14

DIGITAL COMMUNICATION THROUGH FADING MULTIPATH CHANNELS

The previous chapters have described the design and performance of digital communications systems for transmission on either the classical AWGN channel or a linear filter channel with AWGN. We observed that the distortion inherent in linear filter channels requires special signal design techniques and rather sophisticated adaptive equalization algorithms in order to achieve good performance.

In this chapter, we consider the signal design, receiver structure, and receiver performance for more complex channels, namely, channels having randomly time-variant impulse responses. This characterization serves as a model for signal transmission over many radio channels such as shortwave ionospheric radio communication in the 3–30 MHz frequency band (HF), tropospheric scatter (beyond-the-horizon) radio communications in the 300–3000 MHz frequency band (UHF) and 3000–30 000 MHz frequency band (SHF), and ionospheric forward scatter in the 30–300 MHz frequency band (VHF). The time-variant impulse responses of these channels are a consequence of the constantly changing physical characteristics of the media. For example, the ions in the ionospheric layers that reflect the signals transmitted in the HF frequency band are always in motion. To the user of the channel, the motion of the ions appears to be random. Consequently, if the same signal is transmitted at HF in two widely separated time intervals, the two received signals will be different. The time-varying responses that occur are treated in statistical terms.

We shall begin our treatment of digital signalling over fading multipath channels by first developing a statistical characterization of the channel. Then we shall evaluate the performance of several basic digital signaling techniques for communication over such channels. The performance results will demons-

trate the severe penalty in SNR that must be paid as a consequence of the fading characteristics of the received signal. We shall then show that the penalty in SNR can be dramatically reduced by means of efficient modulation/coding and demodulation/decoding techniques.

14-1 CHARACTERIZATION OF FADING MULTIPATH CHANNELS

If we transmit an extremely short pulse, ideally an impulse, over a time-varying multipath channel, the received signal might appear as a train of pulses, as shown in Fig. 14-1-1. Hence, one characteristic of a multipath medium is the time spread introduced in the signal that is transmitted through the channel.

A second characteristic is due to the time variations in the structure of the medium. As a result of such time variations, the nature of the multipath varies with time. That is, if we repeat the pulse-sounding experiment over and over, we shall observe changes in the received pulse train, which will include changes in the sizes of the individual pulses, changes in the relative delays among the pulses, and, quite often, changes in the number of pulses observed in the received pulse train as shown in Fig. 14-1-1. Moreover, the time variations appear to be unpredictable to the user of the channel. Therefore, it is reasonable to characterize the time-variant multipath channel statistically.

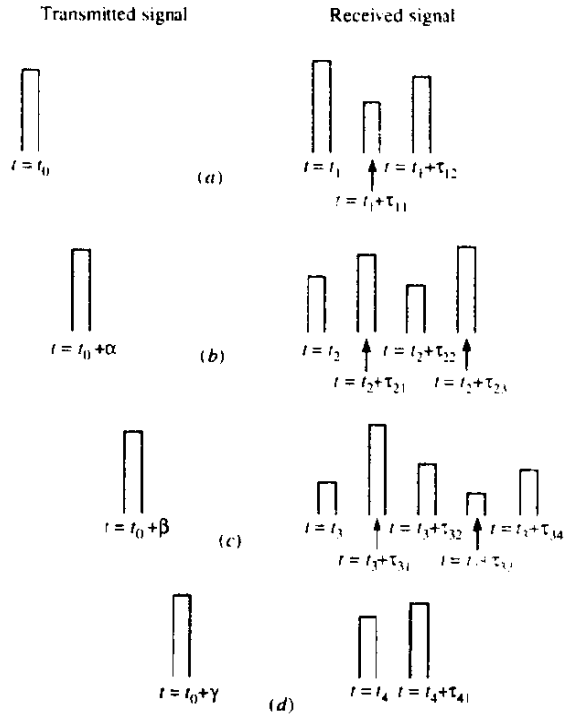

FIGURE 14-1-1 Example of the response of a time-variant multipath channel to a very narrow pulse.

Toward this end, let us examine the effects of the channel on a transmitted signal that is represented in general as

$$s(t) = \text{Re}\left[s_l(t)e^{j2\pi f_c t}\right] \tag{14-1-1}$$

We assume that there are multiple propagation paths. Associated with each path is a propagation delay and an attenuation factor. Both the propagation delays and the attenuation factors are time-variant as a result of changes in the structure of the medium. Thus, the received bandpass signal may be expressed in the form

$$x(t) = \sum_n \alpha_n(t)s(t - \tau_n(t)) \tag{14-1-2}$$

where $\alpha_n(t)$ is the attenuation factor for the signal received on the nth path and $\tau_n(t)$ is the propagation delay for the nth path. Substitution for $s(t)$ from (14-1-1) into (14-1-2) yields the result

$$x(t) = \text{Re}\left\{\left[\sum_n \alpha_n(t)e^{-j2\pi f_c \tau_n(t)}s_l(t - \tau_n(t))\right]e^{j2\pi f_c t}\right\} \tag{14-1-3}$$

It is apparent from (14-1-3) that the equivalent lowpass received signal is

$$r_l(t) = \sum_n \alpha_n(t)e^{-j2\pi f_c \tau_n(t)}s_l(t - \tau_n(t)) \tag{14-1-4}$$

Since $r_l(t)$ is the response of an equivalent lowpass channel to the equivalent lowpass signal $s_l(t)$, it follows that the equivalent lowpass channel is described by the time-variant impulse response

$$c(\tau; t) = \sum_n \alpha_n(t)e^{-j2\pi f_c \tau_n(t)}\delta(\tau - \tau_n(t)) \tag{14-1-5}$$

For some channels, such as the tropospheric scatter channel, it is more appropriate to view the received signal as consisting of a continuum of multipath components. In such a case, the received signal $x(t)$ is expressed in the integral form

$$x(t) = \int_{-\infty}^{\infty} \alpha(\tau; t)s(t - \tau)\,d\tau \tag{14-1-6}$$

where $\alpha(\tau; t)$ denotes the attenuation of the signal components at delay τ and at time instant t. Now substitution for $s(t)$ from (14-1-1) into (14-1-6) yields

$$x(t) = \text{Re}\left\{\left[\int_{-\infty}^{\infty} \alpha(\tau; t)e^{-j2\pi f_c \tau}s_l(t - \tau)\,d\tau\right]e^{j2\pi f_c t}\right\} \tag{14-1-7}$$

Since the integral in (14-1-7) represents the convolution of $s_l(t)$ with an equivalent lowpass time-variant impulse response $c(\tau; t)$, it follows that

$$c(\tau; t) = \alpha(\tau; t)e^{-j2\pi f_c \tau} \tag{14-1-8}$$

where $c(\tau; t)$ represents the response of the channel at time t due to an impulse applied at time $t - \tau$. Thus (14-1-8) is the appropriate definition of the equivalent lowpass impulse response when the channel results in continuous multipath and (14-1-5) is appropriate for a channel that contains discrete multipath components.

Now let us consider the transmission of an unmodulated carrier at frequency f_c. Then $s_l(t) = 1$ for all t, and, hence, the received signal for the case of discrete multipath, given by (14-1-4), reduces to

$$r_l(t) = \sum_n \alpha_n(t) e^{-j2\pi f_c \tau_n(t)}$$

$$= \sum_n \alpha_n(t) e^{-j\theta_n(t)} \qquad (14\text{-}1\text{-}9)$$

where $\theta_n(t) = 2\pi f_c \tau_n(t)$. Thus, the received signal consists of the sum of a number of time-variant vectors (phasors) having amplitudes $\alpha_n(t)$ and phases $\theta_n(t)$. Note that large dynamic changes in the medium are required for $\alpha_n(t)$ to change sufficiently to cause a significant change in the received signal. On the other hand, $\theta_n(t)$ will change by 2π rad whenever τ_n changes by $1/f_c$. But $1/f_c$ is a small number and, hence, θ_n can change by 2π rad with relatively small motions of the medium. We also expect the delays $\tau_n(t)$ associated with the different signal paths to change at different rates and in an unpredictable (random) manner. This implies that the received signal $r_l(t)$ in (14-1-9) can be modeled as a random process. When there are a large number of paths, the central limit theorem can be applied. That is, $r_l(t)$ may be modeled as a complex-valued gaussian random process. This means that the time-variant impulse response $c(\tau; t)$ is a complex-valued gaussian random process in the t variable.

The multipath propagation model for the channel embodied in the received signal $r_l(t)$, given in (14-1-9), results in signal fading. The fading phenomenon is primarily a result of the time variations in the phases $\{\theta_n(t)\}$. That is, the randomly time-variant phases $\{\theta_n(t)\}$ associated with the vectors $\{\alpha_n e^{-j\theta_n}\}$ at times result in the vectors adding destructively. When that occurs, the resultant received signal $r_l(t)$ is very small or practically zero. At other times, the vectors $\{\alpha_n e^{-j\theta_n}\}$ add constructively, so that the received signal is large. Thus, the amplitude variations in the received signal, termed *signal fading*, are due to the time-variant multipath characteristics of the channel.

When the impulse response $c(\tau; t)$ is modeled as a zero-mean complex-valued gaussian process, the envelope $|c(\tau; t)|$ at any instant t is Rayleigh-distributed. In this case the channel is said to be a *Rayleigh fading channel.* In the event that there are fixed scatterers or signal reflectors in the medium, in addition to randomly moving scatterers, $c(\tau; t)$ can no longer be modeled as having zero mean. In this case, the envelope $|c(\tau; t)|$ has a Rice distribution and the channel is said to be a *Ricean fading channel.* Another probability distribution function that has been used to model the envelope of fading

signals is the Nakagami-m distribution. These fading channel models are considered in Section 14-1-2.

14-1-1 Channel Correlation Functions and Power Spectra

We shall now develop a number of useful correlation functions and power spectral density functions that define the characteristics of a fading multipath channel. Our starting point is the equivalent lowpass impulse response $c(\tau; t)$, which is characterized as a complex-valued random process in the t variable. We assume that $c(\tau; t)$ is wide-sense-stationary. Then we define the autocorrelation function of $c(\tau; t)$ as

$$\phi_c(\tau_1, \tau_2; \Delta t) = \tfrac{1}{2}E[c^*(\tau_1; t)c(\tau_2; t + \Delta t)] \tag{14-1-10}$$

In most radio transmission media, the attenuation and phase shift of the channel associated with path delay τ_1 is uncorrelated with the attenuation and phase shift associated with path delay τ_2. This is usually called *uncorrelated scattering*. We make the assumption that the scattering at two different delays is uncorrelated and incorporate it into (14-1-10) to obtain

$$\tfrac{1}{2}E[c^*(\tau_1; t)c(\tau_2; t + \Delta t)] = \phi_c(\tau_1; \Delta t)\delta(\tau_1 - \tau_2) \tag{14-1-11}$$

If we let $\Delta t = 0$, the resulting autocorrelation function $\phi_c(\tau; 0) \equiv \phi_c(\tau)$ is simply the average power output of the channel as a function of the time delay τ. For this reason, $\phi_c(\tau)$ is called the *multipath intensity profile* or *the delay power spectrum* of the channel. In general, $\phi_c(\tau; \Delta t)$ gives the average power output as a function of the time delay τ and the difference Δt in observation time.

In practice, the function $\phi_c(\tau; \Delta t)$ is measured by transmitting very narrow pulses or, equivalently, a wideband signal and cross-correlating the received signal with a delayed version of itself. Typically, the measured function $\phi_c(\tau)$ may appear as shown in Fig. 14-1-2. The range of values of τ over which $\phi_c(\tau)$

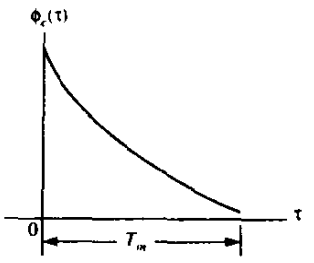

FIGURE 14-1-2 Multipath intensity profile.

is essentially nonzero is called the *multipath spread of the channel* and is denoted by T_m.

A completely analogous characterization of the time-variant multipath channel begins in the frequency domain. By taking the Fourier transform of $c(\tau; t)$ we obtain the time-variant transfer function $C(f; t)$, where f is the frequency variable. Thus,

$$C(f; t) = \int_{-\infty}^{\infty} c(\tau; t) e^{-j2\pi f\tau}\, d\tau \tag{14-1-12}$$

If $c(\tau; t)$ is modeled as a complex-valued zero-mean gaussian random process in the t variable, it follows that $C(f; t)$ also has the same statistics. Under the assumption that the channel is wide-sense-stationary, we define the autocorrelation function

$$\phi_C(f_1, f_2; \Delta t) = \tfrac{1}{2} E[C^*(f_1; t) C(f_2; t + \Delta t)] \tag{14-1-13}$$

Since $C(f; t)$ is the Fourier transform of $c(\tau; t)$, it is not surprising to find that $\phi_C(f_1, f_2; \Delta t)$ is related to $\phi_C(\tau; \Delta t)$ by the Fourier transform. The relationship is easily established by substituting (14-1-12) into (14-1-13). Thus,

$$\begin{aligned}
\phi_C(f_1, f_2; \Delta t) &= \tfrac{1}{2} \int_{-\infty}^{\infty} \int_{-\infty}^{\infty} E[c^*(\tau_1; t) c(\tau_2; t + \Delta t)] e^{j2\pi(f_1\tau_1 - f_2\tau_2)}\, d\tau_1\, d\tau_2 \\
&= \int_{-\infty}^{\infty} \int_{-\infty}^{\infty} \phi_c(\tau_1; \Delta t) \delta(\tau_1 - \tau_2) e^{j2\pi(f_1\tau_1 - f_2\tau_2)}\, d\tau_1\, d\tau_2 \\
&= \int_{-\infty}^{\infty} \phi_c(\tau_1; \Delta t) e^{j2\pi(f_1 - f_2)\tau_1}\, d\tau_1 \\
&= \int_{-\infty}^{\infty} \phi_c(\tau_1; \Delta t) e^{-j2\pi \Delta f \tau_1}\, d\tau_1 \equiv \phi_C(\Delta f; \Delta t)
\end{aligned} \tag{14-1-14}$$

where $\Delta f = f_2 - f_1$. From (14-1-14), we observe that $\phi_C(\Delta f; \Delta t)$ is the Fourier transform of the multipath intensity profile. Furthermore, the assumption of uncorrelated scattering implies that the autocorrelation function of $C(f; t)$ in frequency is a function of only the frequency difference $\Delta f = f_2 - f_1$. Therefore, it is appropriate to call $\phi_C(\Delta f; \Delta t)$ the *spaced-frequency, spaced-time correlation function of the channel.* It can be measured in practice by transmitting a pair of sinusoids separated by Δf and cross-correlating the two separately received signals with a relative delay Δt.

Suppose we set $\Delta t = 0$ in (14-1-14). Then, with $\phi_C(\Delta f; 0) \equiv \phi_C(\Delta f)$ and $\phi_c(\tau; 0) \equiv \phi_c(\tau)$, the transform relationship is simply

$$\phi_C(\Delta f) = \int_{-\infty}^{\infty} \phi_c(\tau) e^{-j2\pi \Delta f \tau}\, d\tau \tag{14-1-15}$$

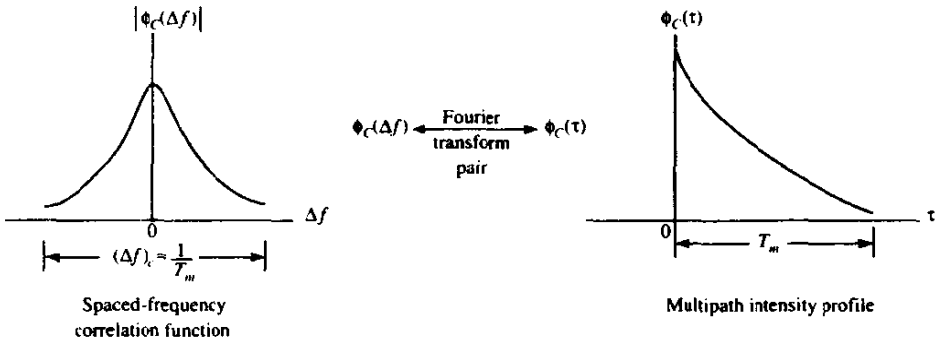

Spaced-frequency correlation function

Multipath intensity profile

FIGURE 14-1-3 Relationship between $\phi_C(\Delta f)$ and $\phi_c(\tau)$.

The relationship is depicted graphically in Fig. 14-1-3. Since $\phi_C(\Delta f)$ is an autocorrelation function in the frequency variable, it provides us with a measure of the frequency coherence of the channel. As a result of the Fourier transform relationship between $\phi_C(\Delta f)$ and $\phi_c(\tau)$, the reciprocal of the multipath spread is a measure of the *coherence bandwidth of the channel.* That is,

$$(\Delta f)_c \approx \frac{1}{T_m} \tag{14-1-16}$$

where $(\Delta f)_c$ denotes the coherence bandwidth. Thus, two sinusoids with frequency separation greater than $(\Delta f)_c$ are affected differently by the channel. When an information-bearing signal is transmitted through the channel, if $(\Delta f)_c$ is small in comparison to the bandwidth of the transmitted signal, the channel is said to be *frequency-selective.* In this case, the signal is severely distorted by the channel. On the other hand, if $(\Delta f)_c$ is large in comparison with the bandwidth of the transmitted signal, the channel is said to be *frequency-nonselective.*

We now focus our attention on the time variations of the channel as measured by the parameter Δt in $\phi_C(\Delta f; \Delta t)$. The time variations in the channel are evidenced as a Doppler broadening and, perhaps, in addition as a Doppler shift of a spectral line. In order to relate the Doppler effects to the time variations of the channel, we define the Fourier transform of $\phi_C(\Delta f; \Delta t)$ with respect to the variable Δt to be the function $S_C(\Delta f; \lambda)$. That is,

$$S_C(\Delta f; \lambda) = \int_{-\infty}^{\infty} \phi_C(\Delta f; \Delta t) e^{-j2\pi\lambda\,\Delta t}\, d\Delta t \tag{14-1-17}$$

With Δf set to zero and $S_C(0; \lambda) \equiv S_C(\lambda)$, the relation in (14-1-17) becomes

$$S_C(\lambda) = \int_{-\infty}^{\infty} \phi_C(\Delta t) e^{-j2\pi\lambda\,\Delta t}\, d\Delta t \tag{14-1-18}$$

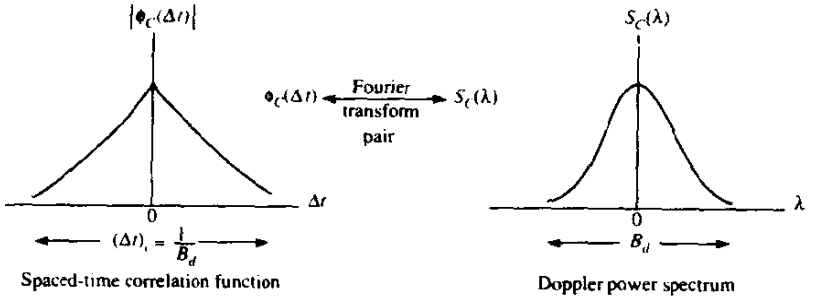

FIGURE 14-1-4 Relationship between $\phi_C(\Delta t)$ and $S_C(\lambda)$.

The function $S_C(\lambda)$ is a power spectrum that gives the signal intensity as a function of the Doppler frequency λ. Hence, we call $S_C(\lambda)$ the *Doppler power spectrum of the channel.*

From (14-1-18), we observe that if the channel is time-invariant, $\phi_C(\Delta t) = 1$ and $S_C(\lambda)$ becomes equal to the delta function $\delta(\lambda)$. Therefore, when there are no time variations in the channel, there is no spectral broadening observed in the transmission of a pure frequency tone.

The range of values of λ over which $S_C(\lambda)$ is essentially nonzero is called the *Doppler spread B_d of the channel.* Since $S_C(\lambda)$ is related to $\phi_C(\Delta t)$ by the Fourier transform, the reciprocal of B_d is a measure of the coherence time of the channel. That is,

$$(\Delta t)_c \approx \frac{1}{B_d} \tag{14-1-19}$$

where $(\Delta t)_c$ denotes the *coherence time.* Clearly, a slowly changing channel has a large coherence time or, equivalently, a small Doppler spread. Figure 14-1-4 illustrates the relationship between $\phi_C(\Delta t)$ and $S_C(\lambda)$.

We have now established a Fourier transform relationship between $\phi_C(\Delta f; \Delta t)$ and $\phi_c(\tau; \Delta t)$ involving the variables $(\tau, \Delta f)$, and a Fourier transform relationship between $\phi_C(\Delta f; \Delta t)$ and $S_C(\Delta f; \lambda)$ involving the variables $(\Delta t, \lambda)$. There are two additional Fourier transform relationships that we can define, which serve to relate $\phi_c(\tau; \Delta t)$ to $S_C(\Delta f; \lambda)$ and, thus, close the loop. The desired relationship is obtained by defining a new function, denoted by $S(\tau; \lambda)$, to be the Fourier transform of $\phi_c(\tau; \Delta t)$ in the Δt variable. That is,

$$S(\tau; \lambda) = \int_{-\infty}^{\infty} \phi_c(\tau; \Delta t) e^{-j2\pi\lambda\,\Delta t}\, d\Delta t \tag{14-1-20}$$

It follows that $S(\tau; \lambda)$ and $S_C(\Delta f; \lambda)$ are a Fourier transform pair. That is,

$$S(\tau; \lambda) = \int_{-\infty}^{\infty} S_C(\Delta f; \lambda) e^{j2\pi\tau\,\Delta f}\, d\Delta f \tag{14-1-21}$$

Furthermore, $S(\tau; \lambda)$ and $\phi_C(\Delta f; \Delta t)$ are related by the double Fourier transform

$$S(\tau; \lambda) = \int_{-\infty}^{\infty} \int_{-\infty}^{\infty} \phi_C(\Delta f; \Delta t) e^{-j2\pi\lambda\,\Delta t} e^{j2\pi\tau\,\Delta f}\, d\Delta t\, d\Delta f \qquad (14\text{-}1\text{-}22)$$

This new function $S(\tau; \lambda)$ is called the *scattering function of the channel.* It provides us with a measure of the average power output of the channel as a function of the time delay τ and the Doppler frequency λ.

The relationships among the four functions $\phi_C(\Delta f; \Delta t)$, $\phi_c(\tau; \Delta t)$, $\phi_C(\Delta f; \lambda)$, and $S(\tau; \lambda)$ are summarized in Fig. 14-1-5.

FIGURE 14-1-5 Relationships among the channel correlation functions and power spectra. [*From Green (1962), with permission.*]

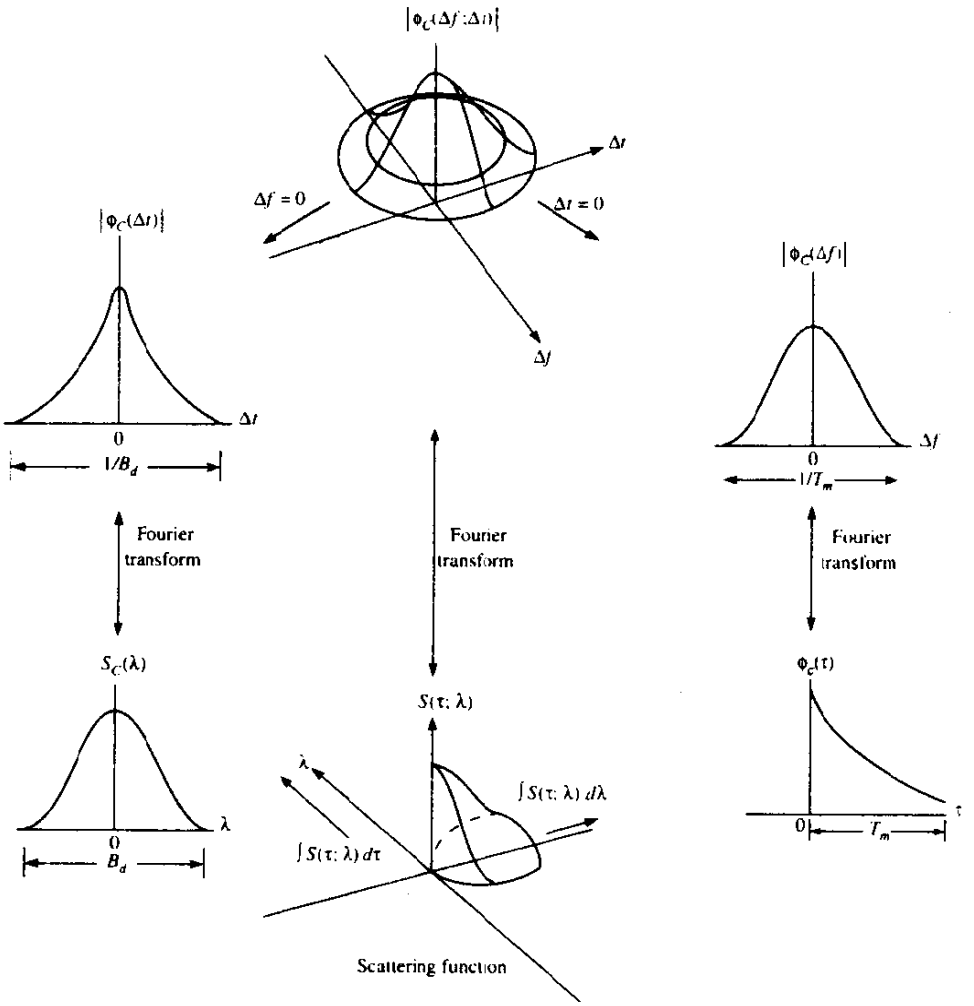

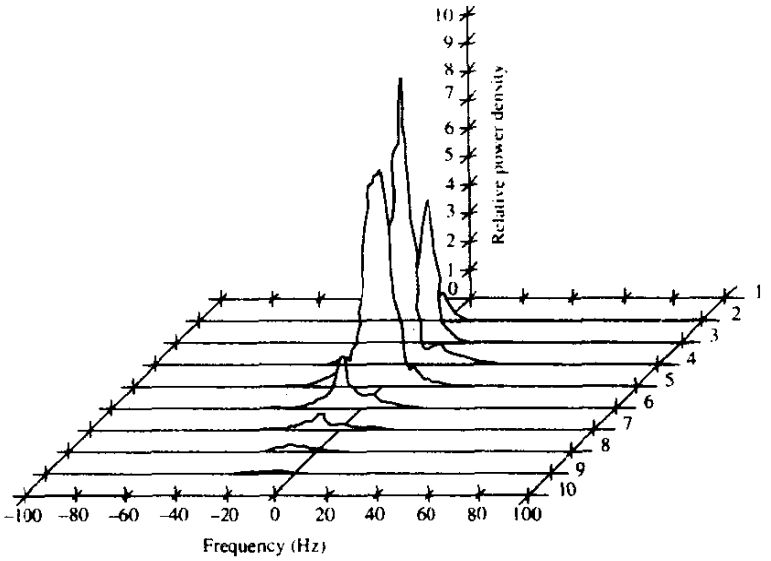

FIGURE 14-1-6 Scattering function of a medium-range tropospheric scatter channel. The taps delay increment is 0.1 μs.

The scattering function $S(\tau; \lambda)$ measured on a 150 mi tropospheric scatter link is shown in Fig. 14-1-6. The signal used to probe the channel had a time resolution of 0.1 μs. Hence, the time-delay axis is quantized in increments of 0.1 μs. From the graph, we observe that the multipath spread $T_m = 0.7$ μs. On the other hand, the Doppler spread, which may be defined as the 3 dB bandwidth of the power spectrum for each signal path, appears to vary with each signal path. For example, in one path it is less than 1 Hz, while in some other paths it is several hertz. For our purposes, we shall take the largest of these 3 dB bandwidths of the various paths and call that the *Doppler spread.*

14-1-2 Statistical Models for Fading Channels

There are several probability distributions that can be considered in attempting to model the statistical characteristics of the fading channel. When there are a large number of scatterers in the channel that contribute to the signal at the receiver, as is the case in ionospheric or tropospheric signal propagation, application of the central limit theorem leads to a gaussian process model for the channel impulse response. If the process is zero-mean, then the envelope of the channel response at any time instant has a Rayleigh probability distribution and the phase is uniformly distributed in the interval $(0, 2\pi)$. That is,

$$p_R(r) = \frac{2r}{\Omega} e^{-r^2/\Omega}, \quad r \geq 0 \tag{14-1-23}$$

where

$$\Omega = E(R^2) \tag{14-1-24}$$

We observe that the Rayleigh distribution is characterized by the single parameter $E(R^2)$.

An alternative statistical model for the envelope of the channel response is the Nakagami-*m* distribution given by the pdf in (2-1-147). In constrast to the Rayleigh distribution, which has a single parameter that can be used to match the fading channel statistics, the Nakagami-*m* is a two-parameter distribution, namely, involving the parameter m and the second moment $\Omega = E(R^2)$. As a consequence, this distribution provides more flexibility and accuracy in matching the observed signal statistics. The Nakagami-*m* distribution can be used to model fading channel conditions that are either more or less severe than the Rayleigh distribution, and it includes the Rayleigh distribution as a special case ($m = 1$). For example, Turin (1972) and Suzuki (1977) have shown that the Nakagami-*m* distribution is the best fit for data signals received in urban radio multipath channels.

The Rice distribution is also a two-parameter distribution. It may be expressed by the pdf given in (2-1-141), where the parameters are s and σ^2. Recall that s^2 is called the *noncentrality parameter* in the equivalent chi-square distribution. It represents the power in the nonfading signal components, sometimes called *specular components,* of the received signal.

There are many radio channels in which fading is encountered that are basically line-of-sight (LOS) communication links with multipath components arising from secondary reflections, or signal paths, from surrounding terrain. In such channels, the number of multipath components is small, and, hence, the channel may be modeled in a somewhat simpler form. We cite two channel models as examples.

As the first example, let us consider an airplane to ground communication link in which there is the direct path and a single multipath component at a delay t_0 relative to the direct path. The impulse response of such a channel may be modeled as

$$c(\tau; t) = \alpha\delta(\tau) + \beta(t)\delta(\tau - \tau_0(t)) \tag{14-1-25}$$

where α is the attenuation factor of the direct path and $\beta(t)$ represents the time-variant multipath signal component resulting from terrain reflections. Often, $\beta(t)$ can be characterized as a zero-mean gaussian random process. The transfer function for this channel model may be expressed as

$$C(f; t) = \alpha + \beta(t)e^{-j2\pi f\tau_0(t)} \tag{14-1-26}$$

This channel fits the Ricean fading model defined previously. The direct path with attenuation α represents the specular component and $\beta(t)$ represents the Rayleigh fading component.

A similar model has been found to hold for microwave LOS radio channels

used for long-distance voice and video transmission by telephone companies throughout the world. For such channels, Rummler (1979) has developed a three-path model based on channel measurements performed on typical LOS links in the 6 GHz frequency band. The differential delay on the two multipath components is relatively small, and, hence, the model developed by Rummler is one that has a channel transfer function

$$C(f) = \alpha[1 - \beta e^{-j2\pi(f-f_0)\tau_0}] \tag{14-1-27}$$

where α is the overall attenuation parameter, β is called a shape parameter which is due to the multipath components, f_0 is the frequency of the fade minimum, and τ_0 is the relative time delay between the direct and the multipath components. This simplified model was used to fit data derived from channel measurements.

Rummler found that the parameters α and β may be characterized as random variables that, for practical purposes, are nearly statistically independent. From the channel measurements, he found that the distribution of β has the form $(1-\beta)^{2.3}$. The distribution of α is well modeled by the lognormal distribution, i.e., $-\log \alpha$ is gaussian. For $\beta > 0.5$, the mean of $-20 \log \alpha$ was found to be 25 dB and the standard deviation was 5 dB. For smaller values of β, the mean decreases to 15 dB. The delay parameter determined from the measurements was $\tau_0 = 6.3$ ns. The magnitude-square response of $C(f)$ is

$$|C(f)|^2 = \alpha^2[1 + \beta^2 - 2\beta \cos 2\pi(f - f_0)\tau_0] \tag{14-1-28}$$

$|C(f)|$ is plotted in Fig. 14-1-7 as a function of the frequency $f - f_0$ for $\tau_0 = 6.3$ ns. Note that the effect of the multipath component is to create a deep attenuation at $f = f_0$ and at multiples of $1/\tau_0 \approx 159$ MHz. By comparison, the typical channel bandwidth is 30 MHz. This model was used by Lundgren and Rummler (1979) to determine the error rate performance of digital radio systems.

FIGURE 14-1-7 Magnitude frequency response of LOS channel model

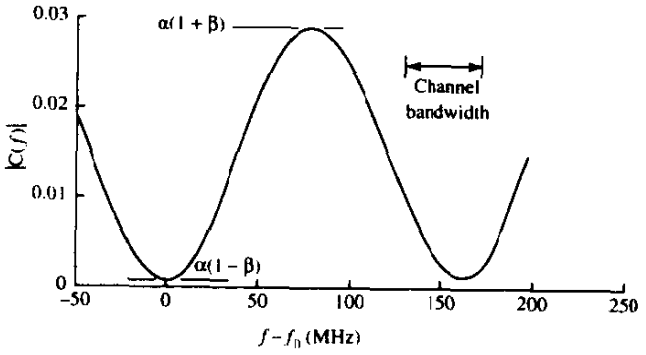

14-2 THE EFFECT OF SIGNAL CHARACTERISTICS ON THE CHOICE OF A CHANNEL MODEL

Having discussed the statistical characterization of time-variant multipath channels generally in terms of the correlation functions described in Section 14-1, we now consider the effect of signal characteristics on the selection of a channel model that is appropriate for the specified signal. Thus, let $s_l(t)$ be the equivalent lowpass signal transmitted over the channel and let $S_l(f)$ denote its frequency content. Then the equivalent lowpass received signal, exclusive of additive noise, may be expressed either in terms of the time domain variables $c(\tau; t)$ and $s_l(t)$ as

$$r_l(t) = \int_{-\infty}^{\infty} c(\tau; t) s_l(t - \tau)\, d\tau \tag{14-2-1}$$

or in terms of the frequency functions $C(f; t)$ and $S_l(f)$ as

$$r_l(t) = \int_{-\infty}^{\infty} C(f; t) S_l(f) e^{j2\pi ft}\, df \tag{14-2-2}$$

Suppose we are transmitting digital information over the channel by modulating (either in amplitude, or in phase, or both) the basic pulse $s_l(t)$ at a rate $1/T$, where T is the signaling interval. It is apparent from (14-2-2) that the time-variant channel characterized by the transfer function $C(f; t)$ distorts the signal $S_l(f)$. If $S_l(f)$ has a bandwidth W greater than the coherence bandwidth $(\Delta f)_c$ of the channel, $S_l(f)$ is subjected to different gains and phase shifts across the band. In such a case, the channel is said to be *frequency-selective*. Additional distortion is caused by the time variations in $C(f; t)$. This type of distortion is evidenced as a variation in the received signal strength, and has been termed *fading*. It should be emphasized that the frequency selectivity and fading are viewed as two different types of distortion. The former depends on the multipath spread or, equivalently, on the coherence bandwidth of the channel relative to the transmitted signal bandwidth W. The latter depends on the time variations of the channel, which are grossly characterized by the coherence time $(\Delta t)_c$ or, equivalently, by the Doppler spread B_d.

The effect of the channel on the transmitted signal $s_l(t)$ is a function of our choice of signal bandwidth and signal duration. For example, if we select the signaling interval T to satisfy the condition $T \gg T_m$, the channel introduces a negligible amount of intersymbol interference. If the bandwidth of the signal pulse $s_l(t)$ is $W \approx 1/T$, the condition $T \gg T_m$ implies that

$$W \ll \frac{1}{T_m} \approx (\Delta f)_c \tag{14-2-3}$$

That is, the signal bandwidth W is much smaller than the coherence bandwidth of the channel. Hence, the channel is frequency-nonselective. In other words,

all of the frequency components in $S_l(f)$ undergo the same attenuation and phase shift in transmission through the channel. But this implies that, within the bandwidth occupied by $S_l(f)$, the time-variant transfer function $C(f;t)$ of the channel is a complex-valued constant in the frequency variable. Since $S_l(f)$ has its frequency content concentrated in the vicinity of $f = 0$, $C(f;t) = C(0;t)$. Consequently, (14-2-2) reduces to

$$r_l(t) = C(0;t)\int_{-\infty}^{\infty} S_l(f)e^{j2\pi ft}\,df$$

$$= C(0;t)s_l(t) \tag{14-2-4}$$

Thus, when the signal bandwidth W is much smaller than the coherence bandwidth $(\Delta f)_c$ of the channel, the received signal is simply the transmitted signal multiplied by a complex-valued random process $C(0;t)$, which represents the time-variant characteristics of the channel. In this case, we say that the multipath components in the received are not resolvable because $W \ll (\Delta f)_c$.

The transfer function $C(0;t)$ for a frequency-nonselective channel may be expressed in the form

$$C(0;t) = \alpha(t)e^{-j\phi(t)} \tag{14-2-5}$$

where $\alpha(t)$ represents the envelope and $\phi(t)$ represents the phase of the equivalent lowpass channel. When $C(0;t)$ is modeled as a zero-mean complex-valued gaussian random process, the envelope $\alpha(t)$ is Rayleigh-distributed for any fixed value of t and $\phi(t)$ is uniformly distributed over the interval $(-\pi, \pi)$. The rapidity of the fading on the frequency-nonselective channel is determined either from the correlation function $\phi_C(\Delta t)$ or from the Doppler power spectrum $S_C(\lambda)$. Alternatively, either of the channel parameters $(\Delta t)_c$ or B_d can be used to characterize the rapidity of the fading.

For example, suppose it is possible to select the signal bandwidth W to satisfy the condition $W \ll (\Delta f)_c$ and the signaling interval T to satisfy the condition $T \ll (\Delta t)_c$. Since T is smaller than the coherence time of the channel, the channel attenuation and phase shift are essentially fixed for the duration of at least one signaling interval. When this condition holds, we call the channel a *slowly fading channel.* Furthermore, when $W \approx 1/T$, the conditions that the channel be frequency-nonselective and slowly fading imply that the product of T_m and B_d must satisfy the condition $T_m B_d < 1$.

The product $T_m B_d$ is called the *spread factor* of the channel. If $T_m B_d < 1$, the channel is said to be *underspread*; otherwise, it is *overspread.* The multipath spread, the Doppler spread, and the spread factor are listed in Table 14-2-1 for several channels. We observe from this table that several radio channels, including the moon when used as a passive reflector, are underspread. Consequently, it is possible to select the signal $s_l(t)$ such that these channels are frequency-nonselective and slowly fading. The slow-fading condition

TABLE 14-2-1 MULTIPATH SPREAD, DOPPLER SPREAD, AND SPREAD FACTOR FOR SEVERAL TIME-VARIANT MULTIPATH CHANNELS

Type of channel	Multipath duration	Doppler spread	Spread factor
Shortwave ionospheric propagation (HF)	10^{-3}–10^{-2}	10^{-1}–1	10^{-4}–10^{-2}
Ionospheric propagation under disturbed auroral conditions (HF)	10^{-3}–10^{-2}	10–100	10^{-2}–1
Ionospheric forward scatter (VHF)	10^{-4}	10	10^{-3}
Tropospheric scatter (SHF)	10^{-6}	10	10^{-5}
Orbital scatter (X band)	10^{-4}	10^{3}	10^{-1}
Moon at max. libration ($f_0 = 0.4$ kmc)	10^{-2}	10	10^{-1}

implies that the channel characteristics vary sufficiently slowly that they can be measured.

In Section 14-3, we shall determine the error rate performance for binary signaling over a frequency-nonselective slowly fading channel. This channel model is, by far, the simplest to analyze. More importantly, it yields insight into the performance characteristics for digital signaling on a fading channel and serves to suggest the type of signal waveforms that are effective in overcoming the fading caused by the channel.

Since the multipath components in the received signal are not resolvable when the signal bandwidth W is less than the coherence bandwidth $(\Delta f)_c$ of the channel, the received signal appears to arrive at the receiver via a single fading path. On the other hand, we may choose $W \gg (\Delta f)_c$, so that the channel becomes frequency-selective. We shall show later that, under this condition, the multipath components in the received signal are resolvable with a resolution in time delay of $1/W$. Thus, we shall illustrate that the frequency-selective channel can be modeled as a tapped delay line (transversal) filter with time-variant tap coefficients. We shall then derive the performance of binary signaling over such a frequency-selective channel model.

14-3 FREQUENCY-NONSELECTIVE, SLOWLY FADING CHANNEL

In this section, we derive the error rate performance of binary PSK and binary FSK when these signals are transmitted over a frequency-nonselective, slowly fading channel. As described in Section 14-2, the frequency-nonselective channel results in multiplicative distortion of the transmitted signal $s_l(t)$. Furthermore, the condition that the channel fades slowly implies that the multiplicative process may be regarded as a constant during at least one

signaling interval. Consequently, if the transmitted signal is $s_i(t)$, the received equivalent lowpass signal in one signaling interval is

$$r_i(t) = \alpha e^{-j\phi} s_i(t) + z(t), \quad 0 \leq t \leq T \tag{14-3-1}$$

where $z(t)$ represents the complex-valued white gaussian noise process corrupting the signal.

Let us assume that the channel fading is sufficiently slow that the phase shift ϕ can be estimated from the received signal without error. In that case, we can achieve ideal coherent detection of the received signal. Thus, the received signal can be processed by passing it through a matched filter in the case of binary PSK or through a pair of matched filters in the case of binary FSK. One method that we can use to determine the performance of the binary communications systems is to evaluate the decision variables and from these determine the probability of error. However, we have already done this for a fixed (time-invariant) channel. That is, for a fixed attenuation α, we have previously derived the probability of error for binary PSK and binary FSK. From (5-2-5), the expression for the error rate of binary PSK as a function of the received SNR γ_b is

$$P_2(\gamma_b) = Q(\sqrt{2\gamma_b}) \tag{14-3-2}$$

where $\gamma_b = \alpha^2 \mathscr{E}_b / N_0$. The expression for the error rate of binary FSK, detected coherently, is given by (5-2-10) as

$$P_2(\gamma_b) = Q(\sqrt{\gamma_b}) \tag{14-3-3}$$

We view (14-3-2) and (14-3-3) as conditional error probabilities, where the condition is that α is fixed. To obtain the error probabilities when α is random, we must average $P_2(\gamma_b)$, given in (14-3-2) and (14-3-3), over the probability density function of γ_b. That is, we must evaluate the integral

$$P_2 = \int_0^\infty P_2(\gamma_b) p(\gamma_b)\, d\gamma_b \tag{14-3-4}$$

where $p(\gamma_b)$ is the probability density function of γ_b when α is random.

Rayleigh Fading Since α is Rayleigh-distributed, α^2 has a chi-square probability distribution with two degrees of freedom. Consequently, γ_b also is chi-square-distributed. It is easily shown that

$$p(\gamma_b) = \frac{1}{\bar{\gamma}_b} e^{-\gamma_b/\bar{\gamma}_b}, \quad \gamma_b \geq 0 \tag{14-3-5}$$

where $\bar{\gamma}_b$ is the average signal-to-noise ratio, defined as

$$\bar{\gamma}_b = \frac{\mathscr{E}_b}{N_0} E(\alpha^2) \tag{14-3-6}$$

The term $E(\alpha^2)$ is simply the average value of α^2.

Now we can substitute (14-3-5) into (14-3-4) and carry out the integration for $P_2(\gamma_b)$ as given by (14-3-2) and (14-3-3). The result of this integration for binary PSK is

$$P_2 = \frac{1}{2}\left(1 - \sqrt{\frac{\bar{\gamma}_b}{1 + \bar{\gamma}_b}}\right) \tag{14-3-7}$$

If we repeat the integration with $P_2(\gamma_b)$ given by (14-3-3), we obtain the probability of error for binary FSK, detected coherently, in the form

$$P_2 = \frac{1}{2}\left(1 - \sqrt{\frac{\bar{\gamma}_b}{2 + \bar{\gamma}_b}}\right) \tag{14-3-8}$$

In arriving at the error rate results in (14-3-7) and (14-3-8), we have assumed that the estimate of the channel phase shift, obtained in the presence of slow fading, is noiseless. Such an ideal condition may not hold in practice. In such a case, the expressions in (14-3-7) and (14-3-8) should be viewed as representing the best achievable performance in the presence of Rayleigh fading. In Appendix C we consider the problem of estimating the phase in the presence of noise and we evaluate the error rate performance of binary and multiphase PSK.

On channels for which the fading is sufficiently rapid to preclude the estimation of a stable phase reference by averaging the received signal phase over many signaling intervals, DPSK, is an alternative signaling method. Since DPSK requires phase stability over only two consecutive signaling intervals, this modulation technique is quite robust in the presence of signal fading. In deriving the performance of binary DPSK for a fading channel, we begin again with the error probability for a nonfading channel, which is

$$P_2(\gamma_b) = \tfrac{1}{2}e^{-\gamma_b} \tag{14-3-9}$$

This expression is substituted into the integral in (14-3-4) along with $p(\gamma_b)$ obtained from (14-3-5). Evaluation of the resulting integral yields the probability of error for binary DPSK, in the form

$$P_2 = \frac{1}{2(1 + \bar{\gamma}_b)} \tag{14-3-10}$$

If we choose not to estimate the channel phase shift at all, but instead employ a noncoherent (envelope or square-law) detector with binary, orthogonal FSK signals, the error probability for a nonfading channel is

$$P_2(\gamma_b) = \tfrac{1}{2}e^{-\gamma_b/2} \tag{14-3-11}$$

When we average $P_2(\gamma_b)$ over the Rayleigh fading channel attenuation, the resulting error probability is

$$P_2 = \frac{1}{2 + \bar{\gamma}_b} \tag{14-3-12}$$

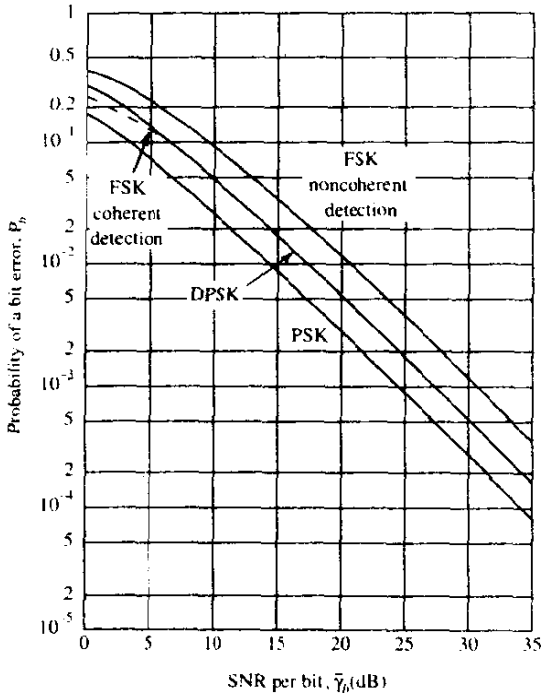

FIGURE 14-3-1 Performance of binary signaling on a Rayleigh fading channel.

The error probabilities in (14-3-7), (14-3-8), (14-3-10), and (14-3-12) are illustrated in Fig. 14-3-1. In comparing the performance of the four binary signaling systems, we focus our attention on the probabilities of error for large SNR, i.e., $\bar{\gamma}_b \gg 1$. Under this condition, the error rates in (14-3-7), (14-3-8), (14-3-10), and (14-3-12) simplify to

$$P_2 \approx \begin{cases} 1/4\bar{\gamma}_b & \text{for coherent PSK} \\ 1/2\bar{\gamma}_b & \text{for coherent, orthogonal FSK} \\ 1/2\bar{\gamma}_b & \text{for DPSK} \\ 1/\bar{\gamma}_b & \text{for noncoherent, orthogonal FSK} \end{cases} \tag{14-3-13}$$

From (14-3-13), we observe that coherent PSK is 3 dB better than DPSK and 6 dB better than noncoherent FSK. More striking, however, is the observation that the error rates decrease only inversely with SNR. In contrast, the decrease in error rate on a nonfading channel is exponential with SNR. This means that, on a fading channel, the transmitter must transmit a large amount of power in order to obtain a low probability of error. In many cases, a large amount of power is not possible, technically and/or economically. An alternative solution to the problem of obtaining acceptable performance on a fading channel is the use of redundancy, which can be obtained by means of diversity techniques, as discussed in Section 14-4.

Nakagami Fading If α is characterized statistically by the Nakagami-m distribution, the random variable $\gamma = \alpha^2 \mathscr{E}_b / N_0$ has the pdf (see Problem 14-15)

$$p(\gamma) = \frac{m^m}{\Gamma(m)\bar{\gamma}^m} \gamma^{m-1} e^{-m\gamma/\bar{\gamma}} \tag{14-3-14}$$

where $\bar{\gamma} = E(\alpha^2)\mathscr{E}/N_0$.

The average probability of error for any of the modulation methods is simply obtained by averaging the appropriate error probability for a nonfading channel over the fading signal statistics.

As an example of the performance obtained with Nakagami-m fading statistics, Fig. 14-3-2 illustrates the probability of error of binary PSK with m as a parameter. We recall that $m = 1$ corresponds to Rayleigh fading. We observe that the performance improves as m is increased above $m = 1$, which is indicative of the fact that the fading is less severe. On the other hand, when $m < 1$, the performance is worse than Rayleigh fading.

Other Fading Signal Statistics Following the procedure described above, one can determine the performance of the various modulation methods for other types of fading signal statistics, such as the Rice distribution.

Error probability results for Rice-distributed fading statistics can be found in the paper by Lindsey (1964), while for Nakagami-m fading statistics, the

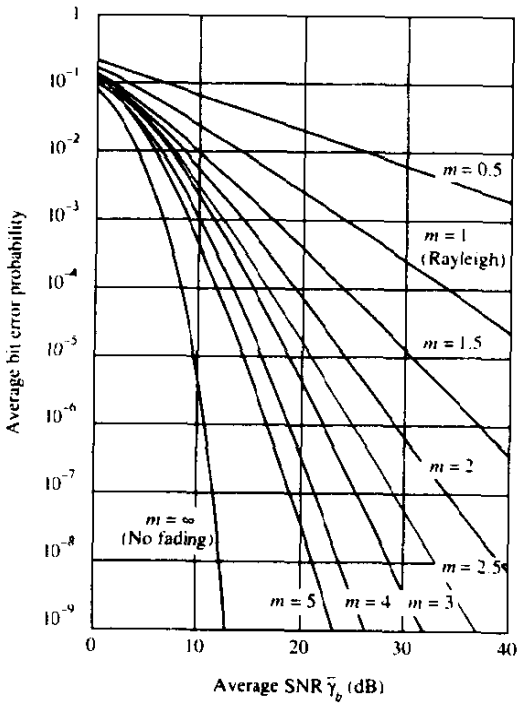

FIGURE 14-3-2 Average error probability for two-phase PSK symbol in nondiversity reception.

reader may refer to the papers by Espòsito (1967), Miyagaki *et al.* (1978), Charash (1979), Al-Hussaini *et al.* (1985), and Beaulieu *et al.* (1991).

14-4 DIVERSITY TECHNIQUES FOR FADING MULTIPATH CHANNELS

Diversity techniques are based on the notion that errors occur in reception when the channel attenuation is large, i.e., when the channel is in a deep fade. If we can supply to the receiver several replicas of the same information signal transmitted over independently fading channels, the probability that all the signal components will fade simultaneously is reduced considerably. That is, if p is the probability that any one signal will fade below some critical value then p^L is the probability that all L independently fading replicas of the same signal will fade below the critical value. There are several ways in which we can provide the receiver with L independently fading replicas of the same information-bearing signal.

One method is to employ *frequency diversity*. That is, the same information-bearing signal is transmitted on L carriers, where the separation between successive carriers equals or exceeds the coherence bandwidth $(\Delta f)_c$ of the channel.

A second method for achieving L independently fading versions of the same information-bearing signal is to transmit the signal in L different time slots, where the separation between successive time slots equals or exceeds the coherence time $(\Delta t)_c$ of the channel. This method is called *time diversity*.

Note that the fading channel fits the model of a bursty error channel. Furthermore, we may view the transmission of the same information either at different frequencies or in difference time slots (or both) as a simple form of repetition coding. The separation of the diversity transmissions in time by $(\Delta t)_c$ or in frequency by $(\Delta f)_c$ is basically a form of block-interleaving the bits in the repetition code in an attempt to break up the error bursts and, thus, to obtain independent errors. Later in the chapter, we shall demonstrate that, in general, repetition coding is wasteful of bandwidth when compared with nontrivial coding.

Another commonly used method for achieving diversity employs multiple antennas. For example, we may employ a single transmitting antenna and multiple receiving antennas. The latter must be spaced sufficiently far apart that the multipath components in the signal have significantly different propagation delays at the antennas. Usually a separation of at least 10 wavelengths is required between two antennas in order to obtain signals that fade independently.

A more sophisticated method for obtaining diversity is based on the use of a signal having a bandwidth much greater than the coherence bandwidth $(\Delta f)_c$ of the channel. Such a signal with bandwidth W will resolve the multipath components and, thus, provide the receiver with several independently fading signal paths. The time resolution is $1/W$. Consequently, with a multipath

spread of T_m s, there are $T_m W$ resolvable signal components. Since $T_m \approx 1/(\Delta f)_c$, the number of resolvable signal components may also be expressed as $W/(\Delta f)_c$. Thus, the use of a wideband signal may be viewed as just another method for obtaining frequency diversity of order $L \approx W/(\Delta f)_c$. The optimum receiver for processing the wideband signal will be derived in Section 14-5. It is called a *RAKE correlator* or a *RAKE matched filter* and was invented by Price and Green (1958).

There are other diversity techniques that have received some consideration in practice, such as angle-of-arrival diversity and polarization diversity. However, these have not been as widely used as those described above.

14-4-1 Binary Signals

We shall now determine the error rate performance for a binary digital communications system with diversity. We begin by describing the mathematical model for the communications system with diversity. First of all, we assume that there are L diversity channels, carrying the same information-bearing signal. Each channel is assumed to be frequency-nonselective and slowly fading with Rayleigh-distributed envelope statistics. The fading processes among the L diversity channels are assumed to be mutually statistically independent. The signal in each channel is corrupted by an additive zero-mean white gaussian noise process. The noise processes in the L channels are assumed to be mutually statistically independent, with identical autocorrelation functions. Thus, the equivalent low-pass received signals for the L channels can be expressed in the form

$$r_{lk}(t) = \alpha_k e^{-j\phi_k} s_{km}(t) + z_k(t), \quad k = 1, 2, \ldots, L, \quad m = 1, 2 \qquad (14\text{-}4\text{-}1)$$

where $\{\alpha_k e^{-j\phi_k}\}$ represent the attenuation factors and phase shifts for the L channels, $s_{km}(t)$ denotes the mth signal transmitted on the kth channel, and $z_k(t)$ denotes the additive white gaussian noise on the kth channel. All signals in the set $\{s_{km}(t)\}$ have the same energy.

The optimum demodulator for the signal received from the kth channel consists of two matched filters, one having the impulse response

$$b_{k1}(t) = s_{k1}^*(T - t) \qquad (14\text{-}4\text{-}2)$$

and the other having the impulse response

$$b_{k2}(t) = s_{k2}^*(T - t) \qquad (14\text{-}4\text{-}3)$$

Of course, if binary PSK is the modulation method used to transmit the information, then $s_{k1}(t) = -s_{k2}(t)$. Consequently, only a single matched filter is required for binary PSK. Following the matched filters is a combiner that forms the two decision variables. The combiner that achieves the best performance is one in which each matched filter output is multiplied by the corresponding complex-valued (conjugate) channel gain $\alpha_k e^{j\phi_k}$. The effect of this multiplication is to compensate for the phase shift in the channel and to

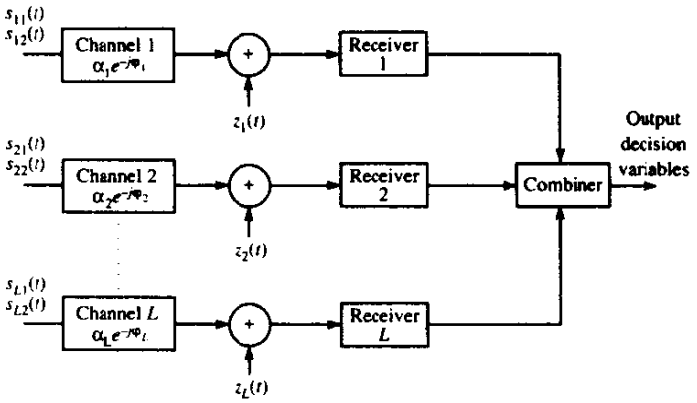

FIGURE 14-4-1 Model of binary digital communications system with diversity.

weight the signal by a factor that is proportional to the signal strength. Thus, a strong signal carries a larger weight than a weak signal. After the complex-valued weighting operation is performed, two sums are formed. One consists of the real parts of the weighted outputs from the matched filters corresponding to a transmitted 0. The second consists of the real part of the outputs from the matched filters corresponding to a transmitted 1. This optimum combiner is called a *maximal ratio combiner* by Brennan (1959). Of course, the realization of this optimum combiner is based on the assumption that the channel attenuations $\{\alpha_k\}$ and the phase shifts $\{\phi_k\}$ are known perfectly. That is, the estimates of the parameters $\{\alpha_k\}$ and $\{\phi_k\}$ contain no noise. (The effect of noisy estimates on the error rate performance of multiphase PSK is considered in Appendix C.

A block diagram illustrating the model for the binary digital communications system described above is shown in Fig. 14-4-1.

Let us first consider the performance of binary PSK with Lth-order diversity. The output of the maximal ratio combiner can be expressed as a single decision variable in the form

$$U = \text{Re}\left(2\mathscr{E}\sum_{k=1}^{L}\alpha_k^2 + \sum_{k=1}^{L}\alpha_k N_k\right)$$
$$= 2\mathscr{E}\sum_{k=1}^{L}\alpha_k^2 + \sum_{k=1}^{L}\alpha_k N_{kr} \tag{14-4-4}$$

where N_{kr} denotes the real part of the complex-valued gaussian noise variable

$$N_k = e^{j\phi_k}\int_0^T z_k(t)s_k^*(t)\,dt \tag{14-4-5}$$

We follow the approach used in Section 14-3 in deriving the probability of error. That is, the probability of error conditioned on a fixed set of attenuation

factors $\{\alpha_k\}$ is obtained first. Then the conditional probability of error is averaged over the probability density function of the $\{\alpha_k\}$.

Rayleigh Fading For a fixed set of $\{\alpha_k\}$ the decision variable U is gaussian with mean

$$E(U) = 2\mathscr{E}\sum_{k=1}^{L}\alpha_k^2 \tag{14-4-6}$$

and variance

$$\sigma_U^2 = 2\mathscr{E}N_0\sum_{k=1}^{L}\alpha_k^2 \tag{14-4-7}$$

For these values of the mean and variance, the probability that U is less than zero is simply

$$P_2(\gamma_b) = Q(\sqrt{2\gamma_b}) \tag{14-4-8}$$

where the SNR per bit, γ_b, is given as

$$\begin{aligned}\gamma_b &= \frac{\mathscr{E}}{N_0}\sum_{k=1}^{L}\alpha_k^2 \\ &= \sum_{k=1}^{L}\gamma_k\end{aligned} \tag{14-4-9}$$

where $\gamma_k = \mathscr{E}\alpha_k^2/N_0$ is the instantaneous SNR on the kth channel. Now we must determine the probability density function $p(\gamma_b)$. This function is most easily determined via the characteristic function of γ_b. First of all, we note that for $L = 1$, $\gamma_b \equiv \gamma_1$ has a chi-square probability density function given in (14-3-5). The characteristic function of γ_1 is easily shown to be

$$\begin{aligned}\psi_{\gamma_1}(jv) &= E(e^{jv\gamma_1}) \\ &= \frac{1}{1 - jv\bar{\gamma}_c}\end{aligned} \tag{14-4-10}$$

where $\bar{\gamma}_c$ is the average SNR per channel, which is assumed to be identical for all channels. That is,

$$\bar{\gamma}_c = \frac{\mathscr{E}}{N_0}E(\alpha_k^2) \tag{14-4-11}$$

independent of k. This assumption applies for the results throughout this section. Since the fading on the L channels is mutually statistically independent, the $\{\gamma_k\}$ are statistically independent, and, hence, the characteristic function for the sum γ_b is simply the result in (14-4-10) raised to the Lth power, i.e.,

$$\psi_{\gamma_b}(jv) = \frac{1}{(1 - jv\bar{\gamma}_c)^L} \tag{14-4-12}$$

But this is the characteristic function of a chi-square-distributed random variable with $2L$ degrees of freedom. It follows from (2-1-107) that the probability density function $p(\gamma_b)$ is

$$p(\gamma_b) = \frac{1}{(L-1)!\bar{\gamma}_c^L}\gamma_b^{L-1}e^{-\gamma_b/\bar{\gamma}_c} \tag{14-4-13}$$

The final step in this derivation is to average the conditional error probability given in (14-4-8) over the fading channel statistics. Thus, we evaluate the integral

$$P_2 = \int_0^\infty P_2(\gamma_b)p(\gamma_b)\,d\gamma_b \tag{14-4-14}$$

There is a closed-form solution for (14-4-14), which can be expressed as

$$P_2 = [\tfrac{1}{2}(1-\mu)]^L \sum_{k=0}^{L-1}\binom{L-1+k}{k}[\tfrac{1}{2}(1+\mu)]^k \tag{14-4-15}$$

where, by definition,

$$\mu = \sqrt{\frac{\bar{\gamma}_c}{1+\bar{\gamma}_c}} \tag{14-4-16}$$

When the average SNR per channel, $\bar{\gamma}_c$, satisfies the condition $\bar{\gamma}_c \gg 1$, the term $\frac{1}{2}(1+\mu) \approx 1$ and the term $\frac{1}{2}(1-\mu) \approx 1/4\bar{\gamma}_c$. Furthermore,

$$\sum_{k=0}^{L-1}\binom{L-1+k}{k} = \binom{2L-1}{L} \tag{14-4-17}$$

Therefore, when $\bar{\gamma}_c$ is sufficiently large (greater than 10 dB), the probability of error in (14-4-15) can be approximated as

$$P_2 \approx \left(\frac{1}{4\bar{\gamma}_c}\right)^L\binom{2L-1}{L} \tag{14-4-18}$$

We observe from (14-4-18) that the probability of error varies as $1/\bar{\gamma}_c$ raised to the Lth power. Thus, with diversity, the error rate decreases inversely with the Lth power of the SNR.

Having obtained the performance of binary PSK with diversity, we now turn our attention to binary, orthogonal FSK that is detected coherently. In this case, the two decision variables at the output of the maximal ratio combiner may be expressed as

$$\begin{aligned} U_1 &= \mathrm{Re}\left(2\mathscr{E}\sum_{k=1}^{L}\alpha_k^2 + \sum_{k=1}^{L}\alpha_k N_{k1}\right) \\ U_2 &= \mathrm{Re}\left(\sum_{k=1}^{L}\alpha_k N_{k2}\right) \end{aligned} \tag{14-4-19}$$

where we have assumed that signal $s_{k1}(t)$ was transmitted and where $\{N_{k1}\}$ and $\{N_{k2}\}$ are the two sets of noise component at the output of the matched filters.

The probability of error is simply the probability that $U_2 > U_1$. This computation is similar to the one performed for PSK, except that we now have twice the noise power. Consequently, when the $\{\alpha_k\}$ are fixed, the conditional probability of error is

$$P_2(\gamma_b) = Q(\sqrt{\gamma_b}) \tag{14-4-20}$$

We use (14-4-13) to average $P_2(\gamma_b)$ over the fading. It is not surprising to find that the result given in (14-4-15) still applies, with $\bar{\gamma}_c$ replaced by $\frac{1}{2}\bar{\gamma}_c$. That is, (14-4-15) is the probability of error for binary, orthogonal FSK with coherent detection, where the parameter μ is defined as

$$\mu = \sqrt{\frac{\bar{\gamma}_c}{2 + \bar{\gamma}_c}} \tag{14-4-21}$$

Furthermore, for large values of $\bar{\gamma}_c$, the performance P_2 can be approximated as

$$P_2 \approx \left(\frac{1}{2\bar{\gamma}_c}\right)^L \binom{2L-1}{L} \tag{14-4-22}$$

In comparing (14-4-22) with (14-4-18), we observe that the 3 dB difference in performance between PSK and orthogonal FSK with coherent detection, which exists in a nonfading, nondispersive channel, is the same also in a fading channel.

In the above discussion of binary PSK and FSK, detected coherently, we assumed that noiseless estimates of the complex-valued channel parameters $\{\alpha_k e^{-j\phi_k}\}$ were used at the receiver. Since the channel is time-variant, the parameters $\{\alpha_k e^{-j\phi_k}\}$ cannot be estimated perfectly. In fact, on some channels, the time variations may be sufficiently fast to preclude the implementation of coherent detection. In such a case, we should consider using either DPSK or FSK with noncoherent detection.

Let us consider DPSK first. In order for DPSK to be a viable digital signaling method, the channel variations must be sufficiently slow so that the channel phase shifts $\{\phi_k\}$ do not change appreciably over two consecutive signaling intervals. In our analysis, we assume that the channel parameters $\{\alpha_k e^{-j\phi_k}\}$ remain constant over two successive signaling intervals. Thus the combiner for binary DPSK will yield as an output the decision variable

$$U = \mathrm{Re}\left[\sum_{k=1}^{L} (2\mathscr{E}\alpha_k e^{-j\phi_k} + N_{k2})(2\mathscr{E}\alpha_k e^{j\phi_k} + N_{k1}^*)\right] \tag{14-4-23}$$

where $\{N_{k1}\}$ and $\{N_{k2}\}$ denote the received noise components at the output of the matched filters in the two consecutive signaling intervals. The probability of error is simply the probability that $U < 0$. Since U is a special case of the general quadratic form in complex-valued gaussian random variables treated in Appendix B, the probability of error can be obtained directly from the results given in that appendix. Alternatively, we may use the error probability given in (12-1-3), which applies to binary DPSK transmitted over L time-invariant

channels, and average it over the Rayleigh fading channel statistics. Thus, we have the conditional error probability

$$P_2(\gamma_b) = (\tfrac{1}{2})^{2L-1} e^{-\gamma_b} \sum_{k=0}^{L-1} b_k \gamma_b^2 \tag{14-4-24}$$

where γ_b is given by (14-4-9) and

$$b_k = \frac{1}{k!} \sum_{n=0}^{L-1-k} \binom{2L-1}{n} \tag{14-4-25}$$

The average of $P_2(\gamma_b)$ over the fading channel statistics given by $p(\gamma_b)$ in (14-4-13) is easily shown to be

$$P_2 = \frac{1}{2^{2L-1}(L-1)!(1+\bar{\gamma}_c)^L} \sum_{k=0}^{L-1} b_k (L-1+k)! \left(\frac{\bar{\gamma}_c}{1+\bar{\gamma}_c}\right)^k \tag{14-4-26}$$

We indicate that the result in (14-4-26) can be manipulated into the form given in (14-4-15), which applies also to coherent PSK and FSK. For binary DPSK, the parameter μ in (14-4-15) is defined as (see Appendix C)

$$\mu = \frac{\bar{\gamma}_c}{1+\bar{\gamma}_c} \tag{14-4-27}$$

For $\bar{\gamma}_c \gg 1$, the error probability in (14-4-26) can be approximated by the expression

$$P_2 \approx \left(\frac{1}{2\bar{\gamma}_c}\right)^L \binom{2L-1}{L} \tag{14-4-28}$$

Orthogonal FSK with noncoherent detection is the final signaling technique that we consider in this section. It is appropriate for both slow and fast fading. However, the analysis of the performance presented below is based on the assumption that the fading is sufficiently slow so that the channel parameters $\{\alpha_k e^{-j\phi_k}\}$ remain constant for the duration of the signaling interval. The combiner for the multichannel signals is a square-law combiner. Its output consists of the two decision variables

$$\begin{aligned} U_1 &= \sum_{k=1}^{L} |2\mathscr{E}\alpha_k e^{-j\phi_k} + N_{k1}|^2 \\ U_2 &= \sum_{k=1}^{L} |N_{k2}|^2 \end{aligned} \tag{14-4-29}$$

where U_1 is assumed to contain the signal. Consequently the probability of error is the probability that $U_2 > U_1$.

As in DPSK, we have a choice of two approaches in deriving the performance of FSK with square-law combining. In Section 12-1, we indicated that the expression for the error probability for square-law combined FSK is the same as that for DPSK with γ_b replaced by $\frac{1}{2}\gamma_b$. That is, the FSK system requires 3 dB of additional SNR to achieve the same performance on a time-invariant channel. Consequently, the conditional error probability for DPSK given in (14-4-24) applies to square-law-combined FSK when γ_b is replaced by $\frac{1}{2}\gamma_b$. Furthermore, the result obtained by averaging (14-4-24) over the fading, which is given by (14-4-26), must also apply to FSK with $\bar{\gamma}_c$ replaced by $\frac{1}{2}\bar{\gamma}_c$. But we also stated previously that (14-4-26) and (14-4-15) are equivalent. Therefore, the error probability given in (14-4-15) also applies to square-law-combined FSK with the parameter μ defined as

$$\mu = \frac{\bar{\gamma}_c}{2 + \bar{\gamma}_c} \tag{14-4-30}$$

An alternative derivation used by Pierce (1958) to obtain the probability that the decision variable $U_2 > U_1$ is just as easy as the method described above. It begins with the probability density functions $p(U_1)$ and $p(U_2)$. Since the complex-valued random variables $\{\alpha_k e^{-j\phi_k}\}$, $\{N_{k1}\}$, and $\{N_{k2}\}$ are zero-mean gaussian-distributed, the decision variables U_1 and U_2 are distributed according to a chi-square probability distribution with $2L$ degrees of freedom. That is,

$$p(U_1) = \frac{1}{(2\sigma_1^2)^L (L-1)!} U_1^{L-1} \exp\left(-\frac{U_1}{2\sigma_1^2}\right) \tag{14-4-31}$$

where

$$\begin{aligned}\sigma_1^2 &= \tfrac{1}{2}E(|2\mathscr{E}\alpha_k e^{-j\phi_k} + N_{k1}|^2) \\ &= 2\mathscr{E}N_0(1 + \bar{\gamma}_c)\end{aligned}$$

Similarly,

$$p(U_2) = \frac{2}{(2\sigma_2^2)^L (L-1)!} U_2^{L-1} \exp\left(-\frac{U_2}{2\sigma_2^2}\right) \tag{14-4-32}$$

where

$$\sigma_2^2 = 2\mathscr{E}N_0$$

The probability of error is just the probability that $U_2 > U_1$. It is left as an exercise for the reader to show that this probability is given by (14-4-15), where μ is defined by (14-4-30).

When $\bar{\gamma}_c \gg 1$, the performance of square-law-detected FSK can be simplified as we have done for the other binary multichannel systems. In this case, the error rate is well approximated by the expression

$$P_2 \approx \left(\frac{1}{\bar{\gamma}_c}\right)^L \binom{2L-1}{L} \tag{14-4-33}$$

The error rate performance of PSK, DPSK, and square-law-detected

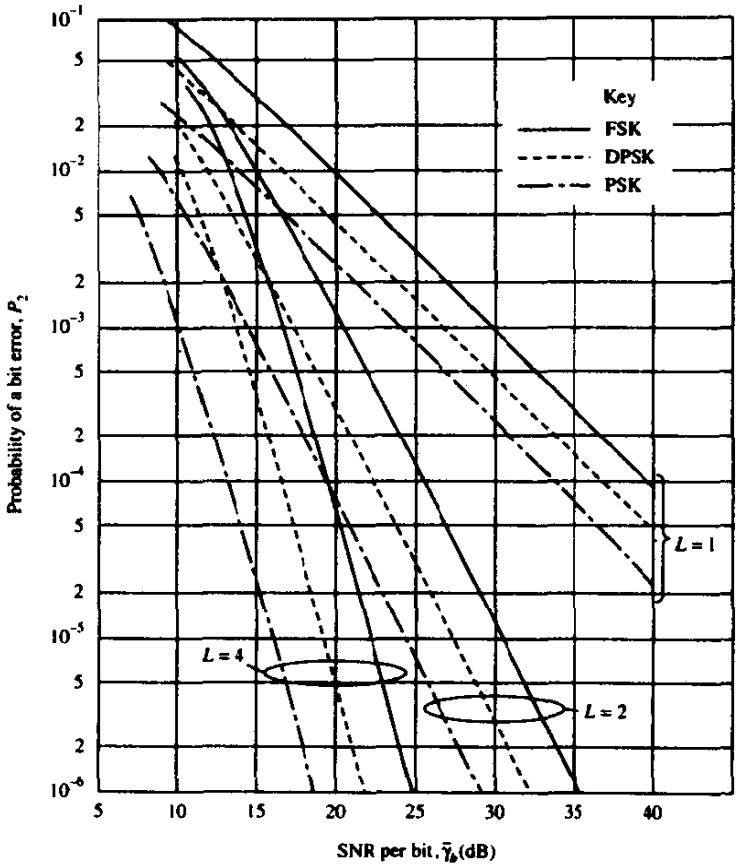

FIGURE 14-4-2 Performance of binary signals with diversity.

orthogonal FSK is illustrated in Fig. 14-4-2 for $L = 1$, 2, and 4. The performance is plotted as a function of the average SNR per bit, $\bar{\gamma}_b$, which is related to the average SNR per channel, $\bar{\gamma}_c$, by the formula

$$\bar{\gamma}_b = L\bar{\gamma}_c \tag{14-4-34}$$

The results in Fig. 14-4-2 clearly illustrate the advantage of diversity as a means for overcoming the severe penalty in SNR caused by fading.

14-4-2 Multiphase Signals

Multiphase signaling over a Rayleigh fading channel is the topic presented in some detail in Appendix C. Our main purpose in this section is to cite the general result for the probability of a symbol error in M-ary PSK and DPSK systems and the probability of a bit error in four-phase PSK and DPSK.

The general result for the probability of a symbol error in M-ary PSK and DPSK is

$$P_M = \frac{(-1)^{L-1}(1-\mu^2)^L}{\pi(L-1)!}\left(\frac{\partial^{L-1}}{\partial b^{L-1}}\left\{\frac{1}{b-\mu^2}\left[\frac{\pi}{M}(M-1)\right.\right.\right.$$
$$\left.\left.\left.-\frac{\mu\sin(\pi/M)}{\sqrt{b-\mu^2\cos^2(\pi/M)}}\cot^{-1}\frac{-\mu\cos(\pi/M)}{\sqrt{b-\mu^2\cos^2(\pi/M)}}\right]\right\}\right)_{b=1} \quad (14\text{-}4\text{-}35)$$

where

$$\mu = \sqrt{\frac{\bar{\gamma}_c}{1+\bar{\gamma}_c}} \quad (14\text{-}4\text{-}36)$$

for coherent PSK and

$$\mu = \frac{\bar{\gamma}_c}{1+\bar{\gamma}_c} \quad (14\text{-}4\text{-}37)$$

for DPSK. Again, $\bar{\gamma}_c$ is the average received SNR per channel. The SNR per bit is $\bar{\gamma}_b = L\bar{\gamma}_c/k$, where $k = \log_2 M$.

The bit error rate for four-phase PSK and DPSK is derived on the basis that the pair of information bits is mapped into the four phases according to a Gray code. The expression for the bit error rate derived in Appendix C is

$$P_b = \frac{1}{2}\left[1 - \frac{\mu}{\sqrt{2-\mu^2}}\sum_{k=0}^{L-1}\binom{2k}{k}\left(\frac{1-\mu^2}{4-2\mu^2}\right)^k\right] \quad (14\text{-}4\text{-}38)$$

where μ is again given by (14-4-36) and (14-4-37) for PSK and DPSK, respectively.

Figure 14-4-3 illustrates the probability of a symbol error of DPSK and coherent PSK for $M = 2$, 4, and 8 with $L = 1$. Note that the difference in performance between DPSK and coherent PSK is approximately 3 dB for all three values of M. In fact, when $\bar{\gamma}_b \gg 1$ and $L = 1$, (14-4-35) is well approximated as

$$P_M \approx \frac{M-1}{(M\log_2 M)[\sin^2(\pi/M)]\bar{\gamma}_b} \quad (14\text{-}4\text{-}39)$$

for DPSK and as

$$P_M \approx \frac{M-1}{(M\log_2 M)[\sin^2(\pi/M)]2\bar{\gamma}_b} \quad (14\text{-}4\text{-}40)$$

for PSK. Hence, at high SNR, coherent PSK is 3 dB better than DPSK on a Rayleigh fading channel. This difference also holds as L is increased.

Bit error probabilities are depicted in Fig. 14-4-4 for two-phase, four-phase, and eight-phase DPSK signaling with $L = 1$, 2, and 4. The expression for the bit error probability of eight-phase DPSK with Gray encoding is not given here, but it is available in the paper by Proakis (1968). In this case, we observe

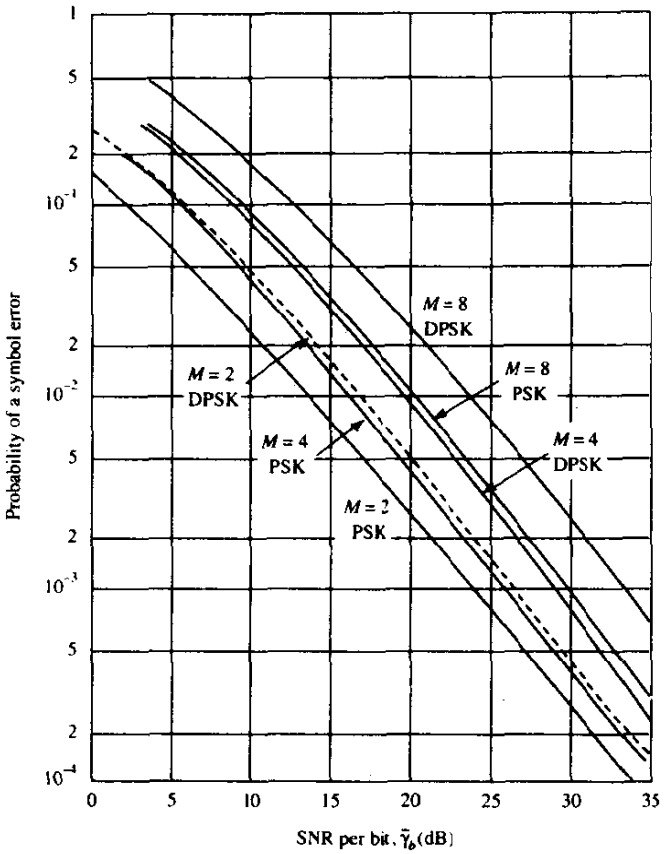

FIGURE 14-4-3 Probability of symbol error for PSK and DPSK for Rayleigh fading.

that the performances for two- and four-phase DPSK are (approximately) the same, while that for eight-phase DPSK is about 3 dB poorer. Although we have not shown the bit error probability for coherent PSK, it can be demonstrated that two- and four-phase coherent PSK also yield approximately the same performance.

14-4-3 *M*-ary Orthogonal Signals

In this sub-section, we determine the performance of M-ary orthogonal signals transmitted over a Rayleigh fading channel and we assess the advantages of higher-order signal alphabets relative to a binary alphabet. The orthogonal signals may be viewed as M-ary FSK with a minimum frequency separation of an integer multiple of $1/T$, where T is the signaling interval. The same information-bearing signal is transmitted on L diversity channels. Each diversity channel is assumed to be frequency-nonselective and slowly fading, and the fading processes on the L channels are assumed to be mutually

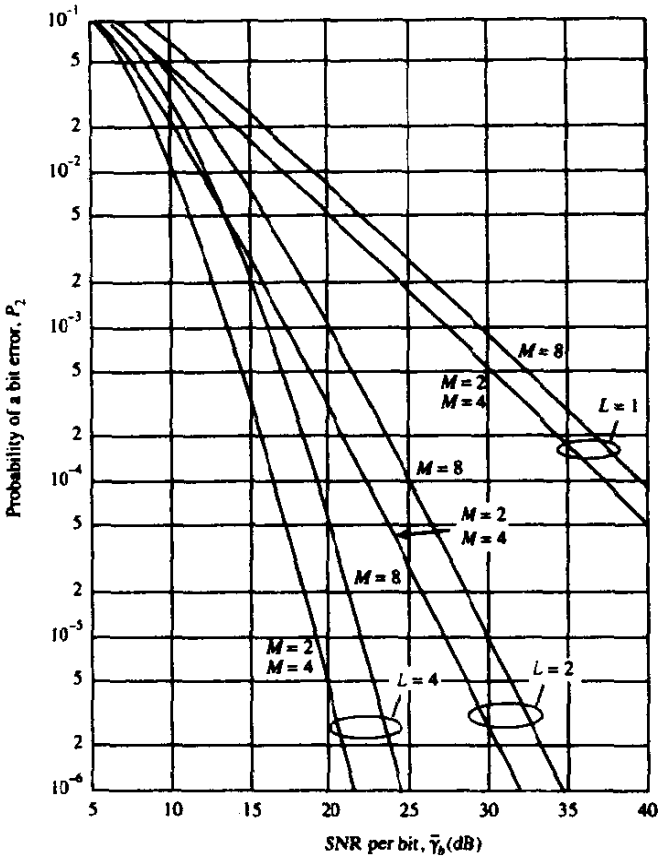

FIGURE 14-4-4 Probability of a bit error for DPSK with diversity for Rayleigh fading.

statistically independent. An additive white gaussian noise process corrupts the signal on each diversity channel. We assume that the additive noise processes are mutually statistically independent.

Although it is relatively easy to formulate the structure and analyze the performance of a maximal ratio combiner for the diversity channels in the M-ary communication system, it is more likely that a practical system would employ noncoherent detection. Consequently, we confine our attention to square-law combining of the diversity signals. The output of the combiner containing the signal is

$$U_1 = \sum_{k=1}^{L} |2\mathscr{E}\alpha_k e^{-j\phi_k} + N_{k1}|^2 \tag{14-4-41}$$

while the outputs of the remaining $M - 1$ combiners are

$$U_m = \sum_{k=1}^{L} |N_{km}|^2, \quad m = 2, 3, 4, \ldots, M \tag{14-4-42}$$

The probability of error is simply 1 minus the probability that $U_1 > U_m$ for $m = 2, 3, \ldots, M$. Since the signals are orthogonal and the additive noise processes are mutually statistically independent, the random variables $U_1, U_2, \ldots, U_M$ are also mutually statistically independent. The probability density function of U_1 was given in (14-4-31). On the other hand, $U_2, \ldots, U_M$ are identically distributed and described by the marginal probability density function in (14-4-32). With U_1 fixed, the joint probability $P(U_2 < U_1, U_3 < U_1, \ldots, U_m < U_1)$ is equal to $P(U_2 < U_1)$ raised to the $M-1$ power. Now,

$$P(U_2 < U_1) = \int_0^{U_1} p(U_2)\, dU_2$$
$$= 1 - \exp\left(-\frac{U_1}{2\sigma_2^2}\right) \sum_{k=0}^{L-1} \frac{1}{k!} \left(\frac{U_1}{2\sigma_2^2}\right)^k \tag{14-4-43}$$

where $\sigma_2^2 = 2\mathscr{E}N_0$. The $M-1$ power of this probability is then averaged over the probability density function of U_1 to yield the probability of a correct decision. If we subtract this result from unity, we obtain the probability of error in the form given by Hahn (1962)

$$P_M = 1 - \int_0^{\infty} \frac{1}{(2\sigma_1^2)^L (L-1)!} U_1^{L-1} \exp\left(-\frac{U_1}{2\sigma_2^2}\right)$$
$$\times \left[1 - \exp\left(-\frac{U_1}{2\sigma_2^2}\right) \sum_{k=0}^{L-1} \frac{1}{k!} \left(\frac{U_1}{2\sigma_2^2}\right)^k\right]^{M-1} dU_1$$
$$= 1 - \int_0^{\infty} \frac{1}{(1+\bar{\gamma}_c)^L (L-1)!} U_1^{L-1} \exp\left(-\frac{U_1}{1+\bar{\gamma}_c}\right)$$
$$\times \left(1 - e^{-U_1} \sum_{k=0}^{L-1} \frac{U_1^k}{k!}\right)^{M-1} dU_1 \tag{14-4-44}$$

where $\bar{\gamma}_c$ is the average SNR per diversity channel. The average SNR per bit is $\bar{\gamma}_b = L\bar{\gamma}_c / \log_2 M = L\bar{\gamma}_c / k$.

The integral in (14-4-44) can be expressed in closed form as a double summation. This can be seen if we write

$$\left(\sum_{k=0}^{L-1} \frac{U_1^k}{k!}\right)^m = \sum_{k=0}^{m(L-1)} \beta_{km} U_1^k \tag{14-4-45}$$

where β_{km} is the set of coefficients in the above expansion. Then it follows that (14-4-44) reduces to

$$P_M = \frac{1}{(L-1)!} \sum_{m=1}^{M-1} \frac{(-1)^{m+1} \binom{M-1}{m}}{(1+m+m\bar{\gamma}_c)^L}$$
$$\times \sum_{k=0}^{m(L-1)} \beta_{km} (L-1+k)! \left(\frac{1+\bar{\gamma}_c}{1+m+m\bar{\gamma}_c}\right)^k \tag{14-4-46}$$

When there is no diversity ($L = 1$), the error probability in (14-4-46) reduces to the simple form

$$P_M = \sum_{m=1}^{M-1} \frac{(-1)^{m+1}\binom{M-1}{m}}{1+m+m\bar{\gamma}_c} \tag{14-4-47}$$

The symbol error rate P_M may be converted to an equivalent bit error rate by multiplying P_M with $2^{k-1}/(2^k-1)$.

Although the expression for P_M given in (14-4-46) is in closed form, it is computationally cumbersome to evaluate for large values of M and L. An alternative is to evaluate P_M by numerical integration using the expression in (14-4-44). The results illustrated in the following graphs were generated from (14-4-44).

First of all, let us observe the error rate performance of M-ary orthogonal signaling with square-law combining as a function of the order of diversity. Figures 14-4-5 and 14-4-6 illustrate the characteristics of P_M for $M = 2$ and 4 as

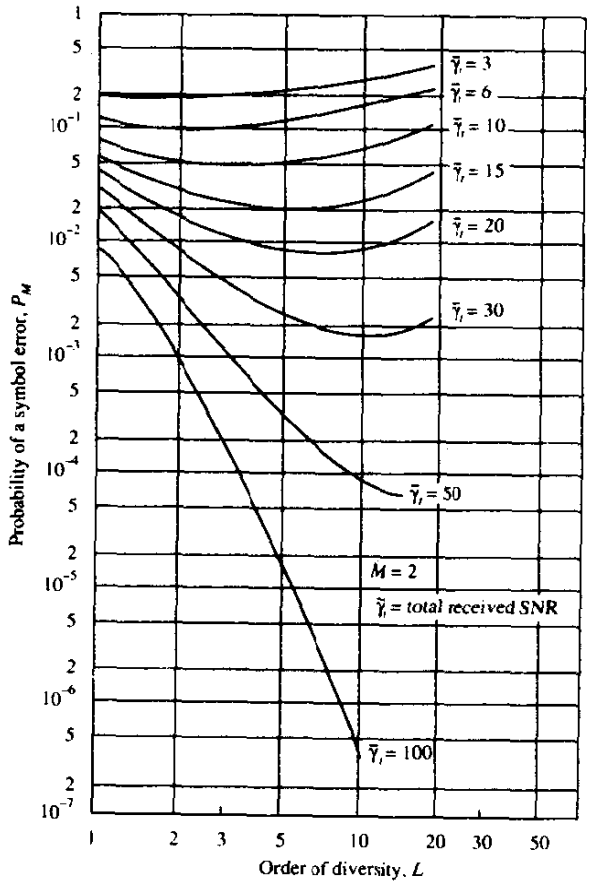

FIGURE 14-4-5 Performance of square-law-detected binary orthogonal signals as a function of diversity.

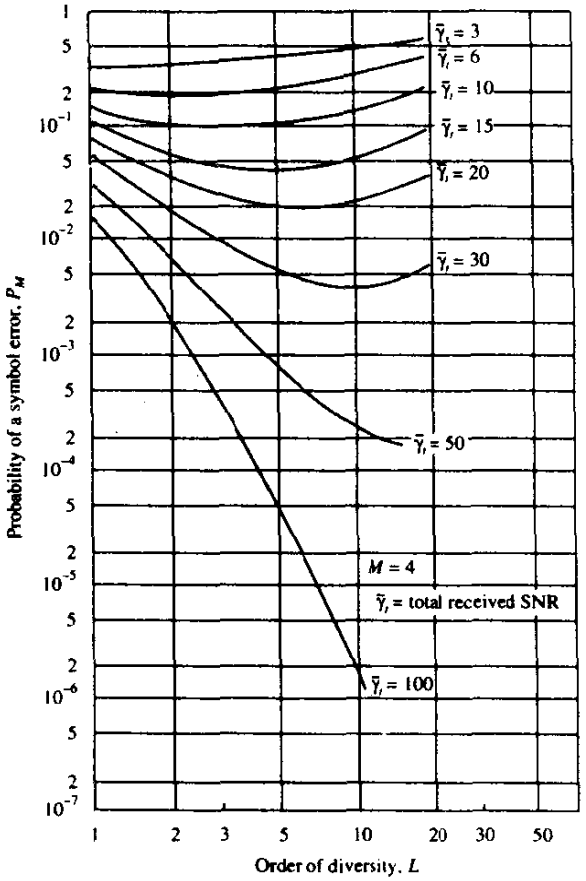

FIGURE 14-4-6 Performance of square-law-detected $M = 4$ orthogonal signals as a function of diversity.

a function of L when the total SNR, defined as $\bar{\gamma}_t = L\bar{\gamma}_c$, remains fixed. These results indicate that there is an optimum order of diversity for each $\bar{\gamma}_t$. That is, for any $\bar{\gamma}_t$, there is a value of L for which P_M is a minimum. A careful observation of these graphs reveals that the minimum in P_M is obtained when $\bar{\gamma}_c = \bar{\gamma}_t/L \approx 3$. This result appears to be independent of the alphabet size M.

Second, let us observe the error rate P_M as a function of the average SNR per bit, defined as $\bar{\gamma}_b = L\bar{\gamma}_c/k$. (If we interpret M-ary orthogonal FSK as a form of coding† and the order of diversity as the number of times a symbol is repeated in a repetition code then $\bar{\gamma}_b = \bar{\gamma}_c/R_c$, where $R_c = k/L$ is the code rate.) The graphs of P_M versus $\bar{\gamma}_b$ for $M = 2, 4, 8, 16, 32$ and $L = 1, 2, 4$ are shown in Fig. 14-4-7. These results illustrate the gain in performance as M increases and L increases. First, we note that a significant gain in performance is obtained by increasing L. Second, we note that the gain in performance obtained with an increase in M is relatively small when L is small. However,

† In Section 14-6, we show that M-ary orthogonal FSK with diversity may be viewed as a block orthogonal code.

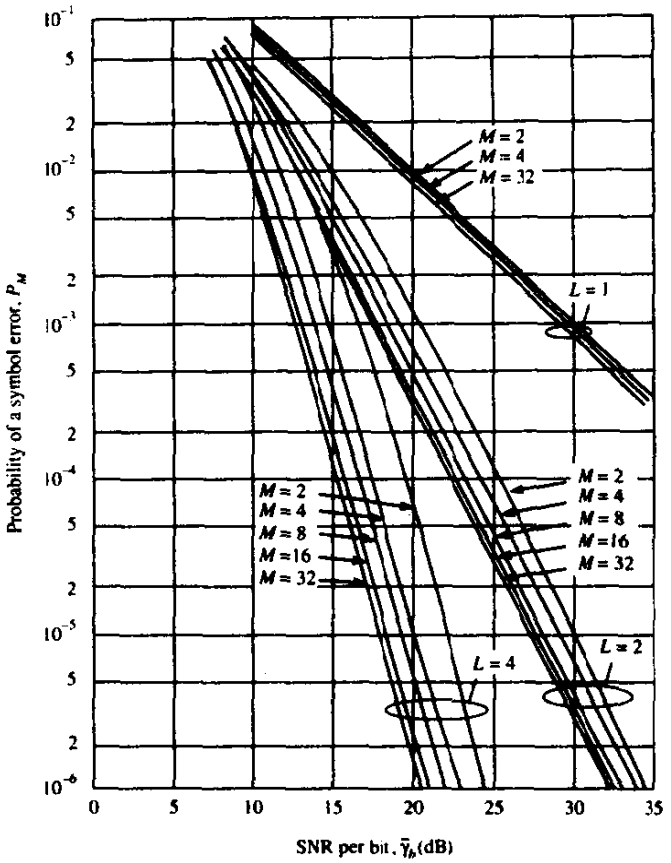

FIGURE 14-4-7 Performance of orthogonal signaling with M and L as parameters.

as L increases, the gain achieved by increasing M also increases. Since an increase in either parameter results in an expansion of bandwidth, i.e.,

$$B_e = \frac{LM}{\log_2 M}$$

the results illustrated in Fig. 14-4-7 indicate that an increase in L is more efficient than a corresponding increase in M. As we shall see in Section 14-6, coding is a bandwidth-effective means for obtaining diversity in the signal transmitted over the fading channel.

Chernoff Bound Before concluding this section, we develop a Chernoff upper bound on the error probability of binary orthogonal signaling with Lth-order diversity, which will be useful in our discussion of coding for fading channels, the topic of Section 14-6. Our starting point is the expression for the two decision variables U_1 and U_2 given by (14-4-29), where U_1 consists of the

square-law-combined signal-plus-noise terms and U_2 consists of square-law-combined noise terms. The binary probability of error, denoted here by $P_2(L)$, as

$$\begin{aligned} P_2(L) &= P(U_2 - U_1 > 0) \\ &= P(X > 0) = \int_0^\infty p(x)\,dx \end{aligned} \tag{14-4-48}$$

where the random variable X is defined as

$$X = U_2 - U_1 = \sum_{k=1}^{L} (|N_{k2}|^2 - |2\mathscr{E}\alpha_k + N_{k1}|^2) \tag{14-4-49}$$

The phase terms $\{\phi_k\}$ in U_1 have been dropped since they do not affect the performance of the square-law detector.

Let $S(X)$ denote the unit step function. Then the error probability in (14-4-48) can be expressed in the form

$$P_2(L) = E[S(X)] \tag{14-4-50}$$

Following the development in Section 2-1-5, the Chernoff bound is obtained by overbounding the unit step function by an exponential function. That is,

$$S(X) \leq e^{\zeta X}, \quad \zeta \geq 0 \tag{14-4-51}$$

where the parameter ζ is optimized to yield a tight bound. Thus, we have

$$P_2(L) = E[S(X)] \leq E(e^{\zeta X}) \tag{14-4-52}$$

Upon substituting for the random variable X from (14-4-49) and noting that the random variables in the summation are mutually statistically independent, we obtain the result

$$P_2(L) \leq \prod_{k=1}^{L} E(e^{\zeta|N_{k2}|^2}) E(e^{-\zeta|2\mathscr{E}\alpha_k + N_{k1}|^2}) \tag{14-4-53}$$

But

$$E(e^{\zeta|N_{k2}|^2}) = \frac{1}{1 - 2\zeta\sigma_2^2}, \quad \zeta < \frac{1}{2\sigma_2^2} \tag{14-4-54}$$

and

$$E(e^{-\zeta|2\mathscr{E}\alpha_k + N_{k1}|^2}) = \frac{1}{1 + 2\zeta\sigma_1^2}, \quad \zeta > \frac{-1}{2\sigma_1^2} \tag{14-4-55}$$

where $\sigma_2^2 = 2\mathscr{E}N_0$, $\sigma_1^2 = 2\mathscr{E}N_0(1 + \bar{\gamma}_c)$, and $\bar{\gamma}_c$ is the average SNR per diversity channel. Note that σ_1^2 and σ_2^2 are independent of k, i.e., the additive noise terms on the L diversity channels as well as the fading statistics are identically distributed. Consequently, (14-4-53) reduces to

$$P_2(L) \leq \left[\frac{1}{(1 - 2\zeta\sigma_2^2)(1 + 2\zeta\sigma_1^2)}\right]^L, \quad 0 \leq \zeta \leq \frac{1}{2\sigma_2^2} \tag{14-4-56}$$

By differentiating the right-hand side of (14-4-56) with respect to ζ, we find that the upper bound is minimized when

$$\zeta = \frac{\sigma_1^2 - \sigma_2^2}{4\sigma_1^2\sigma_2^2} \tag{14-4-57}$$

Substitution of (14-4-57) for ζ into (14-4-56) yields the Chernoff upper bound in the form

$$P_2(L) \leq \left[\frac{4(1+\bar{\gamma}_c)}{(2+\bar{\gamma}_c)^2}\right]^L \tag{14-4-58}$$

It is interesting to note that (14-4-58) may also be expressed as

$$P_2(L) \leq [4p(1-p)]^L \tag{14-4-59}$$

where $p = 1/(2+\bar{\gamma}_c)$ is the probability of error for binary orthogonal signaling on a fading channel without diversity.

A comparison of the Chernoff bound in (14-4-58) with the exact error probability for binary orthogonal signaling and square-law combining of the L diversity signals, which is given by the expression

$$\begin{aligned} P_2(L) &= \left(\frac{1}{1+\bar{\gamma}_c}\right)^L \sum_{k=0}^{L-1} \binom{L-1+k}{k} \left(\frac{1+\bar{\gamma}_c}{2+\bar{\gamma}_c}\right)^k \\ &= p^L \sum_{k=0}^{L-1} \binom{L-1+k}{k} (1-p)^k \end{aligned} \tag{14-4-60}$$

reveals the tightness of the bound. Figure (14-4-8) illustrates this comparison.

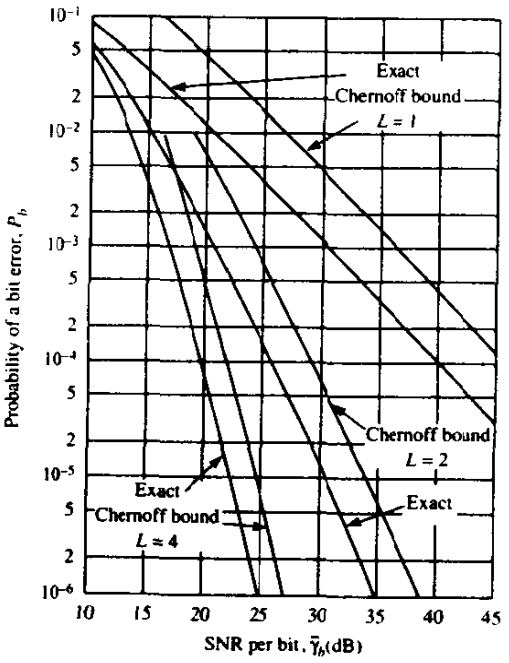

FIGURE 14-4-8 *Comparison of Chernoff bound with exact error probability.*

We observe that the Chernoff upper bound is approximately 6 dB from the exact error probability for $L = 1$, but, as L increases, it becomes tighter. For example, the difference between the bound and the exact error probability is about 2.5 dB when $L = 4$.

Finally we mention that the error probability for M-ary orthogonal signaling with diversity can be upper-bounded by means of the union bound

$$P_M \leq (M-1)P_2(L) \tag{14-4-61}$$

where we may use either the exact expression given in (14-4-60) or the Chernoff bound in (14-4-58) for $P_2(L)$.

14-5 DIGITAL SIGNALING OVER A FREQUENCY-SELECTIVE, SLOWLY FADING CHANNEL

When the spread factor of the channel satisfies the condition $T_m B_d \ll 1$, it is possible to select signals having a bandwidth $W \ll (\Delta f)_c$ and a signal duration $T \ll (\Delta t)_c$. Thus, the channel is frequency-nonselective and slowly fading. In such a channel, diversity techniques can be employed to overcome the severe consequences of fading.

When a bandwidth $W \gg (\Delta f)_c$ is available to the user, the channel can be subdivided into a number of frequency-division multiplexed (FDM) subchannels having a mutual separation in center frequencies of at least $(\Delta f)_c$. Then the same signal can be transmitted on the FDM subchannels, and, thus, frequency diversity is obtained. In this section, we describe an alternative method.

14-5-1 A Tapped-Delay-Line Channel Model

As we shall now demonstrate, a more direct method for achieving basically the same result is to employ a wideband signal covering the bandwidth W. The channel is still assumed to be slowly fading by virtue of the assumption that $T \ll (\Delta t)_c$. Now suppose that W is the bandwidth occupied by the real bandpass signal. Then the band occupancy of the equivalent lowpass signal $s_l(t)$ is $|f| \leq \frac{1}{2}W$. Since $s_l(t)$ is band-limited to $|f| \leq \frac{1}{2}W$, application of the sampling theorem results in the signal representation

$$s_l(t) = \sum_{n=-\infty}^{\infty} s_l\left(\frac{n}{W}\right) \frac{\sin[\pi W(t - n/W)]}{\pi W(t - n/W)} \tag{14-5-1}$$

The Fourier transform of $s_l(t)$ is

$$S_l(f) = \begin{cases} \dfrac{1}{W} \displaystyle\sum_{n=-\infty}^{\infty} s_l(n/W) e^{-j2\pi fn/W} & (|f| \leq \frac{1}{2}W) \\ 0 & (|f| > \frac{1}{2}W) \end{cases} \tag{14-5-2}$$

The noiseless received signal from a frequency-selective channel was previously expressed in the form

$$r_l(t) = \int_{-\infty}^{\infty} C(f;t)S_l(f)e^{j2\pi ft}\,df \tag{14-5-3}$$

where $C(f;t)$ is the time-variant transfer function. Substitution for $S_l(f)$ from (14-5-2) into (14-5-3) yields

$$\begin{aligned} r_l(t) &= \frac{1}{W}\sum_{n=-\infty}^{\infty} s_l(n/W)\int_{-\infty}^{\infty} C(f;t)e^{j2\pi f(t-n/W)}\,df \\ &= \frac{1}{W}\sum_{n=-\infty}^{\infty} s_l(n/W)c(t-n/W;t) \end{aligned} \tag{14-5-4}$$

where $c(\tau;t)$ is the time-variant impulse response. We observe that (14-5-4) has the form of a convolution sum. Hence, it can also be expressed in the alternative form

$$r(t) = \frac{1}{W}\sum_{n=-\infty}^{\infty} s_l(t-n/W)c(n/W;t) \tag{14-5-5}$$

It is convenient to define a set of time-variable channel coefficients as

$$c_n(t) = \frac{1}{W}c\left(\frac{n}{W};t\right) \tag{14-5-6}$$

Then (14-5-5) expressed in terms of these channel coefficients becomes

$$r(t) = \sum_{n=-\infty}^{\infty} c_n(t)s_l(t-n/W) \tag{14-5-7}$$

The form for the received signal in (14-5-7) implies that the time-variant frequency-selective channel can be modeled or represented as a tapped delay line with tap spacing $1/W$ and tap weight coefficients $\{c_n(t)\}$. In fact, we deduce from (14-5-7) that the lowpass impulse response for the channel is

$$c(\tau;t) = \sum_{n=-\infty}^{\infty} c_n(t)\delta(\tau-n/W) \tag{14-5-8}$$

and the corresponding time-variant transfer function is

$$C(f;t) = \sum_{n=-\infty}^{\infty} c_n(t)e^{-j2\pi fn/W} \tag{14-5-9}$$

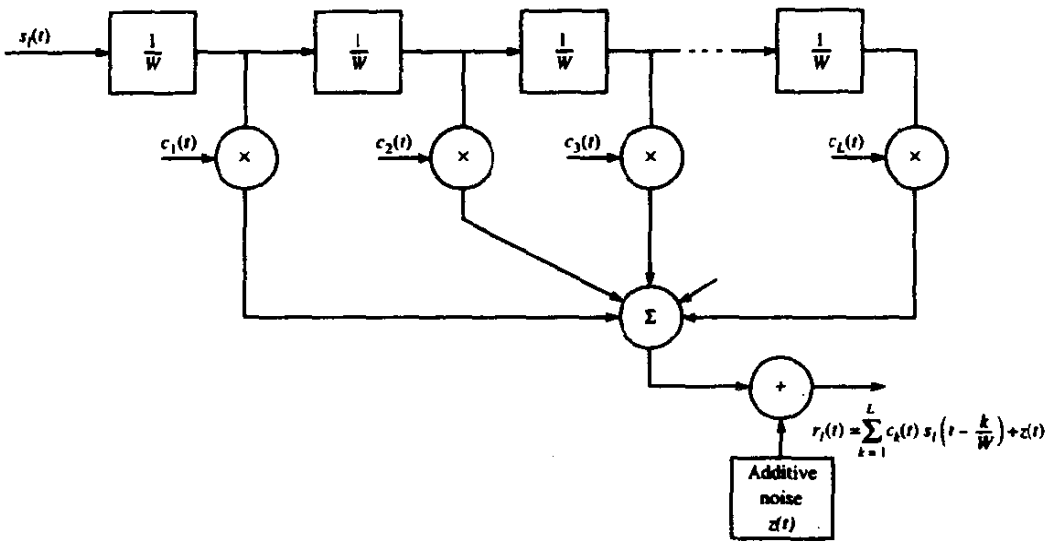

FIGURE 14-5-1 Trapped delay line model of frequency-selective channel.

Thus, with an equivalent lowpass signal having a bandwidth $\frac{1}{2}W$, where $W \gg (\Delta f)_c$, we achieve a resolution of $1/W$ in the multipath delay profile. Since the total multipath spread is T_m, for all practical purposes the tapped delay line model for the channel can be truncated at $L = [T_m W] + 1$ taps. Then the noiseless received signal can be expressed in the form

$$r_l(t) = \sum_{n=1}^{L} c_n(t) s_l\left(t - \frac{n}{W}\right) \tag{14-5-10}$$

The truncated tapped delay line model is shown in Fig. 14-5-1. In accordance with the statistical characterization of the channel presented in Section 14-1, the time-variant tap weights $\{c_n(t)\}$ are complex-valued stationary random processes. In the special case of Rayleigh fading, the magnitudes $|c_n(t)| \equiv \alpha_n(t)$ are Rayleigh-distributed and the phases $\phi_n(t)$ are uniformly distributed. Since the $\{c_n(t)\}$ represent the tap weights corresponding to the L different delays $\tau = n/W$, $n = 1, 2, \ldots, L$, the uncorrelated scattering assumption made in Section 7-1 implies that the $\{c_n(t)\}$ are mutually uncorrelated. When the $\{c_n(t)\}$ are gaussian random processes, they are statistically independent.

14-5-2 The RAKE Demodulator

We now consider the problem of digital signaling over a frequency-selective channel that is modeled by a tapped delay line with statistically independent time-variant tap weights $\{c_n(t)\}$. It is apparent at the outset, however, that the tapped delay line model with statistically independent tap weights provides us

with L replicas of the same transmitted signal at the receiver. Hence, a receiver that processes the received signal in an optimum manner will achieve the performance of an equivalent Lth-order diversity communications system.

Let us consider binary signaling over the channel. We have two equal-energy signals $s_{l1}(t)$ and $s_{l2}(t)$, which are either antipodal or orthogonal. Their time duration T is selected to satisfy the condition $T \gg T_m$. Thus, we may neglect any intersymbol interference due to multipath. Since the bandwidth of the signal exceeds the coherent bandwidth of the channel, the received signal is expressed as

$$\begin{aligned} r_l(t) &= \sum_{k=1}^{L} c_k(t) s_{li}(t - k/W) + z(t) \\ &= v_i(t) + z(t), \quad 0 \leq t \leq T, \quad i = 1, 2 \end{aligned} \tag{14-5-11}$$

where $z(t)$ is a complex-valued zero-mean white gaussian noise process. Assume for the moment that the channel tap weights are known. Then the optimum receiver consists of two filters matched to $v_1(t)$ and $v_2(t)$, followed by samplers and a decision circuit that selects the signal corresponding to the largest output. An equivalent optimum receiver employs cross correlation instead of matched filtering. In either case, the decision variables for coherent detection of the binary signals can be expressed as

$$\begin{aligned} U_m &= \text{Re}\left[\int_0^T r_l(t) v_m^*(t)\, dt\right] \\ &= \text{Re}\left[\sum_{k=1}^{L} \int_0^T r_l(t) c_k^*(t) s_{lm}^*(t - k/W)\, dt\right], \quad m = 1, 2 \end{aligned} \tag{14-5-12}$$

Figure 14-5-2 illustrates the operations involved in the computation of the decision variables. In this realization of the optimum receiver, the two reference signals are delayed and correlated with the received signal $r_l(t)$.

An alternative realization of the optimum receiver employs a single delay line through which is passed the received signal $r_l(t)$. The signal at each tap is correlated with $c_k(t)s_{lm}^*(t)$, where $k = 1, 2, \ldots, L$ and $m = 1, 2$. This receiver structure is shown in Fig. 14-5-3. In effect, the tapped delay line receiver attempts to collect the signal energy from all the received signal paths that fall within the span of the delay line and carry the same information. Its action is somewhat analogous to an ordinary garden rake and, consequently, the name "RAKE receiver" has been coined for this receiver structure by Price and Green (1958).

14-5-3 Performance of RAKE Receiver

We shall now evaluate the performance of the RAKE receiver under the condition that the fading is sufficiently slow to allow us to estimate $c_k(t)$ perfectly (without noise). Furthermore, within any one signaling interval, $c_k(t)$

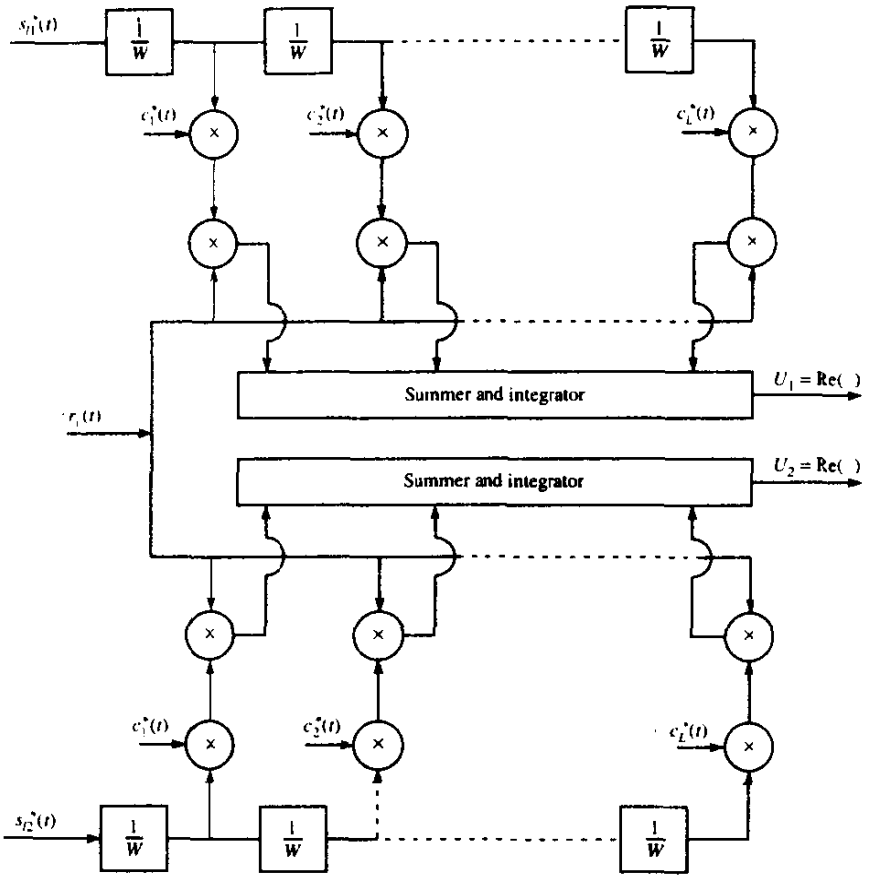

FIGURE 14-5-2 Optimum demodulator for wideband binary signals (delayed reference configuration).

is treated as a constant and denoted as c_k. Thus the decision variables in (14-5-12) may be expressed in the form

$$U_m = \text{Re}\left[\sum_{k=1}^{L} c_k^* \int_0^T r(t) s_{lm}^*(t - k/W)\, dt\right], \quad m = 1, 2 \tag{14-5-13}$$

Suppose the transmitted signal is $s_{l1}(t)$; then the received signal is

$$r_l(t) = \sum_{n=1}^{L} c_n s_{l1}(t - n/W) + z(t), \quad 0 \leq t \leq T \tag{14-5-14}$$

Substitution of (14-5-14) into (14-5-13) yields

$$U_m = \text{Re}\left[\sum_{k=1}^{L} c_k^* \sum_{n=1}^{L} c_n \int_0^T s_{l1}(t - n/W) s_{lm}^*(t - k/W)\, dt\right] + \text{Re}\left[\sum_{k=1}^{L} c_k^* \int_0^T z(t) s_{lm}^*(t - k/W)\, dt\right], \quad m = 1, 2 \tag{14-5-15}$$

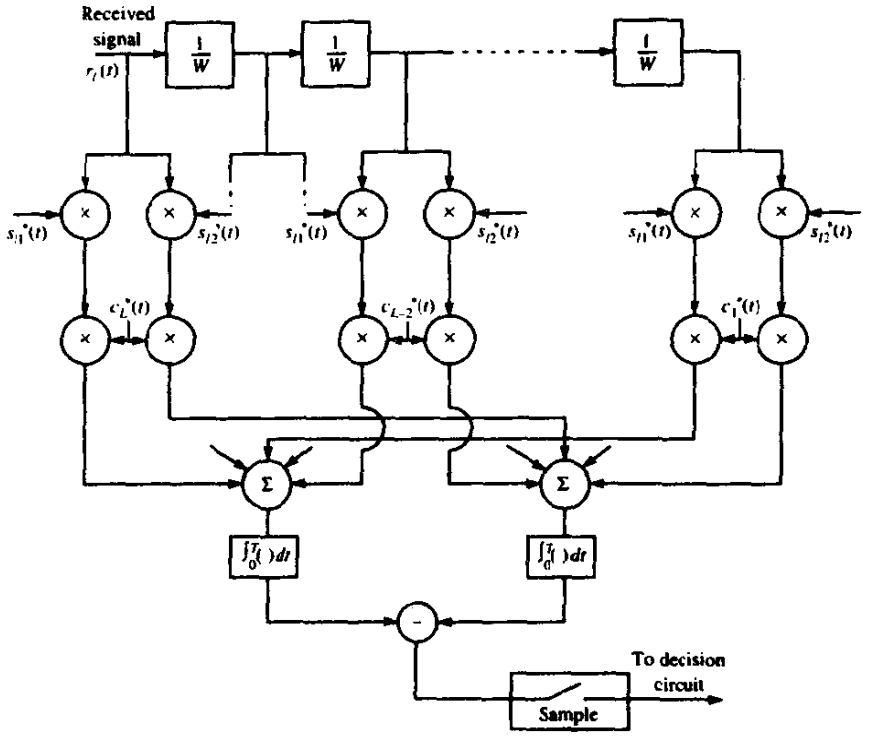

FIGURE 14-5-3 Optimum demodulator for wideband binary signals (delayed received signal configuration).

Usually the wideband signals $s_{l1}(t)$ and $s_{l2}(t)$ are generated from pseudo-random sequences, which result in signals that have the property

$$\int_0^T s_{li}(t - n/W)s_{li}^*(t - k/W)\,dt \approx 0, \qquad k \neq n, \quad i = 1, 2 \tag{14-5-16}$$

If we assume that our binary signals are designed to satisfy this property then (14-5-15) simplifies to†

$$U_m = \text{Re}\left[\sum_{k=1}^{L} |c_k|^2 \int_0^T s_{l1}(t - k/W)s_{lm}^*(t - k/W)\,dt\right] + \text{Re}\left[\sum_{k=1}^{L} c_k^* \int_0^T z(t)s_{lm}^*(t - k/W)\,dt\right], \qquad m = 1, 2 \tag{14-5-17}$$

† Although the orthogonality property specified by (14-5-16) can be satisfied by proper selection of the pseudo-random sequences, the cross-correlation of $s_{l1}(t - n/W)$ with $s_{l1}^*(t - k/W)$ gives rise to a signal-dependent self-noise, which ultimately limits the performance. For simplicity, we do not consider the self-noise term in the following calculations. Consequently, the performance results presented below should be considered as lower bounds (ideal RAKE). An approximation to the performance of the RAKE can be obtained by treating the self-noise as an additional gaussian noise component with noise power equal to its variance.

When the binary signals are antipodal, a single decision variable suffices. In this case, (14-5-17) reduces to

$$U_1 = \text{Re}\left(2\mathscr{E}\sum_{k=1}^{L}\alpha_k^2 + \sum_{k=1}^{L}\alpha_k N_k\right) \tag{14-5-18}$$

where $\alpha_k = |c_k|$ and

$$N_k = e^{j\phi_k}\int_0^T z(t)s_1^*(t - k/W)\,dt \tag{14-5-19}$$

But (14-5-18) is identical to the decision variable given in (14-4-4), which corresponds to the output of a maximal ratio combiner in a system with Lth-order diversity. Consequently, the RAKE receiver with perfect (noiseless) estimates of the channel tap weights is equivalent to a maximal ratio combiner in a system with Lth-order diversity. Thus, when all the tap weights have the same mean-square value, i.e., $E(\alpha_k^2)$ is the same for all k, the error rate performance of the RAKE receiver is given by (14-4-15) and (14-4-16). On the other hand, when the mean square values $E(\alpha_k^2)$ are not identical for all k, the derivation of the error rate performance must be repeated since (14-4-15) no longer applies.

We shall derive the probability of error for binary antipodal and orthogonal signals under the condition that the mean-square values of $\{\alpha_k\}$ are distinct. We begin with the conditional error probability

$$P_2(\gamma_b) = Q(\sqrt{\gamma_b(1-\rho_r)}) \tag{14-5-20}$$

where $\rho_r = -1$ for antipodal signals, $\rho_r = 0$ for orthogonal signals, and

$$\begin{aligned}\gamma_b &= \frac{\mathscr{E}}{N_0}\sum_{k=1}^{L}\alpha_k^2 \\ &= \sum_{k=1}^{L}\gamma_k\end{aligned} \tag{14-5-21}$$

Each of the $\{\gamma_k\}$ is distributed according to a chi-squared distribution with two degrees of freedom. That is,

$$p(\gamma_k) = \frac{1}{\bar{\gamma}_k}e^{-\gamma_k/\bar{\gamma}_k} \tag{14-5-22}$$

where $\bar{\gamma}_k$ is the average SNR for the kth path, defined as

$$\bar{\gamma}_k = \frac{\mathscr{E}}{N_0}E(\alpha_k^2) \tag{14-5-23}$$

Furthermore, from (14-4-10) we know that the characteristic function of γ_k is

$$\psi_{\gamma_k}(jv) = \frac{1}{1 - jv\bar{\gamma}_k} \tag{14-5-24}$$

Since γ_b is the sum of L statistically independent components $\{\gamma_k\}$, the characteristic function of γ_b is

$$\psi_{\gamma_b}(jv) = \prod_{k=1}^{L} \frac{1}{1 - jv\bar{\gamma}_k} \tag{14-5-25}$$

The inverse Fourier transform of the characteristic function in (14-5-25) yields the probability density function of γ_b in the form

$$p(\gamma_b) = \sum_{k=1}^{L} \frac{\pi_k}{\bar{\gamma}_k} e^{-\gamma_b/\bar{\gamma}_k}, \qquad \gamma_b \geq 0 \tag{14-5-26}$$

where π_k is defined as

$$\pi_k = \prod_{\substack{i=1 \\ i \neq k}}^{L} \frac{\bar{\gamma}_k}{\bar{\gamma}_k - \bar{\gamma}_i} \tag{14-5-27}$$

When the conditional error probability in (14-5-20) is averaged over the probability density function given in (14-5-26), the result is

$$P_2 = \tfrac{1}{2} \sum_{k=1}^{L} \pi_k \left[1 - \sqrt{\frac{\bar{\gamma}_k(1 - \rho_r)}{2 + \bar{\gamma}_k(1 - \rho_r)}} \right] \tag{14-5-28}$$

This error probability can be approximated as ($\bar{\gamma}_k \gg 1$)

$$P_2 \approx \binom{2L-1}{L} \prod_{k=1}^{L} \frac{1}{2\bar{\gamma}_k(1 - \rho_r)} \tag{14-5-29}$$

By comparing (14-5-29) for $\rho_r = -1$ with (14-4-18), we observe that the same type of asymptotic behavior is obtained for the case of unequal SNR per path and the case of equal SNR per path.

In the derivation of the error rate performance of the RAKE receiver, we assumed that the estimates of the channel tap weights are perfect. In practice, relatively good estimates can be obtained if the channel fading is sufficiently slow, e.g., $(\Delta t)_c/T \geq 100$, where T is the signaling interval. Figure 14-5-4 illustrates a method for estimating the tap weights when the binary signaling waveforms are orthogonal. The estimate is the output of the lowpass filter at each tap. At any one instant in time, the incoming signal is either $s_{l1}(t)$ or $s_{l2}(t)$. Hence, the input to the lowpass filter used to estimate $c_k(t)$ contains signal plus noise from one of the correlators and noise only from the other correlator. This method for channel estimation is not appropriate for antipodal signals, because the addition of the two correlator outputs results in signal cancellation. Instead, a single correlator can be employed for antipodal signals. Its output is fed to the input of the lowpass filter after the information-bearing signal is removed. To accomplish this, we must introduce a delay of one signaling interval into the channel estimation procedure, as illustrated in Fig. 14-5-5.

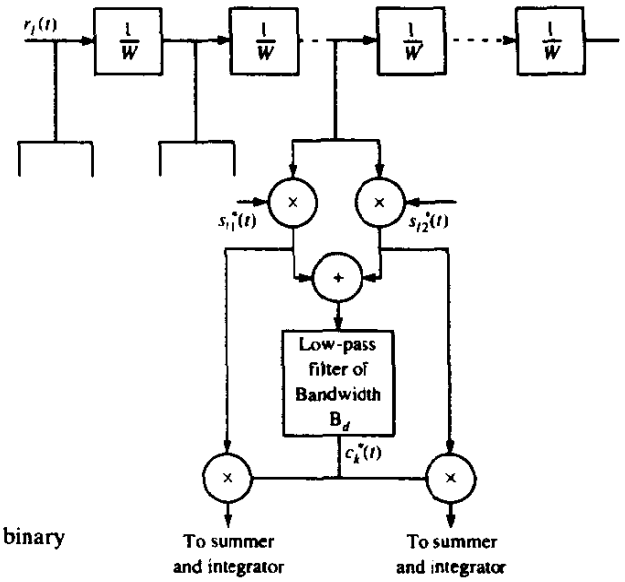

FIGURE 14-5-4 Channel tap weight estimation with binary orthogonal signals.

FIGURE 14-5-5 Channel tap weight estimation with binary antipodal signals.

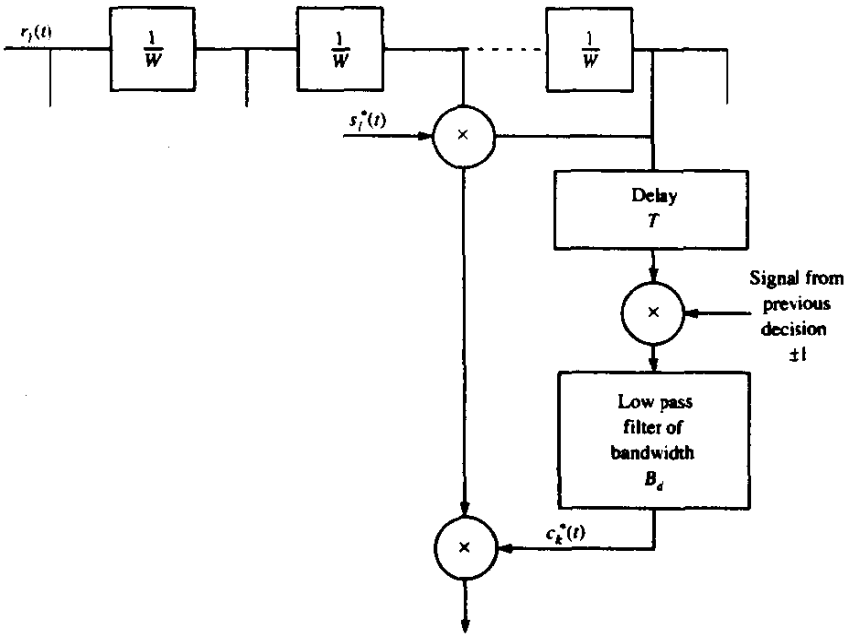

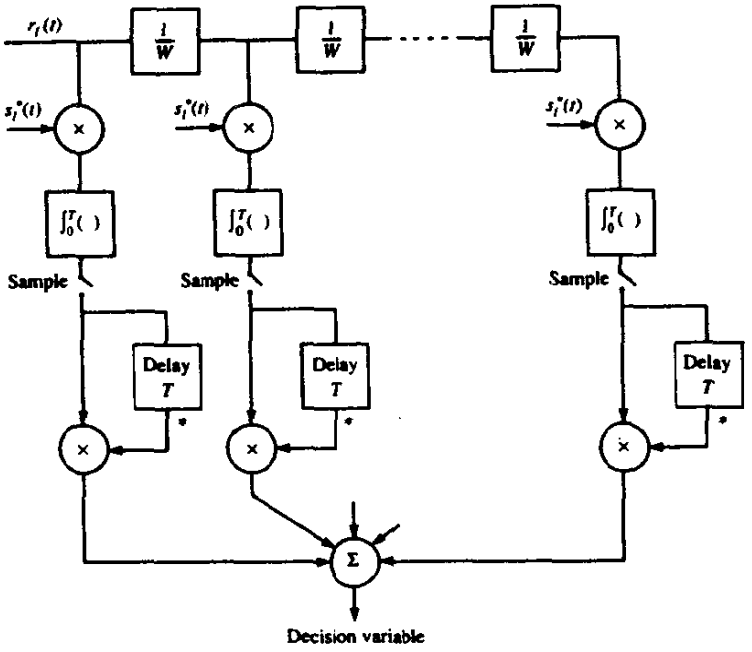

FIGURE 14-5-6 RAKE demodulator for DPSK signals.

That is, first the receiver must decide whether the information in the received signal is $+1$ or -1 and, then, it uses the decision to remove the information from the correlator output prior to feeding it to the lowpass fiter.

If we choose not to estimate the tap weights of the frequency-selective channel, we may use either DPSK signaling or noncoherently detected orthogonal signaling. The RAKE receiver structure for DPSK is illustrated in Fig 14-5-6. It is apparent that when the transmitted signal waveform $s_l(t)$ satisfies the orthogonality property given in (14-5-16), the decision variable is identical that given in (14-4-23) for an Lth-order diversity system. Consequently, the error rate performance of the RAKE receiver for a binary DPSK is identical to that given in (14-4-15) with $\mu = \bar{\gamma}_c/(1 + \bar{\gamma}_c)$, when all the signal paths have the same SNR $\bar{\gamma}_c$. On the other hand, when the SNRs $\{\bar{\gamma}_k\}$ are distinct, the error probability can be obtained by averaging (14-4-24), which is the probability of error conditioned on a time-invariant channel, over the probability density function of γ_b given by (14-5-26). The result of this integration is

$$P_2 = (\tfrac{1}{2})^{2L-1} \sum_{m=0}^{L-1} m! b_m \sum_{k=1}^{L} \frac{\pi_k}{\bar{\gamma}_k} \left(\frac{\bar{\gamma}_k}{1 + \bar{\gamma}_k} \right)^{m+1} \tag{14-5-30}$$

where π_k is defined in (14-5-27) and b_m in (14-4-25).

Finally, we consider binary orthogonal signaling over the frequency-selective channel with square-law detection at the receiver. This type of signal

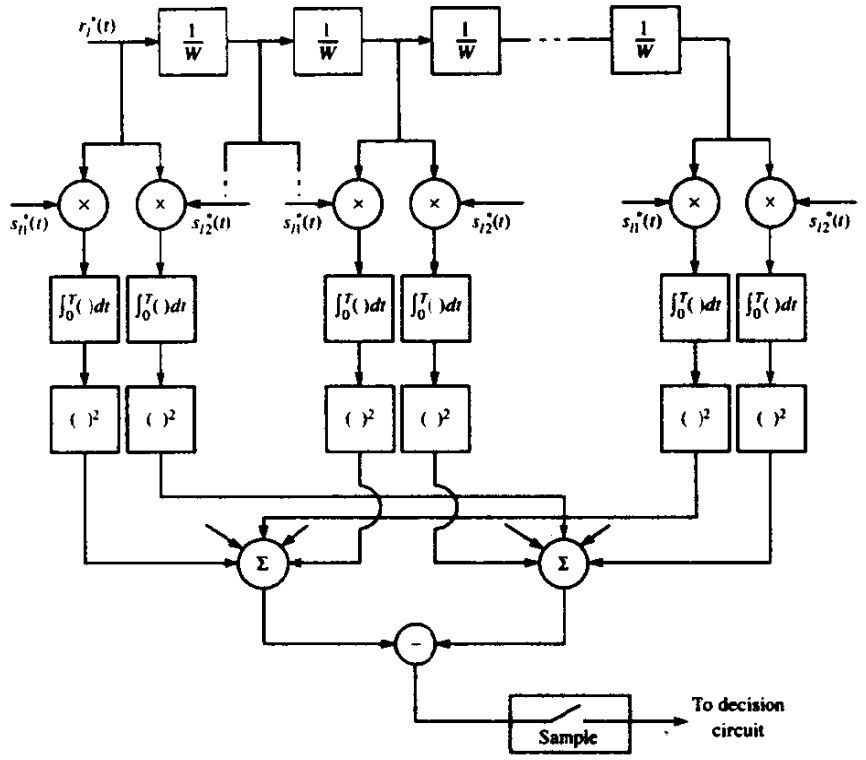

FIGURE 14-5-7 RAKE demodulator for square-law combination of orthogonal signals.

is appropriate when either the fading is rapid enough to preclude a good estimate of the channel tap weights or the cost of implementing the channel estimators is high. The RAKE receiver with square-law combining of the signal from each tap is illustrated in Fig. 14-5-7. In computing its performance, we again assume that the orthogonality property given in (14-5-16) holds. Then the decision variables at the output of the RAKE are

$$U_1 = \sum_{k=1}^{L} |2\mathscr{E}c_k + N_{k1}|^2$$
$$U_2 = \sum_{k=1}^{L} |N_{k2}|^2 \tag{14-5-31}$$

where we have assumed that $s_{j1}(t)$ was the transmitted signal. Again we observe that the decision variables are identical to the ones given in (14-4-29), which apply to orthogonal signals with Lth-order diversity. Therefore, the performance of the RAKE receiver for square-law-detected orthogonal signals is given by (14-4-15) with $\mu = \bar{\gamma}_c/(2 + \bar{\gamma}_c)$ when all the signal paths have the same SNR. If the SNRs are distinct, we can average the conditional error probability given by (14-4-24), with γ_b replaced by $\frac{1}{2}\gamma_b$, over the probability

density function $p(\gamma_b)$ given in (14-5-26). The result of this averaging is given by (14-5-30), with $\bar{\gamma}_k$ replaced by $\frac{1}{2}\bar{\gamma}_k$.

In the above analysis, the RAKE demodulator shown in Fig. 14-5-7 for square-law combination of orthogonal signals is assumed to contain a signal component at each delay. If that is not the case, its performance will be degraded, since some of the tap correlators will contribute only noise. Under such conditions, the low-level, noise-only contributions from the tap correlators should be excluded from the combiner, as shown by Chyi *et al.* (1988).

This concludes our discussion of signaling over a frequency-selective channel. The configurations of the RAKE receiver presented in this section can be easily generalized to multilevel signaling. In fact, if M-ary PSK or DPSK is chosen, the RAKE structures presented in this section remain unchanged. Only the PSK and DPSK detectors that follow the RAKE correlator are different.

14-6 CODED WAVEFORMS FOR FADING CHANNELS

Up to this point, we have demonstrated that diversity techniques are very effective in overcoming the detrimental effects of fading caused by the time-variant dispersive characteristics of the channel. Time- and/or frequency-diversity techniques may be viewed as a form of repetition (block) coding of the information sequence. From this point of view, the combining techniques described previously represent soft-decision decoding of the repetition code. Since a repetition code is a trivial form of coding, we shall now consider the additional benefits derived from more efficient types of codes. In particular, we demonstrate that coding provides an efficient means for obtaining diversity on a fading channel. The amount of diversity provided by a code is directly related to its minimum distance.

As explained in Section 14-4, time diversity is obtained by transmitting the signal components carrying the same information in multiple time intervals mutually separated by an amount equal to or exceeding the coherence time $(\Delta t)_c$ of the channel. Similarly, frequency diversity is obtained by transmitting the signal components carrying the same information in multiple frequency slots mutually separated by an amount of at least equal to the coherence bandwidth $(\Delta f)_c$ of the channel. Thus, the signal components carrying the same information undergo statistically independent fading.

To extend these notions to a coded information sequence, we simply require that the signal waveform corresponding to a particular code or code symbol fade independently of the signal waveform corresponding to any other code bit or code symbol. This requirement may result in inefficient utilization of the available time-frequency space, with the existence of large unused portions in this two-dimensional signaling space. To reduce the inefficiency, a number of code words may be interleaved in time or in frequency or both, in such a manner that the waveform corresponding to the bits or symbols of a given code word fade independently. Thus, we assume that the time-frequency signaling

space is partitioned into nonoverlapping time-frequency cells. A signal waveform corresponding to a code bit or code symbol is transmitted within such a cell.

In addition to the assumption of statistically independent fading of the signal components of a given code word, we also assume that the additive noise components corrupting the received signals are white gaussian processes that are statistically independent and identically distributed among the cells in the time-frequency space. Also, we assume that there is sufficient separation between adjacent cells so that intercell interference is negligible.

An important issue is the modulation technique that is used to transmit the coded information sequence. If the channel fades slowly enough to allow the establishment of a phase reference then PSK or DPSK may be employed. If this is not possible then FSK modulation with noncoherent detection at the receiver is appropriate. In our treatment, we assume that it is not possible to establish a phase reference or phase references for the signals in the different cells occupied by the transmitted signal. Consequently, we choose FSK modulation with noncoherent detection.

A model of the digital communications system for which the error rate performance will be evaluated is shown in Fig. 14-6-1. The encoder may be binary, nonbinary, or a concatenation of a nonbinary encoder with a binary encoder. Furthermore, the code generated by the encoder may be a block code, a convolutional code, or, in the case of concatenation, a mixture of a block code and a convolutional code.

In order to explain the modulation, demodulation, and decoding for FSK-type (orthogonal) signals, consider a linear binary block code in which k information bits are encoded into a block of n bits. For simplicity and without loss of generality, let us assume that all n bits of a code word are transmitted simultaneously over the channel on multiple frequency cells. A code word $\mathbf{C}_i$ having bits $\{c_{ij}\}$ is mapped into FSK signal waveforms in the following way. If $c_{ij} = 0$, the tone f_{0j} is transmitted, and if $c_{ij} = 1$, the tone f_{1j} is transmitted. This means that $2n$ tones or cells are available to transmit the n bits of the code word, but only n tones are transmitted in any signaling interval. Since each code word conveys k bits of information, the bandwidth expansion factor for FSK is $B_e = 2n/k$.

The demodulator for the received signal separates the signal into $2n$

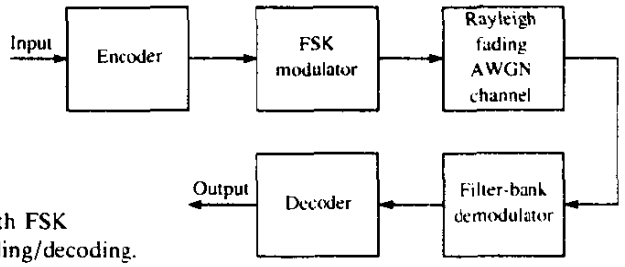

FIGURE 14-6-1 Model of communications system with FSK modulation/demodulation and encoding/decoding.

spectral components corresponding to the available tone frequencies at the transmitter. Thus, the demodulator can be realized as a bank of $2n$ filters, where each filter is matched to one of the possible transmitted tones. The outputs of the $2n$ filters are detected noncoherently. Since the Rayleigh fading and the additive white gaussian noises in the $2n$ frequency cells are mutually statistically independent and identically distributed random processes, the optimum maximum-likelihood soft-decision decoding criterion requires that these filter responses be square-law-detected and appropriately combined for each code word to form the $M = 2^k$ decision variables. The code word corresponding to the maximum of the decision variables is selected. If hard-decision decoding is employed, the optimum maximum-likelihood decoder selects the code word having the smallest Hamming distance relative to the received code word.

Although the discussion above assumed the use of a block code, a convolutional encoder can be easily accommodated in the block diagram shown in Fig. 14-6-1. For example, if a binary convolutional code is employed, each bit in the output sequence may be transmitted by binary FSK. The maximum-likelihood soft-decision decoding criterion for the convolutional code can be efficiently implemented by means of the Viterbi algorithm, in which the metrics for the surviving sequences at any point in the trellis consist of the square-law-combined outputs for the corresponding paths through the trellis. On the other hand, if hard-decision decoding is employed, the Viterbi algorithm is implemented with Hamming distance as the metric.

14-6-1 Probability of Error for Soft-Decision Decoding of Linear Binary Block Codes

Consider the decoding of a linear binary (n, k) code transmitted over a Rayleigh fading channel, as described above. The optimum soft-decision decoder, based on the maximum-likelihood criterion, forms the $M = 2^k$ decision variables

$$U_i = \sum_{j=1}^{n} [(1 - c_{ij})\,|y_{0j}|^2 + c_{ij}\,|y_{1j}|^2]$$

$$= \sum_{j=1}^{n} [|y_{0j}|^2 + c_{ij}(|y_{1j}|^2 - |y_{0j}|^2)], \qquad i = 1, 2, \ldots, 2^k \tag{14-6-1}$$

where $|y_{rj}|^2$, $j = 1, 2, \ldots, n$, and $r = 0, 1$ represent the squared envelopes at the outputs of the $2n$ filters that are tuned to the $2n$ possible transmitted tones. A decision is made in favor of the code word corresponding to the largest decision variable of the set $\{U_i\}$.

Our objective in this section is the determination of the error rate performance of the soft-decision decoder. Toward this end, let us assume that the all-zero code word $\mathbf{C}_1$ is transmitted. The average received signal-to-noise

ratio per tone (cell) is denoted by $\bar{\gamma}_c$. The total received SNR for the n tones in $n\bar{\gamma}_c$ and, hence, the average SNR per bit is

$$\begin{aligned}\bar{\gamma}_b &= \frac{n}{k}\bar{\gamma}_c \\ &= \frac{\bar{\gamma}_c}{R_c}\end{aligned} \tag{14-6-2}$$

where R_c is the code rate.

The decision variable U_1 corresponding to the code word $\mathbf{C}_1$ is given by (14-6-1) with $c_{ij} = 0$ for all j. The probability that a decision is made in favor of the mth code word is just

$$\begin{aligned}P_2(m) &= P(U_m > U_1) = P(U_1 - U_m < 0) \\ &= P\left[\sum_{j=1}^{n}(c_{1j} - c_{mj})(|y_{1j}|^2 - |y_{0j}|^2) < 0\right] \\ &= P\left[\sum_{j=1}^{w_m}(|y_{0j}|^2 - |y_{1j}|^2) < 0\right]\end{aligned} \tag{14-6-3}$$

where w_m is the weight of the mth code word. But the probability in (14-6-3) is just the probability of error for square-law combining of binary orthogonal FSK with w_mth-order diversity. That is,

$$P_2(m) = p^{w_m}\sum_{k=0}^{w_m-1}\binom{w_m - 1 + k}{k}(1-p)^k \tag{14-6-4}$$

$$\leq p^{w_m}\sum_{k=0}^{w_m-1}\binom{w_m - 1 + k}{k} = \binom{2w_m - 1}{w_m}p^{w_m} \tag{14-6-5}$$

where

$$p = \frac{1}{2 + \bar{\gamma}_c} = \frac{1}{2 + R_c\bar{\gamma}_b} \tag{14-6-6}$$

As an alternative, we may use the Chernoff upper bound derived in Section 14-4, which in the present notation is

$$P_2(m) \leq [4p(1-p)]^{w_m} \tag{14-6-7}$$

The sum of the binary error events over the $M - 1$ nonzero-weight code words gives an upper bound on the probability of error. Thus,

$$P_M \leq \sum_{m=2}^{M} P_2(m) \tag{14-6-8}$$

Since the minimum distance of the linear code is equal to the minimum weight, it follows that

$$(1 + R_c\bar{\gamma}_b)^{-w_m} \leq (2 + R_c\bar{\gamma}_b)^{-d_{\min}}$$

The use of this relation in conjunction with (14-6-5) and (14-6-8) yields a simple, albeit looser, upper bound that may be expressed in the form

$$P_M < \frac{\sum_{m=2}^{M} \binom{2w_m - 1}{w_m}}{(2 + R_c \bar{\gamma}_b)^{d_{\min}}} \tag{14-6-9}$$

This simple bound indicates that the code provides an effective order of diversity equal to $d_{\min}$. An even simpler bound is the union bound

$$P_M < (M-1)[4p(1-p)]^{d_{\min}} \tag{14-6-10}$$

which is obtained from the Chernoff bound given in (14-6-7).

As an example serving to illustrate the benefits of coding for a Rayleigh fading channel, we have plotted in Fig. 14-6-2 the performance obtained with the extended Golay (24, 12) code and the performance of binary FSK and quarternay FSK each with dual diversity. Since the extended Golay code requires a total of 48 cells and $k = 12$, the bandwidth expansion factor $B_e = 4$. This is also the bandwidth expansion factor for binary and quaternary FSK with $L = 2$. Thus, the three types of waveforms are compared on the basis of the same bandwidth expansion factor. Note that at $P_b = 10^{-4}$, the Golay code outperforms quaternary FSK by more than 6 dB, and at $P_b = 10^{-5}$, the difference is approximately 10 dB.

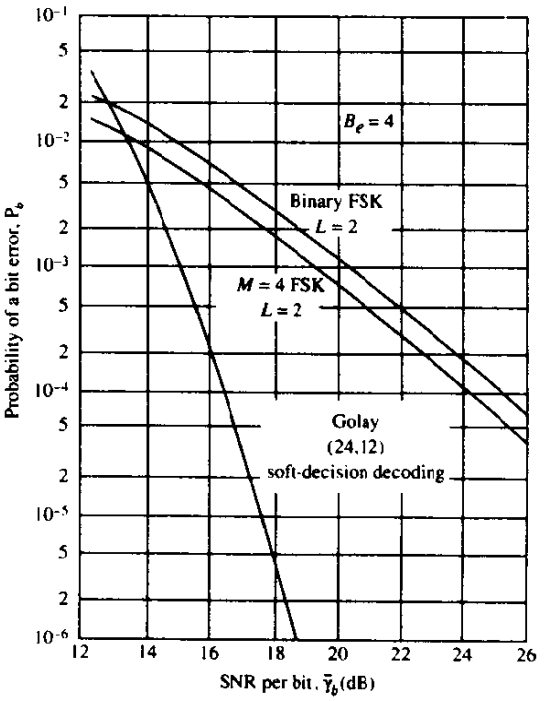

FIGURE 14-6-2 Example of performance obtained with conventional diversity versus coding for $B_e = 4$.

The reason for the superior performance of the Golay code is its large minimum distance ($d_{\min} = 8$), which translates into an equivalent eighth-order ($L = 8$) diversity. In contrast, the binary and quaternary FSK signals have only second-order diversity. Hence, the code makes more efficient use of the available channel bandwidth. The price that we must pay for the superior performance of the code is the increase in decoding complexity.

14-6-2 Probability of Error for Hard-Decision Decoding of Linear Binary Block Codes

Bounds on the performance obtained with hard-decision decoding of a linear binary (n, k) code have already been given in Section 8-1-5. These bounds are applicable to a general binary-input binary-output memoryless (binary symmetric) channel and, hence, they apply without modification to a Rayleigh fading AWGN channel with statistically independent fading of the symbols in the code word. The probability of a bit error needed to evaluate these bounds when binary FSK with noncoherent detection is used as the modulation and demodulation technique is given by (14-6-6).

A particularly interesting result is obtained when we use the Chernoff upper bound on the error probability for hard-decision decoding given by (8-1-89). That is,

$$P_2(m) \leq [4p(1-p)]^{w_m/2} \tag{14-6-11}$$

and P_M is upper-bounded by (14-6-8). In comparison, the Chernoff upper bound for $P_2(m)$ when soft-decision decoding is employed is given by (14-6-7). We observe that the effect of hard-decision decoding is a reduction in the distance between any two code words by a factor of 2. When the minimum distance of a code is relatively small, the reduction of the distances by a factor of 2 is much more noticeable in a fading channel than in a nonfading channel.

For illustrative pruposes we have plotted in Fig. 14-6-3 the performance of the Golay (23, 12) code when hard-decision and soft-decision decoding are used. The difference in performance at $P_b = 10^{-5}$ is approximately 6 dB. This is a significant difference in performance compared with the 2 dB difference between soft- and hard-decision decoding in a nonfading AWGN channel. We also note that the difference in performance increases as P_b decreases. In short, these results indicate the benefits of a soft-decision decoding over hard-decision decoding on a Rayleigh fading channel.

14-6-3 Upper Bounds on the Performance of Convolutional Codes for a Rayleigh Fading Channel

In this subsection, we derive the performance of binary convolutional codes when used on a Rayleigh fading AWGN channel. The encoder accepts k binary digits at a time and puts out n binary digits at a time. Thus, the code rate is $R_c = k/n$. The binary digits at the output of the encoder are transmitted

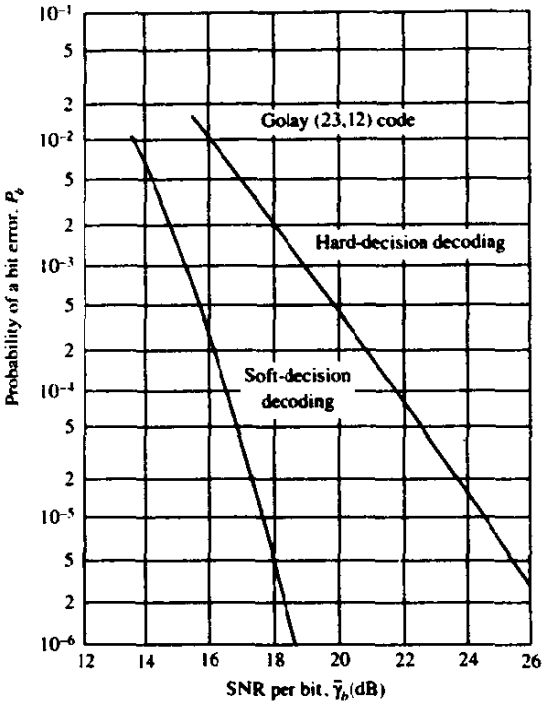

FIGURE 14-6-3 Comparison of performance between hard- and soft-decision decoding.

over the Rayleigh fading channel by means of binary FSK, which is square-law-detected at the receiver. The decoder for either soft- or hard-decision decoding performs maximum-likelihood sequence estimation, which is efficiently implemented by means of the Viterbi algorithm.

First, we consider soft-decision decoding. In this case, the metrics computed in the Viterbi algorithm are simply sums of square-law-detected outputs from the demodulator. Suppose the all-zero sequence is transmitted. Following the procedure outlined in Section 8-2-3, it is easily shown that the probability of error in a pairwise comparison of the metric corresponding to the all-zero sequence with the metric corresponding to another sequence that merges for the first time at the all-zero state is

$$P_2(d) = p^d \sum_{k=0}^{d-1} \binom{d-1+k}{k} (1-p)^k \tag{14-6-12}$$

where d is the number of bit positions in which the two sequences differ and p is given by (14-6-6). That is, $P_2(d)$ is just the probability of error for binary FSK with square-law detection and dth-order diversity. Alternatively, we may use the Chernoff bound in (14-6-7) for $P_2(d)$. In any case, the bit error probability is upperbounded, as shown in Section 8-2-3 by the expression

$$P_b < \frac{1}{k} \sum_{d=d_{\text{free}}}^{\infty} \beta_d P_2(d) \tag{14-6-13}$$

where the weighting coefficients $\{\beta_d\}$ in the summation are obtained from the expansion of the first derivative of the transfer function $T(D, N)$, given by (8-2-25).

When hard-decision decoding is performed at the receiver, the bounds on the error rate performance for binary convolutional codes derived in Section 8-2-4 apply. That is, P_b is again upper-bounded by the expression in (14-6-13), where $P_2(d)$ is defined by (8-2-28) for odd d and by (8-2-29) for even d, or upper-bounded (Chernoff bound) by (8-2-31), and p is defined by (14-6-6).

As in the case of block coding, when the respective Chernoff bounds are used for $P_2(d)$ with hard-decision and soft-decision decoding, it is interesting to note that the effect of hard-decision decoding is to reduce the distances (diversity) by a factor of 2 relative to soft-decision decoding.

The following numerical results illustrate the error rate performance of binary, rate $1/n$, maximal free distance convolutional codes for $n = 2$, 3, and 4 with soft-decision Viterbi decoding. First of all, Fig. 14-6-4 shows the performance of the rate 1/2 convolutional codes for constraint lengths 3, 4, and 5. The bandwidth expansion factor for binary FSK modulation is $B_e = 2n$. Since an increase in the constraint length results in an increase in the complexity of the decoder to go along with the corresponding increase in the minimum free distance, the system designer can weigh these two factors in the selection of the code.

Another way to increase the distance without increasing the constraint

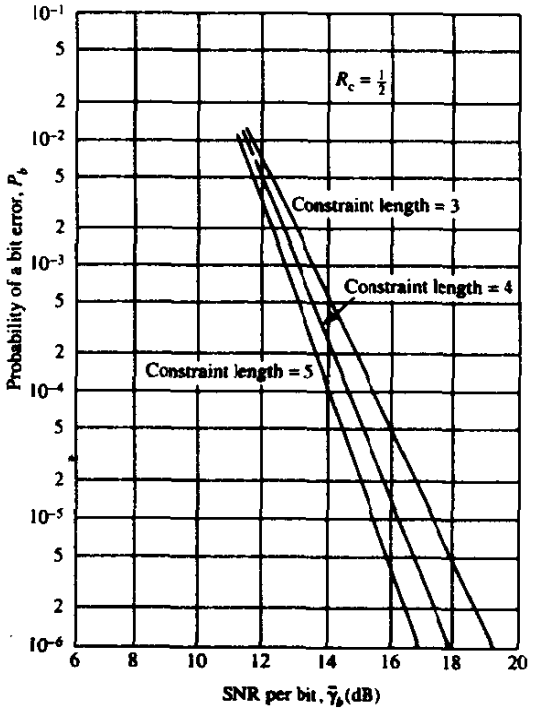

FIGURE 14-6-4 Performance of rate 1/2 binary convolutional codes with soft decision decoding.

length of the code is to repeat each output bit m times. This is equivalent to reducing the code rate by a factor of m or expanding the bandwidth by the same factor. The result is a convolutional code that has a minimum free distance of md_{free}, where d_{free} is the minimum free distance of the original code without repetitions. Such a code is almost as good, from the viewpoint of minimum distance, as a maximum free distance, rate $1/mn$ code. The error rate performance with repetitions is upper-bounded by

$$P_b < \frac{1}{k} \sum_{d_{free}}^{\infty} \beta_d P_2(md) \qquad (14\text{-}6\text{-}14)$$

where $P_2(md)$ is given by (14-6-12). Figure (14-6-5) illustrates the performance of the rate 1/2 codes with repetitions ($m = 1, 2, 3, 4$) for constraint length 5.

14-6-4 Use of Constant-Weight Codes and Concatenated Codes for a Fading Channel

Our treatment of coding for a Rayleigh fading channel to this point was based on the use of binary FSK as the modulation technique for transmitting each of the binary digits in a code word. For this modulation technique, all the 2^k code

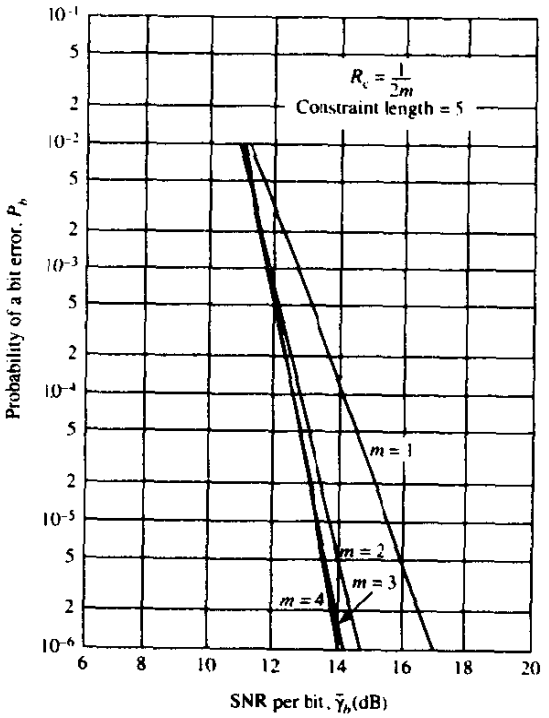

FIGURE 14-6-5 Performance of rate $1/2m$, constraint length 5, binary convolutional codes with soft-decision decoding.

words in the (n, k) code have identical transmitted energy. Furthermore, under the condition that the fading on the n transmitted tones is mutually statistically independent and identically distributed, the average received signal energy for the $M = 2^k$ possible code words is also identical. Consequently, in a soft-decision decoder, the decision is made in favor of the code word having the largest decision variable.

The condition that the received code words have identical average SNR has an important ramification in the implementation of the receiver. If the received code words do not have identical average SNR, the receiver must provide bias compensation for each received code word so as to render it equal energy. In general, the determination of the appropriate bias terms is difficult to implement because it requires the estimation of the average received signal power; hence, the equal-energy condition on the received code words considerably simplifies the receiver processing.

There is an alternative modulation method for generating equal-energy waveforms from code words when the code is constant-weight, i.e., when every code word has the same number of 1s. Note that such a code is nonlinear. Nevertheless, suppose we assign a single tone or cell to each bit position of the 2^k code words. Thus, an (n, k) binary block code has n tones assigned. Waveforms are constructed by transmitting the tone corresponding to a particular bit in a code word if that bit is a 1; otherwise, that tone is not transmitted for the duration of the interval. This modulation technique for transmitting the coded bits is called *on–off keying* (OOK). Since the code is constant-weight, say w, every coded waveform consists of w transmitted tones that depend on the positions of the 1s in each of the code words.

As in FSK, all tones in the OOK signal that are transmitted over the channel are assumed to fade independently across the frequency band and in time from one code word to another. The received signal envelope for each tone is described statistically by the Rayleigh distribution. Statistically independent additive white gaussian noise is assumed to be present in each frequency cell.

The receiver employs maximum-likelihood (soft-decision) decoding to map the received waveform into one of the M possible transmitted code words. For this purpose, n matched filters are employed, each matched to one of the n frequency tones. For the assumed statistical independence of the signal fading for the n frequency cells and additive white gaussian noise, the envelopes of the matched filter outputs are squared and combined to form the M decision variables

$$U_i = \sum_{j=1}^{n} c_{ij} |y_j|^2, \quad i = 1, 2, \ldots, 2^k \tag{14-6-15}$$

where $|y_j|^2$ corresponds to the squared envelope of the filter corresponding to the jth frequency, where $j = 1, 2, \ldots, n$.

It may appear that the constant-weight condition severely restricts our choice of codes. This is not the case, however. To illustrate this point, we

briefly describe some methods for constructing constant-weight codes. This discussion is by no means exhaustive.

Method 1: Nonlinear Transformation of a Linear Code In general, if in each word of an arbitrary binary code we substitute one binary sequence for every occurrence of a 0 and another sequence for each 1, a constant-weight binary block code will be obtained if the two substitution sequences are of equal weights and lengths. If the length of the sequence is v and the original code is an (n, k) code then the resulting constant-weight code will be an (vn, k) code. The weight will be n times the weight of the substitution sequence, and the minimum distance will be the minimum distances of the original code times the distances between the two substitution sequences. Thus, the use of complementary sequences when v is even results in a code with minimum distance $vd_{\min}$ and weight $\frac{1}{2}vn$.

The simplest form of this method is the case $v = 2$, in which every 0 is replaced by the pair 01 and every 1 is replaced by the complementary sequence 10 (or vice versa). As an example, we take as the initial code the (24, 12) extended Golay code. The parameters of the original and the resultant constant-weight code are given in Table 14-6-1.

Note that this substitution process can be viewed as a separate encoding. This secondary encoding clearly does not alter the information content of a code word—it merely changes the form in which it is transmitted. Since the new code word is composed of pairs of bits—one "on" and one "off"—the use of OOK transmission of this code word produces a waveform that is identical to that obtained by binary FSK modulation for the underlying linear code.

Method 2: Expurgation In this method, we start with an arbitrary binary block code and select from it a subset consisting of all words of a certain weight. Several different constant-weight codes can be obtained from one initial code by varying the choice of the weight w. Since the code words of the resulting expurgated code can be viewed as a subset of all possible permutations of any one code word in the set, the term *binary expurgated permutation modulation* (BEXPERM) has been used by Gaarder (1971) to describe such a code. In fact, the constant-weight binary block codes constructed by the other

TABLE 14-6-1 EXAMPLE OF CONSTANT-WEIGHT CODE FORMED BY METHOD 1

Code parameters	Original Golay	Constant-weight
n	24	48
k	12	12
M	4096	4096
$d_{\min}$	8	16
w	variable	24

TABLE 14-6-2 EXAMPLES OF CONSTANT-WEIGHT CODES FORMED BY EXPURGATION

Parameters	Original	Constant weight No. 1	Constant weight No. 2
n	24	24	24
k	12	9	11
M	4096	759	2576
$d_{\min}$	8	≥ 8	≥ 8
w	variable	8	12

methods may also be viewed as BEXPERM codes. This method of generating constant-weight codes is in a sense opposite to the first method in that the word length n is held constant and the code size M is changed. The minimum distance for the constant-weight subset will clearly be no less than that of the original code. As an example, we consider the Golay (24, 12) code and form the two different constant-weight codes shown in Table 14-6-2.

Method 3: Hadamard Matrices This method might appear to form a constant-weight binary block code directly, but it actually is a special case of the method of expurgation. In this method, a Hadamard matrix is formed as described in Section 8-1-2, and a constant-weight code is created by selection of rows (code words) from this matrix. Recall that a Hadamard matrix is an $n \times n$ matrix (*n* even integer) of 1s and 0s with the property that any row differs from any other row in exactly $\frac{1}{2}n$ positions. One row of the matrix is normally chosen as being all 0s.

In each of the other rows, half of the elements are 0s and the other half 1s. A Hadamard code of size $2(n-1)$ code words is obtained by selecting these $n-1$ rows and their complements. By selecting $M = 2^k \leq 2(n-1)$ of these code words, we obtain a Hadamard code, which we denote by $H(n, k)$, where each code word conveys k information bits. The resulting code has constant weight $\frac{1}{2}n$ and minimum distance $d_{\min} = \frac{1}{2}n$.

Since n frequency cells are used to transmit k information bits, the bandwidth expansion factor for the Hadamard $H(n, k)$ code is defined as

$$B_e = \frac{n}{k} \text{ cells per information bit}$$

which is simply the reciprocal of the code rate. Also, the average signal-to-noise ratio (SNR) per bit, denoted by $\bar{\gamma}_b$, is related to the average SNR per cell, $\bar{\gamma}_c$, by the expression

$$\begin{aligned} \bar{\gamma}_c &= \frac{k}{\frac{1}{2}n}\bar{\gamma}_b \\ &= 2\frac{k}{n}\bar{\gamma}_b = 2R_c\bar{\gamma}_b = \frac{2\bar{\gamma}_b}{B_e} \end{aligned} \tag{14-6-16}$$

Let us compare the performance of the constant-weight Hadamard codes under a fixed bandwidth constraint with a conventional M-ary orthogonal set of waveforms where each waveform has diversity L. The M orthogonal waveforms with diversity are equivalent to a block orthogonal code having a block length $n = LM$ and $k = \log_2 M$. For example, if $M = 4$ and $L = 2$, the code words of the block orthogonal code are

$$\mathbf{C}_1 = [1 \quad 1 \quad 0 \quad 0 \quad 0 \quad 0 \quad 0 \quad 0]$$

$$\mathbf{C}_2 = [0 \quad 0 \quad 1 \quad 1 \quad 0 \quad 0 \quad 0 \quad 0]$$

$$\mathbf{C}_3 = [0 \quad 0 \quad 0 \quad 0 \quad 1 \quad 1 \quad 0 \quad 0]$$

$$\mathbf{C}_4 = [0 \quad 0 \quad 0 \quad 0 \quad 0 \quad 0 \quad 1 \quad 1]$$

To transmit these code words using OOK modulation requires $n = 8$ cells, and since each code word conveys $k = 2$ bits of information, the bandwidth expansion factor $B_e = 4$. In general, we denote the block orthogonal code as $O(n, k)$. The bandwidth expansion factor is

$$B_e = \frac{n}{k} = \frac{LM}{k} \tag{14-6-17}$$

Also, the SNR per bit is related to the SNR per cell by the expression

$$\begin{aligned} \bar{\gamma}_c &= \frac{k}{L}\bar{\gamma}_b \\ &= M\left(\frac{k}{n}\right)\bar{\gamma}_b = M\frac{\bar{\gamma}_b}{B_e} \end{aligned} \tag{14-6-18}$$

Now we turn our attention to the performance characteristics of these codes. First, the exact probability of a code word (symbol) error for M-ary orthogonal signaling over a Rayleigh fading channel with diversity was given in closed form in Section 14-4. As previously indicated, this expression is rather cumbersome to evaluate, especially if either L or M or both are large. Instead, we shall use a union bound that is very convenient. That is, for a set of M orthogonal waveforms, the probability of a symbol error can be upper-bounded as

$$\begin{aligned} P_M &\leq (M-1)P_2(L) \\ &= (2^k - 1)P_2(L) < 2^k P_2(L) \end{aligned} \tag{14-6-19}$$

where $P_2(L)$, the probability of error for two orthogonal waveforms, each with diversity L, is given by (14-6-12) with $p = 1/(2 + \bar{\gamma}_c)$. The probability of bit error is obtained by multiplying P_M by $2^{k-1}/(2^k - 1)$, as explained previously.

A simple upper (union) bound on the probability of a code word error for the Hadamard $H(n, k)$ code is obtained by noting the probability of error in deciding between the transmitted code word and any other code word is bounded from above by $P_2(\frac{1}{2}d_{\min})$, where $d_{\min}$ is the minimum distance of the code. Therefore, an upper bound on P_M is

$$P_M \leq (M-1)P_2(\tfrac{1}{2}d_{\min}) < 2^k P_2(\tfrac{1}{2}d_{\min}) \tag{14-6-20}$$

Thus the "effective order of diversity" of the code for OOK modulation is $\frac{1}{2}d_{\min}$. The bit error probability may be approximated as $\frac{1}{2}P_M$, or slightly overbounded by multiplying P_M by the factor $2^{k-1}/(2^k-1)$, which is the factor used above for orthogonal codes. The latter was selected for the error probability computations given below.

Figures 14-6-6 and 14-6-7 illustrate the error rate performance of a selected number of Hadamard codes and block orthogonal codes, respectively, for several bandwidth expansion factors. The advantage resulting from an increase in the size M of the alphabet (or k, since $k = \log_2 M$) and an increase in the bandwidth expansion factor is apparent from observation of these curves. Note, for example, that the $H(20, 5)$ code when repeated twice results in a code that is denoted by ${}_2H(20, 5)$ and has a bandwidth expansion factor $B_e = 8$. Figure 14-6-8 shows the performance of the two types of codes compared on the basis of equal bandwidth expansion factors. It is observed that the error rate curves for the Hadamard codes are steeper than the corresponding curves

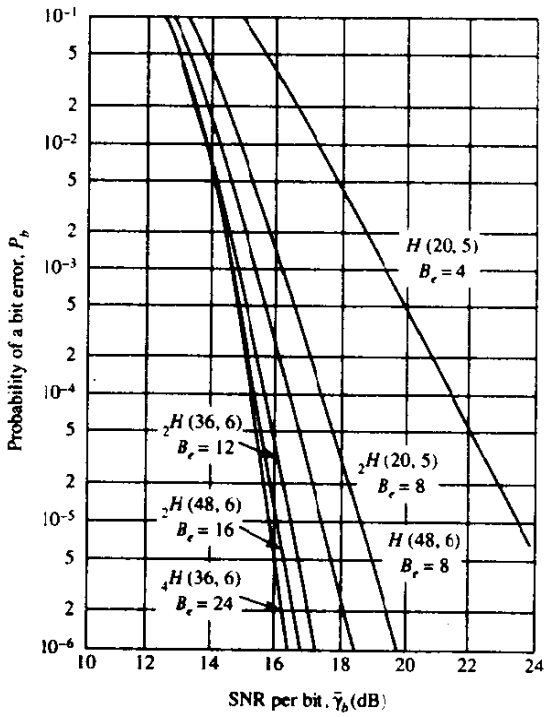

FIGURE 14-6-6 Performance of Hadamard codes.

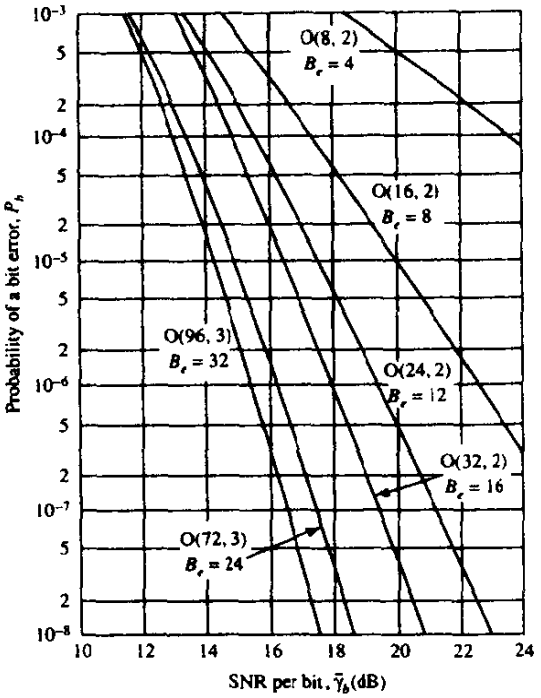

FIGURE 14-6-7 Performance of block orthogonal codes.

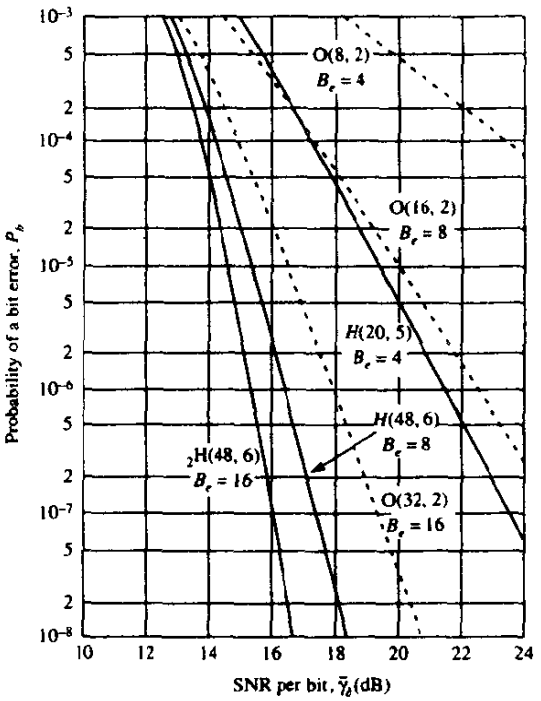

FIGURE 14-6-8 Comparison of performance between Hadamard codes and block orthogonal codes.

for the block orthogonal codes. This characteristic behavior is due simply to the fact that, for the same bandwidth expansion factor, the Hadamard codes provide more diversity than block orthogonal codes. Alternatively, one may say that Hadamard codes provide better bandwidth efficiency than block orthogonal codes. It should be mentioned, however, that at low SNR, a lower-diversity code outperforms a higher-diversity code as a consequence of the fact that, on a Rayleigh fading channel, there is an optimum distribution of the total received SNR among the diversity signals. Therefore, the curves for the block orthogonal codes will cross over the curves for the Hadamard codes at the low-SNR (high-error-rate) region.

Method 4: Concatenation In this method, we begin with two codes: one binary and the other nonbinary. The binary code is the inner code and is an (n, k) constant-weight (nonlinear) block code. The nonbinary code, which may be linear, is the outer code. To distinguish it from the inner code, we use uppercase letters, e.g., an (N, K) code, where N and K are measured in terms of symbols from a q-ary alphabet. The size q of the alphabet over which the outer code is defined cannot be greater than the number of words in the inner code. The outer code, when defined in terms of the binary inner code words rather than q-ary symbols, is the new code.

An important special case is obtained when $q = 2^k$ and the inner code size is chosen to be 2^k. Then the number of words is $M = 2^{kK}$ and the concatenated structure is an (nN, kK) code. The bandwidth expansion factor of this concatenated code is the product of the bandwidth expansions for the inner and outer codes.

Now we shall demonstrate the performance advantages obtained on a Rayleigh fading channel by means of code concatenation. Specifically, we construct a concatenated code in which the outer code is a dual-k (nonbinary) convolutional code and the inner code is either a Hadamard code or a block orthogonal code. That is, we view the dual-k code with M-ary ($M = 2^k$) orthogonal signals for modulation as a concatenated code. In all cases to be considered, soft-decision demodulation and Viterbi decoding are assumed.

The error rate performance of the dual-k convolutional codes is obtained from the derivation of the transfer function given by (8-2-39). For a rate-1/2, dual-k code with no repetitions, the bit error probability, appropriate for the case in which each k-bit output symbol from the dual-k encoder is mapped into one of $M = 2^k$ orthogonal code words, is upper-bounded as

$$P_b < \frac{2^{k-1}}{2^k - 1} \sum_{m=4}^{\infty} \beta_m P_2(m) \tag{14-6-21}$$

where $P_2(m)$ is given by (14-6-12).

For example, a rate-1/2, dual-2 code may employ a 4-ary orthogonal code O(4, 2) as the inner code. The bandwidth expansion factor of the resulting concatenated code is, of course, the product of the bandwidth expansion

factors of the inner and outer codes. Thus, in this example, the rate of the outer code is 1/2 and the inner code is 1/2. Hence, $B_e = (4/2)(2) = 4$.

Note that if every symbol of the dual-k is repeated r times, this is equivalent to using an orthogonal code with diversity $L = r$. If we select $r = 2$ in the example given above, the resulting orthogonal code is denoted as O(8, 2) and the bandwidth expansion factor for the rate-1/2, dual-2 code becomes $B_e = 8$. Consequently, the term $P_2(m)$ in (14-6-21) must be replaced by $P_2(mL)$ when the orthogonal code has diversity L. Since a Hadamard code has an "effective diversity" $\frac{1}{2}d_{\min}$, it follows that when a Hadamard code is used as the inner code with a dual-k outer code, the upper bound on the bit error probability of the resulting concatenated code given by (14-6-21) still applies if $P_2(m)$ is replaced by $P_2(\frac{1}{2}md_{\min})$. With these modifications, the upper bound on the bit error probability given by (14-6-21) has been evaluated for rate-1/2, dual-k convolutional codes with either Hadamard codes or block orthogonal codes as inner codes. Thus the resulting concatenated code has a bandwidth expansion factor equal to twice the bandwidth expansion factor of the inner code.

First, we consider the performance gains due to code concatenation. Figure 14-6-9 illustrates the performance of dual-k codes with block orthogonal inner codes compared with the performance of block orthogonal codes for bandwidth expansion factors $B_e = 4$, 8, 16, and 32. The performance gains due to concatenation are very impressive. For example, at an error rate of 10^{-6} and $B_e = 8$, the dual-k code outperforms the orthogonal block code by 7.5 dB. In

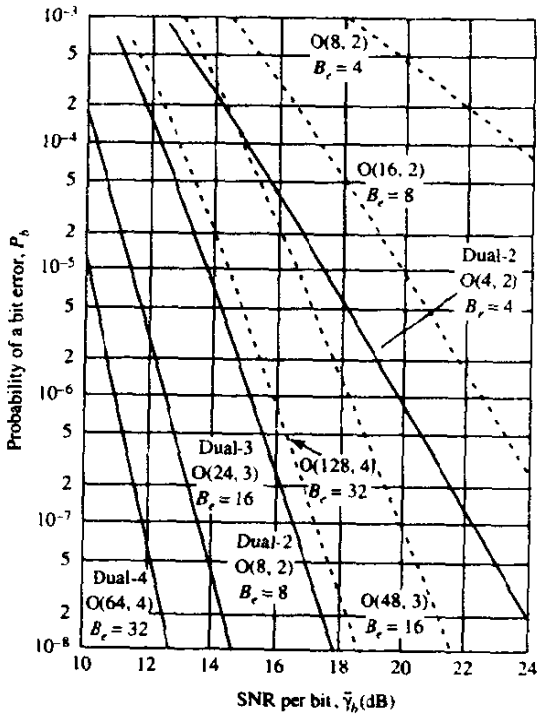

FIGURE 14-6-9 Comparison of performance between block orthogonal codes and dual-k with block orthogonal inner codes.

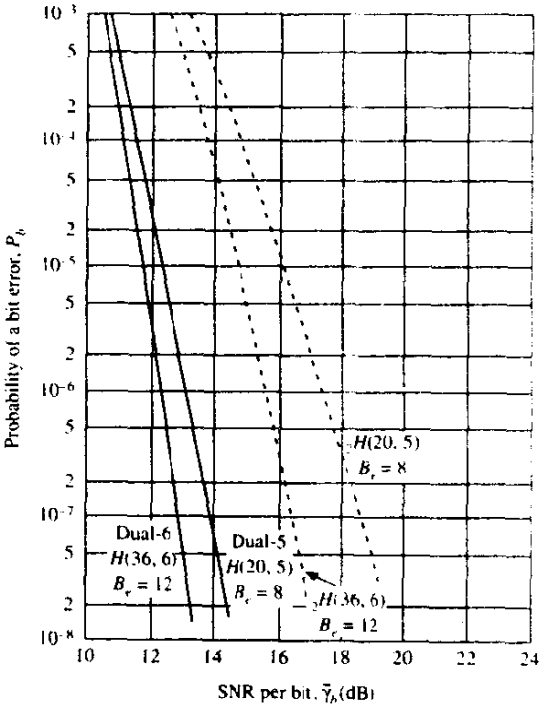

FIGURE 14-6-10 Comparison of performance between Hadamard codes and dual-k codes with Hadamard inner codes.

short, this gain may be attributed to the increased diversity (increase in minimum distance) obtained via code concatenation. Similarly, Fig. 14-6-10 illustrates the performance of two dual-k codes with Hadamard inner codes compared with the performance of the Hadamard codes alone for $B_e = 8$ and 12. It is observed that the performance gains due to code concatenation are still significant, but certainly not as impressive as those illustrated in Fig. 14-6-9. The reason is that the Hadamard codes alone yield a large diversity, so that the increased diversity arising from concatenation does not result in as large a gain in performance for the range of error rates covered in Fig. 14-6-10.

Next, we compare the performance for the two types of inner codes used with dual-k outer codes. Figure 14-6-11 shows the comparison for $B_e = 8$. Note that the $_2H(4, 2)$ inner code has $d_{\min} = 4$, and, hence, it has an effective order of diversity equal to 2. But this dual diversity is achieved by transmitting four frequencies per code word. On the other hand, the orthogonal code O(8, 2) also gives dual diversity, but this is achieved by transmitting only two frequencies per code word. Consequently, the O(8, 2) code is 3 dB better than the $_2H(4, 2)$. This difference in performance is maintained when the two codes are used as inner codes in conjunction with dual-2 code. On the other hand, for $B_e = 8$, one can use the $H(20, 5)$ as the inner code of a dual-5 code, and its performance is significantly better than that of the dual-2 code at low error rates. This improvement in performance is achieved at the expense of an increase in decoding complexity. Similarly, in Fig. 14-6-12, we compare the

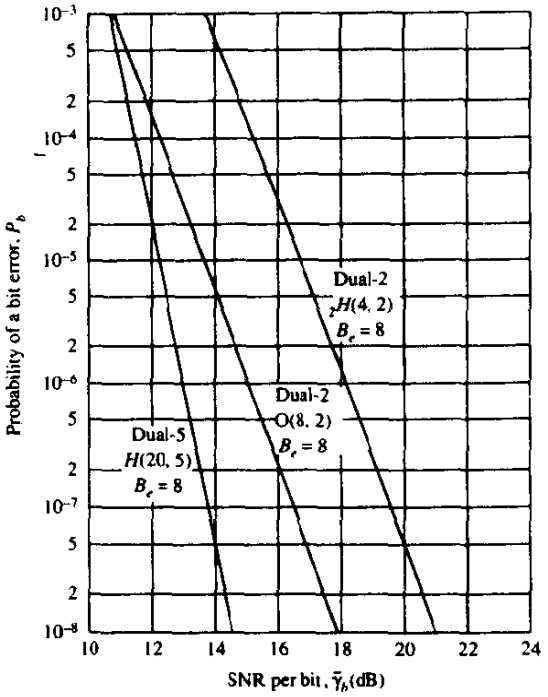

FIGURE 14-6-11 Performance of dual-k codes with either Hadamard or block orthogonal inner code for $B_c = 8$.

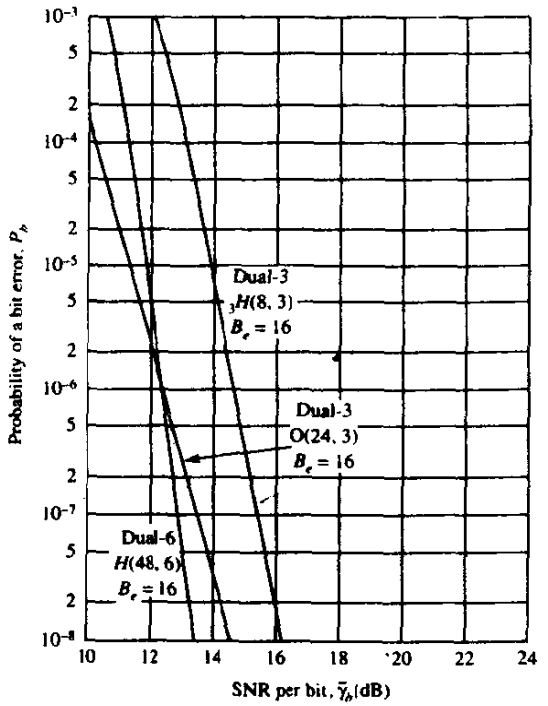

FIGURE 14-6-12 Performance of dual-k codes with either Hadamard or block orthogonal inner code for $B_c = 16$.

performance of the dual-k codes with two types of inner codes for $B_c = 16$. Note that the ${}_3H(8, 3)$ inner code has $d_{\min} = 12$, and, hence, it yields an effective diversity of 6. This diversity is achieved by transmitting 12 frequencies per code word. The orthogonal inner code O(24, 3) gives only third-order diversity, which is achieved by transmitting three frequencies per code word. Consequently the O(24, 3) inner code is more efficient at low SNR, that is, for the range of error rates covered in Fig. 14-6-12. At large SNR, the dual-3 code with the Hadamard ${}_3H(8, 3)$ inner code outperforms its counterpart with the O(24, 3) inner code due to the large diversity provided by the Hadamard code. For the same bandwidth expansion factor $B_c = 16$, one may use a dual-6 code with a $H(48, 6)$ code to achieve an improvement over the dual-3 code with the ${}_3H(8, 3)$ inner code. Again, this improvement in performance (which in this case is not as impressive as that shown in Fig. 14-6-11), must be weighed against the increased decoding complexity inherent in the dual-6 code.

The numerical results given above illustrate the performance advantages in using codes with good distance properties and soft-decision decoding on a Rayleigh fading channel as an alternative to conventional M-ary orthogonal signaling with diversity. In addition, the results illustrate the benefits of code concatenation on such a channel, using a dual-k convolutional code as the outer code and either a Hadamard code or a block orthogonal code as the inner code. Although dual-k codes were used for the outer code, similar results are obtained when a Reed–Solomon code is used for the outer code. There is an even greater choice in the selection of the inner code.

The important parameter in the selection of both the outer and the inner codes is the minimum distance of the resultant concatenated code required to achieve a specified level of performance. Since many codes will meet the performance requirements, the ultimate choice is made on the basis of decoding complexity and bandwidth requirements.

14-6-5 System Design Based on the Cutoff Rate

In the above treatment of coded waveforms, we have demonstrated the effectiveness of various codes for fading channels. In particular, we have observed the benefits of soft-decision decoding and code concatenation as a means for increasing the minimum distance and, hence, the amount of diversity in the coded waveforms. In this subsection, we consider randomly selected code words and derive an upper (union) bound on the error probability that depends on the cutoff rate parameter for the Rayleigh fading channel.

Let us consider the model for the communication system illustrated in Fig. 14-6-1. The modulator has a q-ary orthogonal FSK alphabet. Code words of block length n are mapped into waveforms by selecting n tones from the alphabet of q tones. The demodulation is performed by passing the signal through a bank of q matched filters followed by square-law detectors. The decoding is assumed to be soft-decision. Thus, the square-law detected outputs

from the demodulator are appropriately combined (added) with equal weighting to form M decision variables corresponding to the M possible transmitted code words.

To evaluate the union bound on the probability of error in a Rayleigh fading channel with AWGN, we first evaluate the binary error probability involving the decision variable U_1, which corresponds to the transmitted code word, and any of the other $M-1$ decision variables corresponding to the other code words. Let U_2 be the other decision variable and suppose that U_1 and U_2 have l tones in common. Hence, the contributions to U_1 and U_2 from these l tones are identical and, therefore, cancel out when we form the difference $U_1 - U_2$. Since the two decision variables differ in $n-l$ tones, the probability of error is simply that for a binary orthogonal FSK system with $n-l$ order diversity. The exact form for this probability of error is given by (14-6-4), where $p = 1/(2+\bar{\gamma}_c)$, and $\bar{\gamma}_c$ is the average SNR per tone. For simplicity, we choose to use the Chernoff bound for this binary event error probability, given by (14-6-7), i.e.,

$$P_2(U_1, U_2 \mid l) \leq [4p(1-p)]^{n-l} \tag{14-6-22}$$

Now, let us average over the ensemble of binary communication systems. There are q^n possible code words, from which we randomly select two code words. Thus, each code word is selected with equal probability. Then, the probability that two randomly selected code words have l tones in common is

$$P(l) = \binom{n}{l}\left(\frac{1}{q}\right)^l\left(1-\frac{1}{q}\right)^{n-l} \tag{14-6-23}$$

When we average (14-6-22) over the probability distribution of l given by (14-6-23), we obtain

$$\begin{aligned}\overline{P_2(U_1, U_2)} &= \sum_{l=0}^{n} P_2(U_1, U_2 \mid l)P(l) \\ &\leq \left\{\sum_{l=0}^{n}\binom{n}{l}\left(\frac{1}{q}\right)^l\left[4\left(1-\frac{1}{q}\right)p(1-p)\right]^{n-l}\right. \\ &\leq \left\{\frac{1}{q}[1+4(q-1)p(1-p)]\right\}^n \end{aligned} \tag{14-6-24}$$

Finally, the union bound for communication systems that use $M = 2^k$ randomly selected code words is simply

$$\bar{P}_M \leq (M-1)\overline{P_2(U_1, U_2)} < M\overline{P_2(U_1, U_2)} \tag{14-6-25}$$

By combining (14-6-24) with (14-6-25), we obtain the upper bound on the symbol error probability as

$$\bar{P}_M < 2^{-n(R_0 - R_c)} \tag{14-6-26}$$

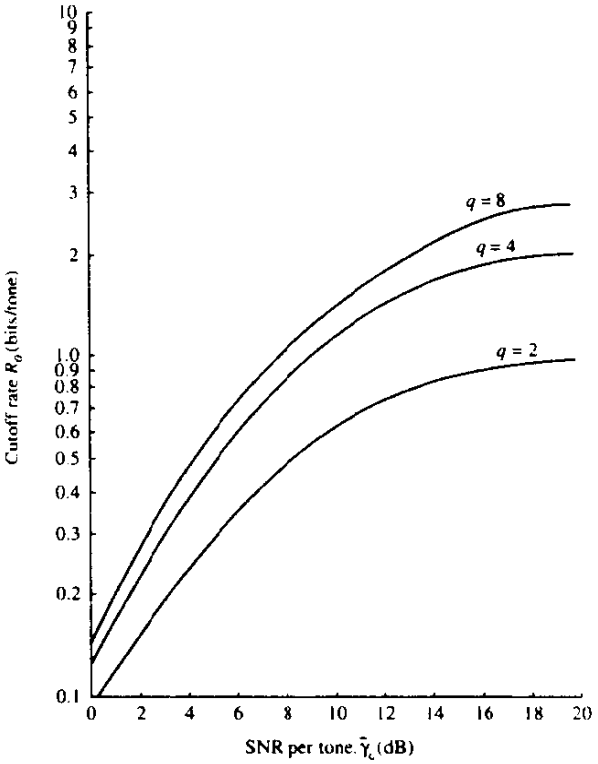

URE 14-6-13 Cutoff rate as a function of $\bar{\gamma}_c$ for Rayleigh fading channel.

where $R_c = k/n$ is the code rate and R_0 is the cutoff rate defined as

$$R_0 = \log_2 \frac{q}{1 + 4(q-1)p(1-p)} \tag{14-6-27}$$

with

$$p = \frac{1}{2 + \bar{\gamma}_c} \tag{14-6-28}$$

Graphs of R_0 as a function of $\bar{\gamma}_c$ are shown in Fig. 14-6-13 for $q = 2$, 4, and 8.

A more interesting form of (14-6-26) is obtained if we express $\bar{P}_M$ in terms of the SNR per bit. In particular, (14-6-26) may be expressed as

$$\bar{P}_M < 2^{-k[\bar{\gamma}_b g(q, \bar{\gamma}_c) - 1]} \tag{14-6-29}$$

where, by definition,

$$\begin{aligned} g(q, \bar{\gamma}_c) &= \frac{R_0}{\bar{\gamma}_c} \\ &= \frac{1}{\bar{\gamma}_c} \log_2 \left[\frac{q}{1 + 4(q-1)p(1-p)} \right] \end{aligned} \tag{14-6-30}$$

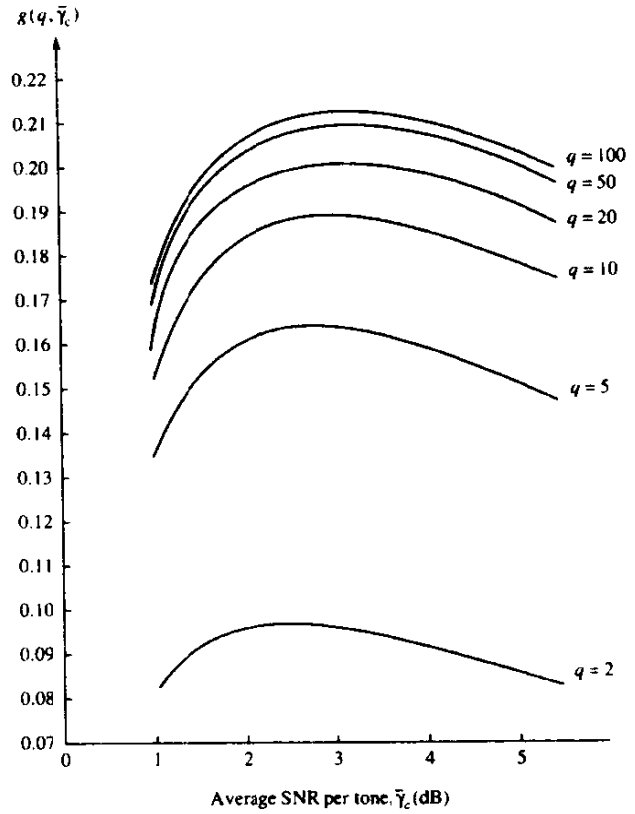

FIGURE 14-6-14 Graph of function $g(q, \bar{\gamma}_c)$.

Graphs of $g(q, \bar{\gamma}_c)$ as a function of $\bar{\gamma}_c$ are plotted in Fig. 14-6-14, with q as a parameter. First, we note thate is an optimum $\bar{\gamma}_c$ for each value of q that minimizes the probability of error. For large q, this value is approximately $\bar{\gamma}_c = 3$ (5 dB), which is consistent with our previous observation for ordinary square-law diversity combining. Furthermore, as $q \to \infty$, the function $g(q, \bar{\gamma}_c)$ approaches a limit, which is

$$\lim_{q \to \infty} g(q, \bar{\gamma}_c) = g_\infty(\bar{\gamma}_c) = \frac{1}{\bar{\gamma}_c} \log_2 \left[\frac{(2 + \bar{\gamma}_c)^2}{4(1 + \bar{\gamma}_c)} \right] \tag{14-6-31}$$

The value of $g_\infty(\bar{\gamma}_c)$ evaluated at $\bar{\gamma}_c = 3$ is

$$\begin{aligned} g_\infty(3) &= \max_{\bar{\gamma}_c} g_\infty(\bar{\gamma}_c) \\ &= 0.215 \end{aligned} \tag{14-6-32}$$

Therefore, the error probability in (14-6-29) for this optimum division of total SNR is

$$\bar{P}_M < 2^{-0.215k(\bar{\gamma}_b - 4.65)} \tag{14-6-33}$$

This result indicates that the probability of error can be made arbitrarily small with optimum SNR per code chip, if the average SNR per bit $\bar{\gamma}_b > 4.65$ (6.7 dB). Even a relatively modest value of $q = 20$ comes close to this minimum value. As seen from Fig. 14-6-14, $g(20, 3) = 0.2$, so that $P_M \to 0$, provided $\bar{\gamma}_b > 5$ (7 dB). On the other hand, if $q = 2$, the maximum value of $g(2, \bar{\gamma}_c) \approx 0.096$ and the corresponding minimum SNR per bit is 10.2 dB.

In the case of binary FSK waveforms ($q = 2$), we may easily compare the cutoff rate for the unquantized (soft-decision) demodulator output with the cutoff rate for binary quantization, for which

$$R_Q = 1 - \log[1 + \sqrt{4p(1-p)}], \qquad Q = 2$$

as was given in (8-1-104). Figure 14-6-15 illustrates the graphs for R_0 and R_Q. Note that the difference between R_0 and R_Q is approximately 3 dB for rates below 0.3 and the difference increases rapidly at high rates. This loss may be reduced significantly by increasing the number of quantization levels to $Q = 8$ (three bits).

Similar comparisons in the relative performance between unquantized soft-decision decoding and quantized decision decoding can also be made for $q > 2$.

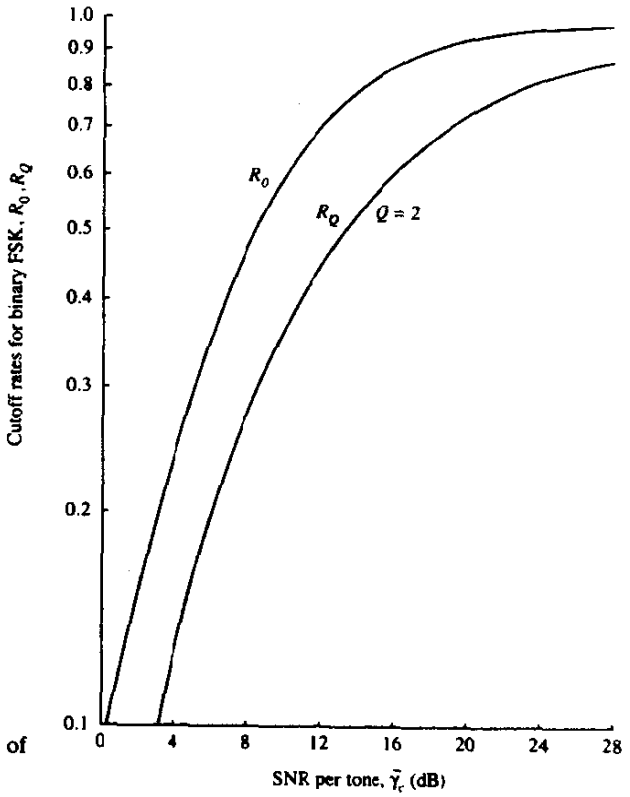

FIGURE 14-6-15 Cutoff rate for (unquantized) soft-decision and hard-decision decoding of coded binary FSK.

14-6-6 Trellis-Coded Modulation

Trellis-coded modulation was described in Section 8-3 as a means for achieving a coding gain on bandwidth-constrained channels, where we wish to transmit at a bit-rate-to-bandwidth ratio $R/W > 1$. For such channels, the digital communication system is designed to use bandwidth-efficient multilevel or multiphase modulation (PAM, PSK, DPSK, or QAM), which allows us to achieve an $R/W > 1$. When coding is applied in signal design for a bandwidth constrained channel, a coding gain is desired without expanding the signal bandwidth. This goal can be achieved, as described in Section 8-3, by increasing the number of signal points in the constellation over the corresponding uncoded system to compensate for the redundancy introduced by the code, and designing the trellis code so that the euclidean distance in a sequence of transmitted symbols corresponding to paths that merge at any node in the trellis is larger than the euclidean distance per symbol in an uncoded system.

In contrast, the coding schemes that we have described above in conjunction with FSK modulation expand the bandwidth of the modulated signal for the purpose of achieving signal diversity. Coupled with FSK modulation, which is not bandwidth-efficient, the coding schemes we have described are inappropriate for use on bandwidth-constrained channels.

In designing trellis-coded signal waveforms for fading channels, we may use the same basic principles that we have learned and applied in the design of conventional coding schemes. In particular, the most important objective in any coded signal design for fading channels is to achieve as large a signal diversity as possible. This implies that successive output symbols from the encoder must be interleaved or sufficiently separated in transmission, either in time or in frequency, so as to achieve independent fading in a sequence of symbols that equals or exceeds the minimum free distance of the trellis code. Therefore, we may represent such a trellis-coded modulation system by the block diagram in Fig. 14-6-16, where the interleaver is viewed broadly as a device that separates the successive coded symbols so as to provide independent fading on each symbol (through frequency or time separation of symbols) in the sequence. The receiver consists of a signal demodulator whose output is deinterleaved and fed to the trellis decoder.

FIGURE 14-6-16 Block diagram of trellis-coded modulation systems.

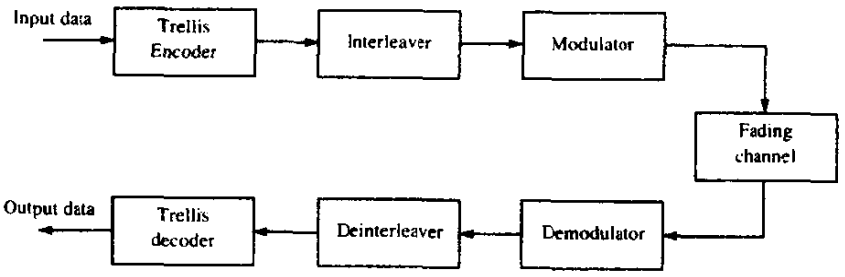

As indicated above, the candidate modulation methods that achieve high bandwidth efficiency are M-ary PSK, DPSK, QAM and PAM. The choice depends to a large extent on the channel characteristics. If there are rapid amplitude variations in the received signal, QAM and PAM may be particularly vulnerable, because a wideband automatic gain control (AGC) must be used to compensate for the channel variations. In such a case, PSK or DPSK are more suitable, since the information is conveyed by the signal phase and not by the signal amplitude. DPSK provides the additional benefit that carrier phase coherence is required only over two successive symbols. However, there is an SNR degradation in DPSK relative to PSK.

In the design of the trellis code, our objective is to achieve as large a free distance as possible, since this parameter is equivalent to the amount of diversity in the received signal. In conventional Ungerboeck trellis coding, each branch in the trellis corresponds to a single M-ary (PSK, DPSK, QAM) output channel symbol. Let us define the *shortest error event path* as the error event path with the smallest number of nonzero distances between itself and the correct path, and let L be its length. In other words, L is the Hamming distance between the M-ary symbols on the shortest error event path and those in the correct path. Hence, if we assume that the transmitted sequence corresponds to the all-zero path in the trellis, L is the number of branches in the shortest-length path with a nonzero M-ary symbol. In a trellis diagram with parallel paths, the paths are constrained to have a shortest error event length of one branch, so that $L = 1$. This means that such a trellis code provides no diversity in a fading channel and, hence, the probability of error is inversely proportional to the SNR per symbol. Therefore, in conventional trellis coding for a fading channel, it is undesirable to design a code that has parallel paths in its trellis, because such a code yields no diversity. This is the case in a conventional rate-$m/(m + 1)$ trellis code, where we are forced to have parallel paths when the number of states is less than 2^m.

One possible way to increase the minimum free distance and, thus, the order of diversity in the code, is to introduce asymmetry in the signal point constellation. This approach appears to be somewhat effective, and has been investigated by Simon and Divsalar (1985), Divsalar and Yuen (1984), and Divsalar *et al.* (1987).

A more effective way to increase the distance L and, thus, the order of diversity is to employ multiple trellis-coded modulation (MTCM). In MTCM, illustrated in Fig. 14-6-17, b input bits to the encoder are coded into c output bits, which are then subdivided into k groups, each of m bits, such that $c = km$. Each m-bit group is mapped into an M-ary symbol. Thus, we obtain the M-ary output symbols. The special case $k = 1$ corresponds to the conventional Ungerboeck codes. With k M-ary output symbols, it is possible to design trellis codes with parallel paths having a distance $L = k$. Thus, we can achieve an error probability that decays inversely as $(\mathcal{E}/N_0)^k$.

An important consideration in the design of the decoder for the trellis code is the use of any side information regarding the channel attenuation for each

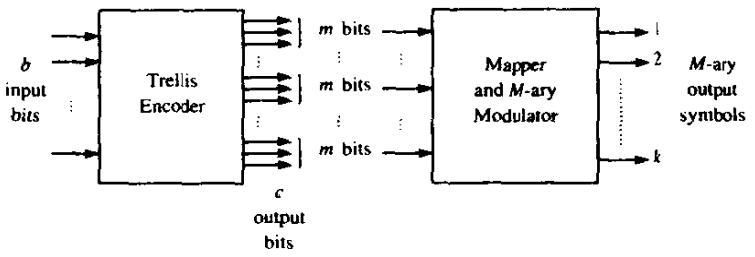

FIGURE 14-6-17 Block diagram of MTCM transmitter.

symbol. In the case of FSK modulation with square-law combination at the decoder to form the decision metrics, it is not necessary to know the channel attenuation for demodulated symbols. However, with coherent detection, the optimum euclidean distance metric for each demodulated symbol is of the form $|r_n - \alpha_n s_n|^2$, where α_n is the channel attenuation for the transmitted symbol s_n and r_n is the demodulation output. Hence, the sum of branch metrics for any given path through the trellis is of the form

$$D(\mathbf{r}, \mathbf{s}^{(i)}) = \sum_n |r_n - \alpha_n s_n^{(i)}|^2$$

where the superscript (i) indicates the ith path through the trellis. Therefore, the estimation of the channel attenuation must be performed in order to realize the optimum trellis decoder. The estimation of the channel attenuation and phase shift, is considered in Appendix C for the case of PSK modulation and demodulation. The effect of the quality of the attenuation and phase estimates on the performance of PSK (uncoded) modulation is also assessed in Appendix C.

14-7 BIBLIOGRAPHICAL NOTES AND REFERENCES

In this chapter, we have considered a number of topics concerned with digital communications over a fading multipath channel. We began with a statistical characterization of the channel and then described the ramifications of the channel characteristics on the design of digital signals and on their performance. We observed that the reliability of the communication system is enhanced by the use of diversity transmission and reception. Finally we demonstrated that channel encoding and soft-decision decoding provide a bandwidth-efficient means for obtaining diversity over such channels.

The pioneering work on the characterization of fading multipath channels and on signal and receiver design for reliable digital communications over such channels was done by Price (1954, 1956). This work was followed by additional significant contributions from Price and Green (1958, 1960), Kailath (1960, 1961), and Green (1962). Diversity transmission and diversity combining techniques under a variety of channel conditions have been considered in the papers by Pierce (1958), Brennan (1959), Turin (1961, 1962), Pierce and Stein

(1960), Barrow (1963), Bello and Nelin (1962a, b, 1963), Price (1962a, b), and Lindsey (1964).

Our treatment of coding for fading channels has relied on contributions from a number of researchers. In particular, the use of dual-k codes with M-ary orthogonal FSK was proposed in publications by Viterbi and Jacobs (1975) and Odenwalder (1976). The importance of coding for digital communications over a fading channel was also emphasized in a paper by Chase (1976). The benefits derived from concatenated coding with soft-decision decoding for a fading channel were demonstrated by Pieper *et al.* (1978). There, a Reed–Solomon code was used for the outer code and a Hadamard code was selected as the inner code. The performance of dual-k codes with either block orthogonal codes or Hadamard codes as inner code were investigated by Proakis and Rahman (1979). The error rate performance of maximal free distance binary convolutional codes was evaluated by Rahman (1981). Finally, the derivation of the cutoff rate for Rayleigh fading channels is due to Wozencraft and Jacobs (1965).

Trellis-coded modulation for fading channels has been investigated by many researchers, whose work was motivated to a large extent by applications to mobile and cellular communications. The book by Biglieri *et al.* (1991) gives a tutorial treatment of this topic and contains a large number of references to the technical literature.

Our treatment of digital communications over fading channels focused primarily on the Rayleigh fading channel model. For the most part, this is due to the wide acceptance of this model for describing the fading effects on many radio channels and to its mathematical tractability. Although other statistical models, such as a Ricean fading model or the Nakagami fading model may be more appropriate for characterizing fading on some real channels, the general approach in the design of reliable communications presented in this chapter carries over.

PROBLEMS

14-1 The scattering function $S(\tau; \lambda)$ for a fading multipath channel is nonzero for the range of values $0 \leq \tau \leq 1$ ms and -0.1 Hz $\leq \lambda \leq 0.1$ Hz. Assume that the scattering function is approximately uniform in the two variables.

a Give numerical values for the following parameters:

(i) the multipath spread of the channel;
(ii) the Doppler spread of the channel;
(iii) the coherence time of the channel;
(iv) the coherence bandwidth of the channel;
(v) the spread factor of the channel.

b Explain the meaning of the following, taking into consideration the answers given in (a):

(i) the channel is frequency-nonselective;
(ii) the channel is slowly fading;
(iii) the channel is frequency-selective.

c Suppose that we have a frequency allocation (bandwidth) of 10 kHz and we wish to transmit at a rate of 100 bits/s over this channel. Design a binary communications system with frequency diversity. In particular, specify (i) the type of modulation, (ii) the number of subchannels, (iii) the frequency separation between adjacent carriers, and (iv) the signaling interval used in your design. Justify your choice of parameters.

14-2 Consider a binary communications system for transmitting a binary sequence over a fading channel. The modulation is orthogonal FSK with third-order frequency diversity ($L = 3$). The demodulator consists of matched filters followed by square-law detectors. Assume that the FSK carriers fade independently and identically according to a Rayleigh envelope distribution. The additive noises on the diversity signals are zero-mean gaussian with autocorrelation functions $\frac{1}{2}E[z_k^*(t)z_k(t+\tau)] = N_0\delta(\tau)$. The noise processes are mutually statistically independent.

a The transmitted signal may be viewed as binary FSK with square-law detection, generated by a repetition code of the form

$$1 \rightarrow \mathbf{C}_1 = [1 \quad 1 \quad 1], \qquad 0 \rightarrow \mathbf{C}_0 = [0 \quad 0 \quad 0]$$

Determine the error rate performance P_{2u} for a hard-decision decoder following the square-law-detected signals.

b Evaluate P_{2u} for $\bar{\gamma}_c = 100$ and 1000.

c Evaluate the error rate P_2, for $\bar{\gamma}_c = 100$ and 1000 if the decoder employs soft-decision decoding.

d Consider the generalization of the result in (a). If a repetition code of block length L (L odd) is used, determine the error probability P_{2u} of the hard-decision decoder and compare that with P_2, the error rate of the soft-decision decoder. Assume $\bar{\gamma} \gg 1$.

14-3 Suppose that the binary signal $s_i(t)$ is transmitted over a fading channel and the received signal is

$$r_i(t) = \pm a s_i(t) + z(t), \qquad 0 \leq t \leq T$$

where $z(t)$ is zero-mean white gaussian noise with autocorrelation function

$$\phi_{zz}(\tau) = N_0\delta(\tau)$$

The energy in the transmitted signal is $\mathcal{E} = \frac{1}{2}\int_0^T |s_i(t)|^2\,dt$. The channel gain a is specified by the probability density function

$$p(a) = 0.1\delta(a) + 0.9\delta(a - 2)$$

a Determine the average probability of error P_2 for the demodulator that employs a filter matched to $s_i(t)$.

b What value does P_2 approach as $\mathcal{E}/N_0$ approaches infinity.

c Suppose that the same signal is transmitted on two statistically *independently fading* channels with gains a_1 and a_2, where

$$p(a_k) = 0.1\delta(a_k) + 0.9\delta(a_k - 2), \qquad k = 1, 2$$

The noises on the two channels are statistically independent and identically distributed. The demodulator employs a matched filter for each channel and

simply adds the two filter outputs to form the decision variable. Determine the average P_2.

d For the case in (c) what value does P_2 approach as $\mathcal{E}/N_0$ approaches infinity.

14-4 A multipath fading channel has a multipath spread of $T_m = 1$ s and a Doppler spread $B_d = 0.01$ Hz. The total channel bandwidth at bandpass available for signal transmission is $W = 5$ Hz. To reduce the effects of intersymbol interference, the signal designer selects a pulse duration $T = 10$ s.

a Determine the coherence bandwidth and the coherence time.

b Is the channel frequency selective? Explain.

c Is the channel fading slowly or rapidly? Explain.

d Suppose that the channel is used to transmit binary data via (antipodal) coherently detected PSK in a frequency diversity mode. Explain how you would use the available channel bandwidth to obtain frequency diversity and determine how much diversity is available.

e For the case in (d), what is the *approximate* SNR required per diversity to achieve an error probability of 10^{-6}?

f Suppose that a wideband signal is used for transmission and a RAKE-type receiver is used for demodulation. How many taps would you use in the RAKE receiver?

g Explain whether or not the RAKE receiver can be implemented as a coherent receiver with maximal ratio combining.

h If binary orthogonal signals are used for the wideband signal with square-law postdetection combining in the RAKE receiver, what is the *approximate* SNR required to achieve an error probability of 10^{-6}?(assume that all taps have the same SNR.)

14-5 In the binary communications system shown in Fig. P14-5, $z_1(t)$ and $z_2(t)$ are statistically independent white gaussian noise processes with zero mean and identical autocorrelation functions $\phi_{zz}(\tau) = N_0\delta(\tau)$. The sampled values U_1 and U_2 represent the *real parts* of the matched filter outputs. For example, if $s_i(t)$ is transmitted, then we have

$$U_1 = 2\mathcal{E} + N_1$$
$$U_2 = N_1 + N_2$$

where $\mathcal{E}$ is the transmitted signal energy and

$$N_k = \text{Re}\left[\int_0^T s_i^*(t) z_k(t)\, dt\right], \quad k = 1, 2$$

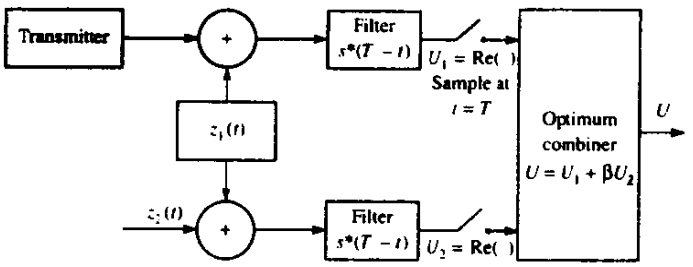

FIGURE P14-5

It is apparent that U_1 and U_2 are correlated gaussian variables while N_1 and N_2 are independent gaussian variables. Thus,

$$p(n_1) = \frac{1}{\sqrt{2\pi}\sigma} \exp\left(-\frac{n_1^2}{2\sigma^2}\right)$$

$$p(n_2) = \frac{1}{\sqrt{2\pi}\sigma} \exp\left(-\frac{n_2^2}{2\sigma^2}\right)$$

where the variance of N_k is $\sigma^2 = 2\mathscr{E}N_0$.

a Show that the joint probability density function for U_1 and U_2 is

$$p(U_1, U_2) = \frac{1}{2\pi\sigma^2} \exp\left\{-\frac{1}{2\sigma^2}[(U_1 - 2\mathscr{E})^2 - U_2(U_1 - 2\mathscr{E}) + \tfrac{1}{2}U_2^2]\right\}$$

if $s(t)$ is transmitted and

$$p(U_1, U_2) = \frac{1}{2\pi\sigma^2} \exp\left\{-\frac{1}{2\sigma^2}[(U_1 + 2\mathscr{E})^2 - U_2(U_1 + 2\mathscr{E}) + \tfrac{1}{2}U_2^2]\right\}$$

if $-s(t)$ is transmitted.

b Based on the likelihood ratio, show that the optimum combination of U_1 and U_2 results in the decision variable

$$U = U_1 + \beta U_2$$

where β is a constant. What is the optimum value of β?

c Suppose that $s(t)$ is transmitted. What is the probability density function of U?

d What is the probability of error assuming that $s(t)$ was transmitted? Express your answer as a function for the SNR $\mathscr{E}/N_0$.

e What is the loss in performance if only $U = U_1$ is the decision variable?

14-6 Consider the model for a binary communications system with diversity as shown in Fig. P14-6. The channels have fixed attenuations and phase shifts. The $\{z_k(t)\}$ are

FIGURE P14-6

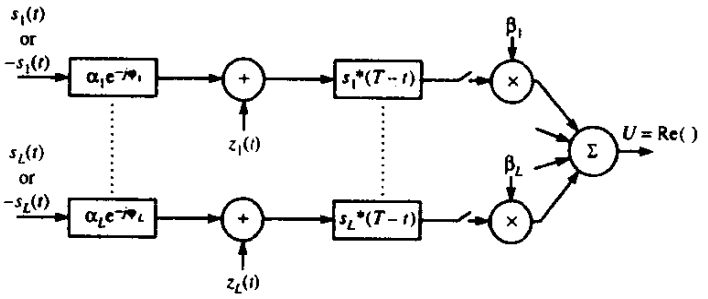

complex-valued white gaussian noise processes with zero mean and autocorrelation functions

$$\phi_{z_k z_k}(t) = \tfrac{1}{2}E[z_k^*(t)z_k(t+\tau)] = N_{0k}\delta(\tau)$$

(Note that the spectral densities $\{N_{0k}\}$ are all different.) Also, the noise processes $\{z_k(t)\}$ are mutually statistically independent. The $\{\beta_k\}$ are complex-valued weighting factors to be determined. The decision variable from the combiner is

$$U = \text{Re}\left(\sum_{k=1}^{L} \beta_k U_k\right) \gtrless_{-1}^{1} 0$$

a Determine the pdf $p(U)$ when $+1$ is transmitted.
b Determine the probability of error P_2 as a function of the weights $\{\beta_k\}$.
c Determine the values of $\{\beta_k\}$ that minimize P_2.

14-7 Determine the probability of error for binary orthogonal signaling with Lth-order diversity over a Rayleigh fading channel. The pdfs of the two decision variables are given by (14-4-31) and (14-4-32).

14-8 The rate-1/3, $L = 3$, binary convolutional code with transfer function given by (8-2-5) is used for transmitting data over a Rayleigh fading channel via binary PSK.
a Determine and plot the probability of error for hard-decision decoding. Assume that the transmitted waveforms corresponding to the coded bits fade independently.
b Determine and plot the probability of error for soft-decision decoding. Assume that the waveforms corresponding to the coded bits fade independently.

14-9 A binary sequence is transmitted via binary antipodal signaling over a Rayleigh fading channel with Lth-order diversity. When $s_i(t)$ is transmitted, the received equivalent lowpass signals are

$$r_k(t) = \alpha_k e^{-j\phi_k} s_i(t) + z_k(t), \qquad k = 1, 2, \ldots, L$$

The fading among the L subchannels is statistically independent. The additive noise terms $\{z_k(t)\}$ are zero-mean, statistically independent and identically distributed white gaussian noise processes with autocorrelation function $\phi_{z_k z_k}(\tau) = N_0\delta(\tau)$. Each of the L signals is passed through a filter matched to $s_i(t)$ and the output is phase-corrected to yield

$$U_k = \text{Re}\left[e^{j\phi_k}\int_0^T r_k(t)s_i^*(t)\,dt\right], \qquad k = 1, 2, \ldots, L$$

The $\{U_k\}$ are combined by a linear combiner to form the decision variable

$$U = \sum_{k=1}^{L} U_k$$

a Determine the pdf of U conditional on fixed values for the $\{a_k\}$.
b Determine the expression for the probability of error when the $\{\alpha_k\}$ are statistically independent and identically distributed Rayleigh random variables.

14-10 The Chernoff bound for the probability of error for binary FSK with diversity L in Rayleigh fading was shown to be

$$P_2(L) < [4p(1-p)]^L = \left[4\frac{1+\bar{\gamma}_c}{(2+\bar{\gamma}_c)^2}\right]^L$$
$$< 2^{-\bar{\gamma}_b g(\bar{\gamma}_c)}$$

where

$$g(\bar{\gamma}_c) = \frac{1}{\bar{\gamma}_c}\log_2\left[\frac{(2+\bar{\gamma}_c)^2}{4(1+\bar{\gamma}_c)}\right]$$

a Plot $g(\bar{\gamma}_c)$ and determine its approximate maximum value and the value of $\bar{\gamma}_c$ where the maximum occurs.

b For a given $\bar{\gamma}_b$, determine the optimal order of diversity.

c Compare $P_2(L)$, under the condition that $g(\bar{\gamma}_c)$ is maximized (optimal diversity), with the error probability for binary FSK in AWGN with no fading, which is

$$P_2 = \tfrac{1}{2}e^{-\gamma_b/2}$$

and determine the penalty in SNR due to fading and noncoherent (square-law) combining.

14-11 A DS spread-spectrum system is used to resolve the multipath signal components in a two-path radio signal propagation scenario. If the path length of the secondary path is 300 m longer than that of the direct path, determine the minimum chip rate necessary to resolve the multipath components.

14-12 A baseband digital communication system employs the signals shown in Fig. P14-12(*a*) for the transmission of two equiprobable messages. It is assumed that the communication problem studied here is a "one-shot" communication problem; that is, the above messages are transmitted just once and no transmission takes place afterward. The channel has no attenuation ($\alpha = 1$), and the noise is AWG with power spectral density $\frac{1}{2}N_0$.

a Find an appropriate orthonormal basis for the representation of the signals.

b In a block diagram, give the precise specifications of the optimum receiver using matched filters. Label the diagram carefully.

c Find the error probability of the optimum receiver.

d Show that the optimum receiver can be implemented by using just *one* filter

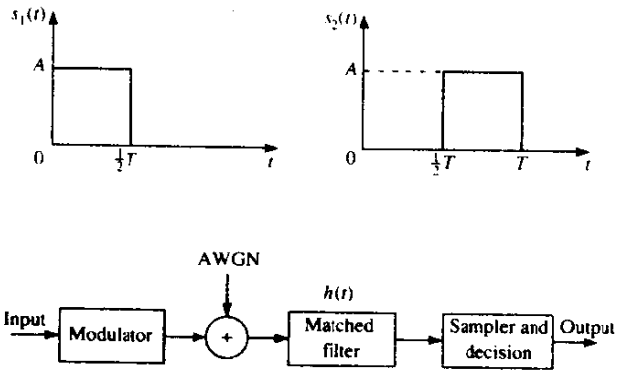

FIGURE P14-12

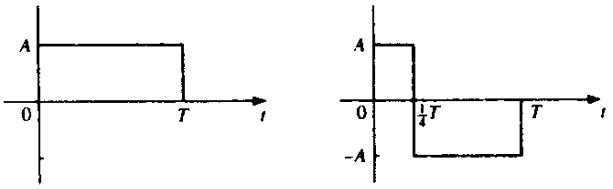

FIGURE P14-14

(see the block diagram in Fig. P14-12(*b*). What are the characteristics of the matched filter and the sampler and decision device?

e Now assume that the channel is not ideal but has an impulse response of $c(t) = \delta(t) + \frac{1}{2}\delta(t - \frac{1}{2}T)$. Using the same matched filter as (d), design an optimum reciever.

f Assuming that the channel impulse response is $c(t) = \delta(t) + a\delta(t - \frac{1}{2}T)$, where a is a random variable uniformly distributed on [0, 1], and using the same matched filter as in (d), design the optimum receiver.

14-13 A communication system employs dual antenna diversity and binary orthogonal FSK modulation. The received signals at the two antennas are

$$r(t) = \alpha_1 s(t) + n_1(t)$$
$$r_2(t) = \alpha_2 s(t) + n_2(t)$$

where α_1 and α_2 are statistically iid Rayleigh random variables, and $n_1(t)$ and $n_2(t)$ are statistically independent, zero-mean white gaussian random processes with power-spectral density $\frac{1}{2}N_0$. The two signals are demodulated, squared and then combined (summed) prior to detection.

a Sketch the functional block diagram of the entire receiver, including the demodulator, the combiner and the detector.

b Plot the probability of error for the detector and compare the result with the case of no diversity.

14-14 The two equivalent lowpass signals shown in Fig. P14-14 are used to transmit a binary sequence. The equivalent lowpass impulse response of the channel is $h(t) = 4\delta(t) - 2\delta(t - T)$. To avoid pulse overlap between successive transmissions, the transmission rate in bits/s is selected to be $R = 1/2T$. The transmitted signals are equally probable and are corrupted by additive zero-mean white gaussian noise having an equivalent lowpass representation $z(t)$ with an autocorrelation function

$$\phi_{zz}(\tau) = \tfrac{1}{2}E[z^*(t)z(t + \tau)] = N_0\delta(\tau)$$

a Sketch the two possible equivalent lowpass noise-free *received* waveforms.

b Specify the optimum receiver and sketch the equivalent lowpass impulse responses of all filters used in the optimum receiver. Assume *coherent detection* of the signals.

14-15 Verify the relation in (14-3-14) by making the change of variable $\gamma = \alpha^2\mathcal{E}_b/N_0$ in the Nakagami-m distribution.